Optimization of Shallow Closed-loop Geothermal Systems

Dissertation

der Mathematisch-Naturwissenschaftlichen Fakultät

der Eberhard Karls Universität Tübingen

zur Erlangung des Grades eines

Doktors der Naturwissenschaften

(Dr. rer. nat.)

vorgelegt von

Jozsef Hecht Méndez

aus Baruta, Venezuela

Tübingen

2012

Tag der mündlichen Qualifikation:	10.05.2012
Dekan:	Prof. Dr. Wolfgang Rosenstiel
1. Berichterstatter:	Jun.-Prof. Dr. habil. Philipp Blum
2. Berichterstatter:	Prof. Dr.-Ing. Olaf A. Cirpka

To my beloved family

…there is no greater challenge in life
than to identify your own limitations
and try to overcome them day by day…

Table of contents

Kurzfassung

Erdgekoppelte Wärmepumpen mit vertikalen Sonden haben sich als die bevorzugte geothermische Technologie zum Heizen und Kühlen von kleinen und großen Gebäuden etabliert. Dieses Verfahren nutzt oberflächennahe geothermische Energie durch die Extraktion oder Injektion von Wärme über Erdwärmesonden (EWS). Bei großräumigen Anwendungen erfolgt der Wärmetransfer über einem Sondenfeld mit multiplen EWS. In der derzeitigen Praxis der EWS-Planung werden bei großräumigen Anlagen alle EWS in Sondenfeldern auf gleiche Weise betrieben. Zudem wird der Einfluss des Grundwassers auf den Wärmetransport im Untergrund bei der EWS-Planung selten berücksichtigt. Die vorliegende Arbeit untersucht das Potential der individuellen Einstellung der einzelnen EWS für unterschiedliche hydro-geothermale Bedingungen. Ein besonderes Augenmerk wurde hierbei auf die durch den Betrieb der EWS bedingten Temperaturänderungen im Untergrund gelegt. Die Hauptfrage ist, inwieweit der konzertierte Wärmeentzug multipler EWS verbessert werden kann. Für die Erörterung der Frage wurden zwei Simulationsoptimierungsverfahren entwickelt. Das erste Verfahren verwendet superpositionierte analytische Modelle, um die Beeinträchtigung der Grundwassertemperatur durch multiple beieinander liegende EWS zu simulieren. Die Vorhersagen der Modelle werden für die Evaluierung einer Zielfunktion für die Optimierung des Betriebs individueller EWS in einem Sondenfeld genutzt. Dies wird innerhalb eines linearen Programmierungsframework erreicht. Zwei *real-case* orientierte Anwendungsfälle für die Wärmeversorgung sind berücksichtigt. Im ersten Anwendungsfall ist das Vorhandensein des Grundwasserflusses vernachlässigt, während für den zweiten Fall unterschiedliche Grundwasserströmungsregime berücksichtigt sind. Die Temperaturverteilung der optimierten und nicht-optimierten EWS-Felder wird durch umfassende numerische Modelle verglichen. Im Allgemeinen kann durch optimierte EWS-Felder die thermische Beeinträchtigung reduziert und extreme lokale Abkühlungen verhindert werden. Im rein

konduktiven Fall wird der maximale Temperaturunterschied im Untergrund um 18% reduziert. Für die konvektionsdominierten Fälle sind die Temperaturänderungen immer geringer, sogar wenn das Grundwasser die lokalen Temperaturanomalien ausgleicht. Zudem kann die Temperatur der zirkulierenden Wärmetransportflüssigkeit innerhalb der optimierten EWS um 1°C erhöht werden, was für die Verbesserung der Wärmepumpenleistung von Vorteil ist. Darüber hinaus erzeugt die optimale Einstellung der Sonden charakteristische Betriebsmuster, die von der Zeit und der Grundwasserfließgeschwindigkeit abhängig sind. Das zweite Simulationsoptimierungsverfahren koppelt die numerische Simulation des Wärmetransports der geothermischen Systeme mit heuristischen Optimierungsalgorithmen. Die Leistungsfähigkeit von drei evolutionären Algorithmen (mit je zwei Varianten) wird für die Maximierung des Gesamtenergieentzugs der EWS-Felder, die in einem heterogenen Aquifer installiert sind, getestet. Zusätzlich wird ein optimales Positionierungsschema für mehrere EWS innerhalb einer vordefinierten Fläche gesucht. Innerhalb der evaluierten Algorithmen ergeben die Optimierungsmethoden Differential Evolution (mit Linesearch-Verfahren, LS-DE) und Partikel-Schwarm Optimierung (PSO) die besten Ergebnisse. Für die gegebene maximale Temperaturänderung im Untergrund (2,5 K) können optimierte Lösungen beträchtliche Energieextraktionsraten erreichen. Die in der Praxis übliche EWS-Planung kann im Vergleich zu den optimierten EWS-Feldern nur 33% der Energieextraktion erreichen.

Abstract

Vertical ground source heat pump systems have been established as the preferred geothermal technology for providing space heating and cooling to both small and large buildings. This technology utilizes shallow geothermal energy by extracting or injecting heat through a borehole heat exchanger (BHE). In large-scale applications, heat transfer is accomplished by using a field of multiple BHEs. Standard design practices for large-scale applications are based on equal operation of the BHEs. Moreover, groundwater often influences the thermal transport in the ground, but it is rarely considered. In the presented work, the potential of individual adjustment of BHEs for different hydro-geothermal conditions is investigated. Special attention is given to the subsurface temperature changes exerted by the operation of the BHEs. The main question is whether the concerted energy extraction of multiple BHEs can be improved, and how. For tackling this question, two simulation-optimization procedures are developed. The first procedure uses superimposed analytical models to simulate ground temperature impacts from operating multiple adjacent BHEs. The predictions of the models are used to evaluate an objective function to optimize individual BHE operation in the field. This is solved within a linear programming framework. Two real-case oriented application cases for heating energy supply are considered. In the first application case, the presence of groundwater flow is neglected, while for the second case, various groundwater flow regimes are considered. Temperature distributions from optimized and non-optimized BHEs, for given operation times, are then compared by comprehensive numerical models. In general, optimized BHEs can reduce the thermal impact, and extreme local cooling can be avoided. In the purely conductive case, the maximum ground temperature change is decreased by 18% compared to the non-optimized field. For the advection-dominated cases, even when flowing groundwater balances local anomalies, the temperature changes in the optimized field are always smaller. Also, the temperature of the circulating heat carrier fluid within the optimized

BHEs can be increased by 1°C, which is favourable for improving the heat pump performance. In addition, the optimal adjustment of the boreholes produces characteristic load patterns that depend on time and groundwater flow velocity. The second simulation-optimization approach couples heat transport numerical simulation of geothermal systems with heuristic optimization algorithms. The performance of three evolutionary algorithms (each with 2 variants) is tested for maximizing the total energy extraction of BHE fields installed in a heterogeneous aquifer. In addition, an optimal positioning scheme of the BHEs within a predefined area is inquired. Among the evaluated algorithms, Differential Evolution (with line search, LS-DE) and Particle Swarm Optimization (PSO) perform best. For the given maximum temperature change in the subsurface (2.5 K) optimized solutions can reach substantial energy extraction rates. In comparison, BHE application according to standard planning practice can only reach 33% of the energy extraction of the optimized field.

1. Introduction

1.1 Background

Geothermal technologies play an important role in fulfilling energy safety, economic growth and climate change mitigation (IEA, 2011). These technologies make use of the heat stored in solids and fluids in the subsurface for a large variety of application such as: electricity generation, space heating and cooling, and bathing, among others. For electricity generation, high-temperature (high-enthalpy) geothermal resources are needed (>150°C), while for space heating and other direct-use applications, intermediate- to low-temperature resources are sufficient (<150°C). In particular, low-enthalpy geothermal systems, commonly used for heating and cooling of buildings, operate at much lower temperatures (<32°C) (ASHRAE, 1995). The use of low-temperature geothermal energy is beneficial since it is available everywhere, it is, to some extent, renewable, and is often economically superior to application of alternative technologies (Nagano et al., 2006; Blum et al., 2010; Rybach, 2010).

The subsurface temperature regime is usually very stable, and only close to surface water bodies and at the upper boundary to the atmosphere, seasonal dynamics can be observed that are reflected by temperature variations of more than 1°C. Low-enthalpy geothermal systems (i.e., shallow geothermal systems) make use of this stable energy source to provide heating and cooling to small and large facilities. Among direct-use applications, shallow geothermal technologies have the highest energy usage (49%) and the highest increment rate on energy utilization, estimated at 20% for the last fifteen years (Lund et al., 2010). At the end of 2009, the number of installed systems worldwide was about 2.94 million. This estimation includes small and large systems with installed capacities ranging between 5.5 kW to 150 kW. In Europe, for 2011 more than 1 million installations are reported (Bayer et al., 2012).

Different types of shallow geothermal systems are available. The most common ones are the ground source heat pump systems (GSHP) or closed-loop systems, and the groundwater heat

pump systems (GWHP) or open-loop systems (Figure 1-1). GSHP systems tap the geothermal energy, using a synthetic circulating fluid (heat carrier) within a pipe system installed vertically or horizontally in the ground. This pipe system is called a borehole heat exchanger (BHE) and is connected to a heat pump installed aboveground. The heat pump decreases the temperature of the heat carrier fluid and accumulates the extracted energy for running the in-house heating system. During this process, the heat pump also consumes energy, e.g. for an electricity driven compressor. The closed geothermal system can be used in reversed mode to provide cooling as well. Here, the ground is used as a temperature sink of the heat collected in a building.

GWHP systems apply the groundwater directly as heat carrier fluid. In the popular doublet system, a groundwater production well and an injection well are implemented. Further applications of shallow geothermal technologies are the underground thermal energy storage systems (UTES), standing column well systems and pile systems. These systems, essentially, are modifications of the two aforementioned basic variants. Besides specific advantages of each technological alternative, the GSHP system has been established as the preferable choice, representing about 80% of the worldwide installed units (Lund, personal communication).

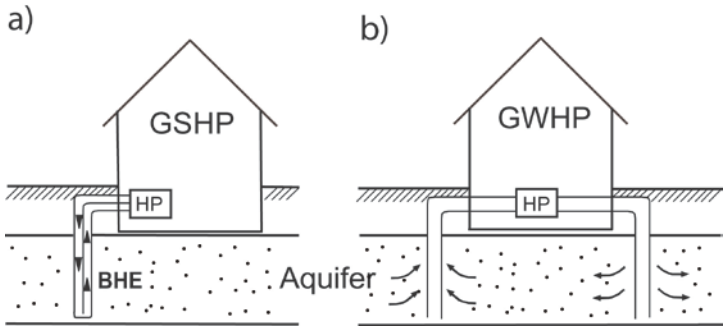

Figure 1-1. Description of shallow geothermal system. a) Ground Source Heat Pump (GSHP) with a vertical Borehole Heat Exchanger (BHE) and b) Ground Water Heat Pump (GWHP) with the doublet system. HP corresponds to the Heat Pump (modified from Hecht-Méndez et al., 2010).

GSHP systems should be properly sized in order to fulfill a certain energy demand. This is usually done by standard technical guidelines, as for instance, the Design and Installation

Standards of the International Ground Source Heat Pump Association (IGSHPA, 1991), the German Guidelines for Thermal Use of the Underground (VDI, 2001) or the Handbook of Application from the American Society of Heating, Refrigerating and Air-Conditioning Engineers (ASHRAE, 2007). The total energy demand of a given facility is estimated based on the energetic consumption of the facility itself and the climatic conditions where it is located. This delivers an energy load profile (commonly daily or monthly). The total length of the BHE loop is then oriented at the total energy demand. For instance, for small applications (heat pump with installed capacity from 5.5 kW to 12 kW), one or two BHEs with lengths ranging between 50-150 m are sufficient (assuming an energy extraction rate from the underground of about 50 W m^{-1}). For larger buildings or district heating systems (>12 kW) the use of multiple BHEs, often with a total length of hundreds of meters, is necessary.

Due to technical and/or legal reasons, BHEs in Germany are typically installed down to a maximum of 100 meters (Haehnlein et al., 2010). Therefore depending on available space, the total energy demand is fulfilled by using square arrays or longitudinal lattices of BHEs (Fujii et al., 2005; Katsura et al., 2008; Katsura et al., 2009). In practice, the operation of multiple BHEs is accomplished by using each BHE equally, i.e. the total heat carrier fluid flow rate is uniformly distributed among all BHEs. In addition, on-off cycles of the GSHP system affect all boreholes simultaneously. The design of small and large systems has traditionally been done by following such operative schemes, disregarding the possibility of regulating each borehole independently. Another common assumption in current GSHP system design is that groundwater flow is absent. Consequently, the potential contribution of moving groundwater to subsurface heat transport is neglected. However, BHEs are often installed in aquifers. Aquifers are geologic formations that contain and allow for the movement of significant amounts of water. They can occur at various depths and their dimensions can vary from a few centimeters to large ranges of meters. Groundwater flow velocities can vary by several orders of magnitude depending on the permeability of the aquifer matrix. Since the hydraulic

characteristics of aquifers are relevant for heat transport and are spatially variable, they should be well understood and should also be included at the design stage of a shallow geothermal system.

1.2 Subsurface heat transport simulation of shallow geothermal systems

Heat transport in water saturated porous media is – with some simplification - analogous to the transport of solutes (de Marsily, 1986; Häfner et al., 1992). This is based on the principle of heat conservation, which resembles the mass balance in solute transport, and by assuming an instantaneous thermal equilibrium between the solid and fluid. Accordingly, both phenomena are described by the same governing equation, namely the Advection-Dispersion Equation.

Two main heat transport mechanisms in porous media are distinguished: heat transfer due to temperature gradients or conductive heat transport, and heat transfer due to the moving groundwater or convective heat transfer. During conduction, the heat moves from high temperature to low temperature regions, through both the solids and the fluids contained in the total pore volume. In contrast, convective heat transport occurs only in the fluid phase and it refers to the transport of heat driven by a fluid moving at a certain velocity (Häfner et al., 1992). In the present study, fluid motion, or groundwater movement, solely occurs as a response to pressure gradients (i.e. absence of density gradients).

When GSHP systems are operated, a thermal anomaly (thermal plume) is induced in the ground by the energy extracted or injected through the BHE(s). Since BHEs are very long, for example, in comparison to wells, they are often described as line sources. Often, the temperature distribution around these line sources is vertically integrated, and for simplification, only a two-dimensional, projected thermal plume is inspected (e.g. Sutton et al., 2003; Diao et al., 2004; Metzger et al., 2004; Marcotte et al., 2010; Molina-Giraldo et al., 2011a). In the absence of groundwater flow, a concentric (projected) thermal plume develops

around a single BHE. In the case of multiple boreholes, the temperature change underground is larger due to the mutual thermal interaction between adjacent BHEs and mitigated lateral conductive heat supply. Groundwater flow elongates the thermal plume in the downgradient flow direction, resulting in an extended cigar-shaped plume (Rybach and Monguillo, 2006).

Subsurface temperature changes due to shallow geothermal systems can be predicted by analytical or numerical models. Classical analytical equations developed for heat transport in porous media can be used for estimating the temperature response of the ground due to an infinite or finite line source/sink as in the case of BHEs (Carslaw and Jaeger, 1959; Zeng et al. 2002). An important assumption behind these analytical equations is that the thermal and hydraulic parameters of the involved materials are independent of the temperature. An advantage of using analytical solutions is that spatially and temporally variable ground temperatures can be efficiently approximated. Since BHE systems are often in contact with aquifers, the use of analytical solutions that include convective heat transport, as for instance the moving infinite (finite) line source model (Sutton et al., 2003; Diao et al., 2004; Metzger et al., 2004; Molina-Giraldo et al., 2011a; Molina-Giraldo et al., 2011b), is desirable. Various analytical solutions have been used for dimensioning BHEs (Xu and Spliter, 2006). Due to their robustness, straightforward applicability and the short calculation time, analytical equations are appealing for BHE planning and iterative optimization. However, since they are only applicable for homogeneous conditions, heterogeneities of the thermal and hydraulic parameters cannot be assessed by these approaches.

An apparent limitation is that they were originally developed for a single source or sink. Nevertheless, based on the fact that energy is an extensive and additive variable, this limitation can be overcome using the superposition principle (Diao et al., 2004; Marcotte et al., 2010). The temperature, as calculated by these analytical approaches, depends linearly on the BHE energy load. Based on this linearity, the principle of superposition can be applied: The temperature differences caused by individual BHEs can be added together in order to

obtain the overall temperature field for multiple BHEs. In addition, although the analytical solutions were originally developed for a constant heat extraction/injection rate or constant load, time dependent heat pulses can also be superimposed (Bernier and Randriamiarinjatovo, 2001; Bernier et al., 2004; Marcotte and Pasquier, 2008; Michopoulos and Kyriakis, 2009; Marcotte et al., 2010; Michopoulos and Kyriakis, 2010). Consequently, the temperature change at any location in the vicinity of a single BHE or a BHE field with time variable energy loads can be calculated.

As an alternative to analytical equations, computer-based numerical models can be used for heat transport simulation in homogenous and heterogeneous porous media. Several models based on finite-elements, finite-differences or finite-volumes are currently available. In general, numerical heat transport models have been widely used for the design of BHEs, regional heat transport modeling, seasonal aquifer thermal energy storage and technical-economic system design (Tsang et al., 1981; Chiasson et al., 2000; Schmidt and Hellström, 2005). The development of numerical codes for heat and solute transport has been closely related to the advent of more powerful computers. In the early stage of numerical simulation, only simple, one-dimensional problems were inspected while, today, more complicated problems with complex boundary conditions can be efficiently handled (Anderson, 2009). Available heat transport simulation codes allow for simulating one, two, and three-dimensional problems.

In the many numerical models that account for groundwater flow, the coupling of the fluid flow simulation and the heat transport calculation is done by means of Darcy´s velocity. As it is common in the analytical equations for BHE simulation, some numerical codes do not consider temperature dependencies of the hydraulic and thermal parameters (e.g. MODFLOW/MT3DMS, TRADIKON3D). Other codes take into account this aspect and include other features, such as chemical processes or mechanical deformation (e.g. FEFLOW, SHEMAT, BASI2, FRACture, ROCKFLOW/GeoSys). Since the temperature differences

from the BHE induced thermal plumes commonly reach only a few Kelvin (<10 K) and the installation of BHEs are in the upper part of the subsurface using a closed pipe, however, chemical or mechanical processes are typically not of concern for BHE simulation.

Ideally, numerical models couple the heat transport inside the BHE and the transport in the aquifer. However this is rarely done and computationally demanding. Since the overall performance of a GSHP system depends on the temperature of the circulating fluid, it represents a fundamental parameter for design of GSHP systems (Bernier, 2006). For approximating the temperature of the circulating fluid, semi-analytical approaches, as for instance the g-functions (Eskilson, 1987), are available. These functions are implemented in semi-analytical codes such as SBM, EED, GHLPRO and TRNSYS-DST (Eskilson, 1986; Hellström et al., 1996; Hellstrom and Sanner, 1997; Spliter, 2000). However, these codes still have limitations: they can only handle pure conductive underground conditions (no groundwater flow), assume an equal operation of the BHEs in multiple arrays and are restricted to a number of fixed geometrical arrays of multiple BHEs.

1.3 Optimization of shallow geothermal systems

Optimization is any systematic procedure that, by means of quantitative methods, provides an optimal solution or an approximation of a given problem (Littger, 1992). The problem must be initially described by a mathematical model, in which some objective, the variables and the constraints (if exist) are identified. The objective should be a quantitative measure of the performance of the target system, which, at the same time, depends on important characteristics of the system and is quantified by variables. The constraints represent limiting aspects of the variables (Nocedal and Wright, 1999).

A mathematical definition of optimization is to find the best (optimal) solution from a given set of possible solutions (i.e. the search space) that minimizes or maximizes a function, the objective function (OF), which is subject to certain constraints on its variables (Nocedal and

Wright, 1999). In the last decades, several optimization algorithms have been developed based on: the characteristics of the OF, the search space size and the expected optimal solution (global solution or an approximation of it that meets a prescribed criterion).

Various computer-based optimization methodologies have been applied for improving technical and economic aspects of shallow geothermal systems (Zhao et al., 2003; Höfker et al., 2007; Zogou and Stamatelos, 2007; Dickinson et al., 2009; Sanaye and Niroomand, 2009; Sayyaadi et al., 2009; Kjellsson et al., 2010; Kranz and Bartels, 2010). In general, these procedures aim at both saving installation and operational costs, or they intend to find optimum operation strategies for a given geothermal system. For the first task, the optimization attempts to minimize the overall cost of the system based on: 1) the analysis of integral components, as for instance, heat pump condenser and evaporator, heat exchanger sizing, or 2) through rescheduling the heat pump operational time. For the second task, in order to predict an ideal operation strategy, analyses of yearly, monthly or even daily energy extraction/injection rates (loads), as well as assessments of the input and output temperature at some components of the system, are part for the optimization procedure. Zhao et al. (2003) use a variable metric algorithm for finding an optimal design method for geothermal open systems. The optimization procedure attempts to minimize total costs per unit time and for investment costs for a predefined system.

Examples for operation strategy optimization are presented by Wall (1991), Höfker et al. (2007), and Kranz and Bartels (2010). Wall (1991) uses the Lagrange multipliers method for optimizing heat pump components design, defining the problem by a thermoeconomics analysis. The thermoeconomics analysis is a comprehensive and frequently used assessment that simultaneously combines both economic and technical aspects of a thermal system (Bejan et al. 1996). In Wall's investigation, it is determined that some components of the heat pump, such as the expansion valve and the electric motor, must be further developed in order to obtain an optimal system. Höfker et al. (2007) predict required heating loads for various

building energy demands, categorized by the end-user type. In this work, stationary heat transport building simulations are linked with geothermal simulation, to determine heating loads for the buildings and the size of the BHE. Kranz and Bartels (2010) assess the heat recovery factor of an Aquifer Thermal Energy Storage (ATES) incorporated at the German Parliament Building. By means of numerical simulations, they found out that in order to enhance the operation of the system, the temperatures at the production and injection wells must be reconsidered.

The reported optimization methods are mainly applied to either components of the on-the-surface system or to GWHP systems (open-loop). In contrast, there are only a few applications of optimization methods to GSHP systems. These will be reviewed in more detail in the following.

Sanaye and Niroomand (2009) apply thermal simulations of BHE's and the Nelder-Mead method for finding optimal design parameters for GSHP systems. Results of the Nelder-Mead method are then validated using real-coded standard genetic algorithms. The OF is based on the total annual costs of the geothermal system, i.e. the annual cost of power consumption and capital investment. For given design and system operation parameters, input and output temperatures of the BHE and the heat pump are predicted. These are used to constrain the temperature for the circulating heat carrier fluid. For a base case, most favorable BHE parameters, such as inlet and outlet temperature of the groundwater source, pipe diameter, depth and number of boreholes, are predicted. Also, optimal parameters for the heat pumps (saturated temperature and pressure of condenser and evaporator) are calculated. In addition, optimization of the geothermal system for seven scenarios with different climates and soil types is performed. For the base case, the differences between the Nelder-Mead and the genetic algorithm results are lower than 0.52% for the total annual costs and 3.2% for the design parameter values.

Sayyaadi et al. (2009) present three optimization procedures: 1) thermodynamic single objective, 2) thermoeconomic single objective and 3) multi-objective optimization, to vertical GSHP systems. The first and second approaches aim at minimizing the total irreversibility of the GSHP system and the total cost of the system, respectively. The multi-objective optimization considers, simultaneously, both thermodynamic and thermoeconomic aspects. Two OFs (defined for the optimization procedures 1 and 2) are defined. Moreover, eight decision variables and ten constraints are formulated. The optimization is done via a real-coded evolution strategy. They show that using thermodynamic criteria provides an optimal system set up with higher exergetic efficiencies and performance, but at the expense of higher costs. In contrast, thermoeconomic optimization offers a system configuration with lower expenses, although some freedom is given to the thermodynamic behavior of the system. In comparison, the multi-objective optimization produces more balanced results between both single objective approaches.

The few previous studies on the optimization of GSHP systems mainly focus on the design of physical components of the systems and economic benefits. However, the time-dependent evolution of thermal plumes, which plays a substantial role for the efficiency of a heat-pump-based system, is not included. In the present study, two different mathematical models are used for the description of the ground temperature changes due to multiple BHE operations. In the first model, the subsurface temperature changes due to a GSHP system is simulated by superimposed analytical solutions. By this, the ground is regarded as homogeneous medium and the primary objective is minimizing the induced temperature change in the ground. Since the mathematical model is based on analytical solutions, linear programming is selected for solving the optimization problem. In the second model, the ground temperature change, from BHE operation in a heterogeneous aquifer, is simulated using a numerical code. In the presented application case, the objectives are to maximize the total energy extraction of a GSHP system and to optimally position a given number of BHEs to fulfill a given heating

energy demand. Due to the non-linearity and potential non-convexity of the objective function, Evolutionary Algorithms are applied. In the following, linear programming and heuristic optimization methods, such as Evolutionary Algorithms, are shortly compared.

Linear Programming (LP) algorithms deal with optimization problems, in which the objective function is a linear function subjected to linear constraints on the variables. This type of optimization is a subset of the class of problems known as combinatorial optimization (Pardalos and Resende, 2002). The search space of possible solutions of combinatorial problems is finite, however, it can be of exponential size. Therefore, several algorithms for combinatorial optimization problems have been developed. In LP, two techniques are most common: Simplex-Type algorithms and Interior-Point Methods. An advantage of LP is that it has a convex search space and therefore, the optimal solution attained, always corresponds to a global solution.

Evolutionary Algorithms (EA) belong to the so-called heuristic optimization techniques (Pardalos and Resende, 2002). They are iterative procedures and mainly applied to search for optimal solutions of complex non-convex problems (commonly, combinatorial optimization problems). The population-based EAs are inspired by the natural selection process of the biological evolution. Initially, a set of (mostly) randomly generated individuals, which represent possible solutions of a given problem, are evaluated using a fitness function (evaluation). Only the fittest individuals are then selected as parents for the next population (reproduction) and are then modified by two different operators: mutation, and recombination. An important feature of these algorithms is the possibility to evaluate several possible solutions for a given problem simultaneously. The major differences between EAs and other traditional optimization techniques are that: 1) they often use a coding for the variables instead of the variables themselves (e.g. binary genetic algorithms), 2) they search from a population of points, not from a single point, 3) additional information, as well as derivative rules, are not necessary and, 4) they mostly apply stochastic transition rules (Goldberg, 1953).

As a consequence, the versatile heuristics are often the best choice for potentially non-convex and complex (e.g. noisy, with data gaps) problems. However, in contrast to linear programming, they are much more computationally demanding.

1.4 Research questions

The present study aims to answer the following research questions:

1. Can the energy extraction of a GSHP system, using multiple BHEs, be optimized by establishing certain temperature constraints in the underground?

2. Based on the assumption that superimposed analytical solutions are a valid approach for predicting the ground temperature changes due to closed-loop shallow geothermal systems, can the energy extraction of an array of BHEs be formulated and efficiently be solved in a linear programming framework?

3. How is the influence of different groundwater flow conditions on the optimal energy extraction strategy of a GSHP system with multiple BHEs?

4. Considering that hydraulic and thermal parameters of the ground are temperature independent, as commonly assumed for the simulation of GSHP systems, can a temperature independent solute transport numerical code be applied for modeling thermal plumes induced by BHEs?

5. Is it possible to optimize the energy extraction of multiple BHEs and their localization considering a heterogeneous ground by using numerical models coupled to heuristic optimization algorithms?

1.5 Thesis outline

Results from the investigations carried out throughout this PhD thesis are subdivided in four chapters. Each chapter corresponds to individual manuscripts that are already published (Chapters 2, 4 and 5) or currently under review (Chapter 3).

The second Chapter of this thesis presents the development of an innovative simulation-optimization procedure for BHE fields using a classical analytical solution for heat transport in saturated porous media (Carslaw and Jaeger, 1959) in a purely conductive scenario (no groundwater flow). Additionally, the temperatures of the circulating fluid within the pipes are simulated using a semi-analytical modeling code. Based on spatial and temporal superposition of infinite line sources, which represent the BHEs, a linear program is formulated to calculate optimal energy extraction rates for multiple BHEs. The objective function is oriented at minimizing the maximum temperature change in the ground. The LP-based optimization procedure is tested for a base case, represented by a GSHP system with 25 BHEs. Typical monthly energy demands for buildings in Central Europe are defined. Finally, the thermal conditions, after 30 years of operation, using energy extractions, predicted by the optimization approach, are contrasted to those from standard system operation.

In Chapter 3, the capabilities of the simulation-optimization procedure developed in the previous chapter are extended for situations in which the presence of groundwater flow cannot be neglected. This is done by replacing the analytical solution used in the optimization procedure by an analytical equation based on the moving infinite line source theory (Metzger et al., 2003). This way, the beneficial effect of convective heat transport in aquifers, as demonstrated in previous studies, is incorporated in the BHE field optimization approach. The same configuration of the GSHP system is used as in the model described in Chapter 2, however, for this work, 15 scenarios with different groundwater flow regimes are considered. The scenarios are defined in order to cover different heat transport conditions, varying from

conductive dominated to convective dominated. For the optimized solutions, the ground temperature distributions, as well as the temperature of the circulating fluid, are simulated in detail by a finite-element numerical code.

In Chapter 4, focus is set on the assessment of a solute transport numerical code (MT3DMS) for heat transport simulation of shallow geothermal systems. Here, the mathematical analogy between the governing equations of solute, heat transport is considered and the temperature dependencies of hydraulic and thermal parameters are neglected. The main goal of this work is to demonstrate the applicability of the solute transport model for heat transport simulation for common operational conditions of GSHP systems. Thermal plume simulations of two- and three-dimensional scenarios for different groundwater flow velocities are performed. The results are compared with analytical solutions for heat and solute transport in saturated porous media. The presented feasible application of MT3DMS for heat transport simulation of closed-loop geothermal systems lays the groundwork for the development of the optimization approach presented in Chapter 5.

In the last Chapter of this study, a new simulation-optimization approach is developed for optimizing the energy extraction rates and the positioning of multiple BHEs of a GSHP system, considering a heterogeneous ground. An iterative simulation-optimization approach is implemented using MT3DMS and five different evolutionary algorithms combined with a line search procedure. After determining the groundwater flow field (by MODFLOW 2000) with a given hydraulic conductivity distribution, heat transport simulations are performed for candidate solutions. In this approach, the maximum temperature change of the ground is defined as optimization criterion in order to comply with potential environmental concerns (Hähnlein et al., 2010). The performance of the evolutionary algorithms and the suggested optimal solutions are compared.

1.6 References

Anderson, M.P., 2009. The Evolution of Ground Water. Ground Water 47, 469-469.

ASHRAE, HVAC Applications, in: ASHRAE Handbook, American Society of Heating, Refrigeration and Air-Conditioning Engineers, Atlanta, 1995.

ASHRAE, Geothermal Energy, in: Handbook of Applications, chapter 32, American Society of Heating, Refrigeration and Air-Conditioning Engineers, Atlanta, 2007.

Bayer, P., Saner, D., Bolay, S., Rybach, L., Blum, P., 2012. Greenhouse gas emission savings of ground source heat pump systems in Europe: A Review, Renewable and Sustainable Energy Reviews 16, 1256-1267.

Bejan, A., Tsatsaronis, G., Moran, M., 1996. Thermal Design and Optimization, John Wiley & Sons, Inc., New York.

Bernier, M., 2006. Closed-loop ground-coupled heat pump systems. ASHRAE Journal 48, 12-19.

Bernier, M., Randriamiarinjatovo, D., Annual simulations of heat pump systems with vertical ground heat exchangers, in: eSim2001-The Canadian conference on building energy simulation, Ottawa, 2001, pp. 8.

Bernier, M.A., Pinel, P., Labib, R., Paillot, R., 2004. A Multiple Load Aggregation Algorithm for Annual Hourly Simulations of GCHP Systems. HVAC & R Research 10, 471-488.

Blum, P., Campillo, G., Münch, W., Kölbel, T., 2010., CO2 savings of ground source heat pump systems - A regional analysis. Renewable Energy 35, 122-127.

Carslaw, H.S., Jäger., J.C., 1959. Conduction of Heat in Solids, 2nd ed., Oxford University Press, New York.

Chiasson, A.C., Rees, S.J., Spliter, J.D., 2000. A preliminary assessment of the effects of ground-water flow on closed-loop ground-source heat pump systems. ASHRAE Transactions 106, 380-393.

de Marsily, G., 1986. Quantitative Hydrogeology, Academic Press, Orlando.

Diao, N., Li, Q., Fang, Z., 2004. Heat transfer in ground heat exchangers with groundwater advection. International Journal of Thermal Sciences 43, 1203-1211.

Dickinson, J., Jackson, T., Matthews, M., Cripps, A., 2009. The economic and environmental optimisation of integrating ground source energy systems into buildings. Energy 34, 2215-2222.

Eskilson, P., 1986. Superposition Borehole Model. Manual for computer code, in: Department of Mathematical Physics, University of Lund, Lund.

Eskilson, P., 1987. Thermal Analysis of Heat Extraction Boreholes, in: Department of Mathematical Physics, University of Lund, Lund.

Fujii, H., Itoi, R., Fujii, J., Uchida, Y., 2005. Optimizing the design of large-scale ground-coupled heat pump systems using groundwater and heat transport modeling. Geothermics 34, 347-364.

Goldberg, D., 1953. Genetic Algorithms in Search, Optimization and Machine Learning, Addison Wesley Longman, Inc., Massachusetts.

Hähnlein, S., Bayer, P., Blum, P., 2010. International legal status of the use of shallow geothermal energy. Renewable and Sustainable Energy Reviews 14, 2611-2625.

Häfner, F., Sames, D., Voigt, H.-D., 1992. Wärme- und Stofftransport, Springer, Heidelberg.

Hecht-Méndez, J., Molina-Giraldo, N., Blum, P., Bayer, P., 2010. Evaluating MT3DMS for heat transport simulation of closed geothermal systems. Ground Water 48, 741-756.

Hellström, G., Mazzarella, L., Pahud, D., 1996. Duct Ground Storage Model – TRNSYS version, Department of Mathematical Physics, University of Lund, Lund.

Hellstrom, G., Sanner, B., 1997. EED – Earth Energy Designer, Version 1.0, User's Manual, Prof. Dr. Knoblich & Partner GmbH, Wetzlar.

Höfker, G., Winkler, K., Bracke, R., 2007. Optimierung geothermischer Energiesysteme am Beispiel eines städtebaulichen Entwicklungsvorhabens. Bauphysik 29, 17-20.

IEA, Tehcnology roadmaps - Geothermal heat and power, in: I.E. Agency (Ed.), Paris, 2011.

IGSHPA, 1991. Design and Installations Standards, International Ground Source Heat Pump Association, Oklahoma.

Katsura, T., Nagano, K., Narita, S., Takeda, S., Nakamura, Y., Okamoto, A., 2009. Calculation algorithm of the temperatures for pipe arrangement of multiple ground heat exchangers. Applied Thermal Engineering 29, 906-919.

Katsura, T., Nagano, K., Takeda, S., 2008. Method of calculation of the ground temperature for multiple ground heat exchangers. Applied Thermal Engineering 28, 1995-2004.

Kjellsson, E., Hellström, G., Perers, B., 2010. Optimization of systems with the combination of ground-source heat pump and solar collectors in dwellings. Energy 35, 2667-2673.

Kranz, S., Bartels, J., 2010. Simulation and data based optimisation of an operational seasonal aquifer thermal energy storage. In: S. University (Ed.), Proceeding of the 2010 World Geothermal Congress. Bali, Indonesia, 25-29 April, pp. 6.

Littger, K., 1992. Optimierung: eine Einführung in rechnergestützte Methoden, Springer, Heidelberg.

Lund, J.W., Freeston, D.H., Boyd, T.L., 2010. Direct Utilization of Geothermal Energy 2010 Worldwide Review. In: S. University (Ed.), Proceeding of the 2010 World Geothermal Congress. Bali, Indonesia, 25-29 April, pp. 23.

Marcotte, D., Pasquier, P., 2008. Fast fluid and ground temperature computation for geothermal ground-loop heat exchanger systems. Geothermics 37, 651-665.

Marcotte, D., Pasquier, P., Sheriff, F., Bernier, M., 2010. The importance of axial effects for borehole design of geothermal heat-pump systems. Renewable Energy 35, 763-770.

Metzger, T., Didierjean, S., Maillet, D., 2004. Optimal experimental estimation of thermal dispersion coefficients in porous media. International Journal of Heat and Mass Transfer 47, 3341-3353.

Michopoulos, A., Kyriakis, N., 2009. A New Energy Analysis Tool for Ground Source Heat Pump Systems. Energy and Buildings 41, 937-941.

Michopoulos, A., Kyriakis, N., 2010. The influence of a vertical ground heat exchanger length on the electricity consumption of the heat pumps. Renewable Energy 35, 1403-1407.

Molina-Giraldo, N., Bayer, P., Blum, P., 2011a. Evaluating the influence of thermal dispersion on temperature plumes from geothermal systems using analytical solutions. International Journal of Thermal Sciences 50, 1223-1231.

Molina-Giraldo, N., Blum, P., Zhu, K., Bayer, P., Fang, Z., 2011b. A moving finite line source model to simulate borehole heat exchangers with groundwater advection. International Journal of Thermal Sciences 50, 2506-2513.

Nagano, K., Katsura, T., Takeda, S., 2006. Development of a design and performance prediction tool for the ground source heat pump system. Applied Thermal Engineering 26, 1578-1592.

Nocedal, J., Wright, S.J., 1999. Numerical Optimization, Springer, New York.

Pardalos, P.M., Resende, M.G.C., 2002. Handbook of Applied Optimization, Oxford University Press, Inc., New York.

Rybach, L.; 2010. Status and Prospects of Geothermal Energy. In: S. University (Ed.), Proceeding of the 2010 World Geothermal Congress. Bali, Indonesia, 25-29 April, pp. 5.

Rybach, L., Monguillo, M., 2006. Geothermal sustainability - A review with identified research needs. Geothermal Resource Council Transactions 30, 1083 - 1090.

Sanaye, S., Niroomand, B., 2009. Thermal-economic modeling and optimization of vertical ground-coupled heat pump. Energy Conversion and Management 50, 1136-1147.

Sayyaadi, H., Amlashi, E.H., Amidpour, M., 2009. Multi-objective optimization of a vertical ground source heat pump using evolutionary algorithm. Energy Conversion and Management 50, 2035-2046.

Schmidt, T., Hellström, G., Ground source cooling - Working paper on usable tools and methods, in, EU Commission SAVE program and Nordic Energy research, 2005, pp. 21.

Spliter, J.D., 2000. GLHEPRO - a design tool for comercial building ground loop heat exchangers. In: (Ed.), Proceesings of 4th international heat pumps in cold climetes conference. Aylmer, 17th-18th August, pp. 15.

Sutton, M.G., Nutter, D.W., Couvillion, R.J., 2003. A ground resistance for vertical bore heat exchangers with groundwater flow. Journal of Energy Resources Technology 125, 183-189.

Tsang, C.F., Buscheck, T., Doughty, C., 1981. Aquifer thermal energy storage: A numerical simulation of Auburn University Field Experiments. Water Resour. Res. 17, 647-658.

VDI, Thermische Nutzung des Untergrundes, teil 2, in: V.D. Ingenieure (Ed.), VDI-Verlag, Düsseldorf, 2001.

Wall, G., 1991. Optimization of refrigeration machinery. International Journal of Refrigeration 14, 336-340.

Xu, X., Spliter, J.D., 2006. Modeling of vertical ground loop heat exchangers with variable convective resistance and thermal mass of the fluid. In: (Ed.), 10th international conference on thermal energy storage – Ecostock. Pomona, NJ, pp. 8.

Zeng, H.Y., Diao, N.R., Fang, Z.H., 2002. A finite line-source model for boreholes in geothermal heat exchangers. Heat Transfer − Asian Research 31, 558-567.

Zhao, Y., Shigang, Z., Xun, L., 2003. Cost-effective optimal design of groundwater source heat pumps. Applied Thermal Engineering 23, 1595-1603.

Zogou, O., Stamatelos, A., 2007. Optimization of thermal performance of a building with ground source heat pump system. Energy Conversion and Management 48, 2853-2863.

2. Optimization of energy extraction for closed shallow geothermal systems using linear programming[1]

Abstract: The objective of the study is to optimize the performance and thereby to mitigate the environmental impact of ground source heat pump (GSHP) systems using multiple borehole heat exchangers (BHEs) by including variable energy loads. Hence, an optimization procedure is developed that is able to predict temperature distributions in the subsurface. Optimized BHE fields are able to keep the maximum temperature change in the subsurface about 18% lower than BHE fields which feature equal flow rates for all BHEs. Thus, the long-term temperature anomaly can be mitigated and the possibility of extracting a higher amount of energy, while keeping temperature thresholds or environmental constraints, arises.

[1] Reproduced from: de Paly, M., Hecht-Méndez, J., Beck, M., Blum, P., Zell, A., Bayer, P., 2012. Optimization of energy extraction for closed shallow geothermal systems using linear programming. Geothermics 43, 57-65.

2.1 Introduction

Shallow geothermal technologies that directly use the heat stored in the subsurface are counted among the most sustainable choices for space heating (Rybach and Mongillo, 2006; Saner et al., 2010). Depending on the supplied primary energy for the heat pumps and the efficiency of installation CO_2 can be avoided or even reduced (Nagano et al., 2006; Blum et al., 2010). In areas of normal or low geothermal gradient, heat pumps can be applied to extract the energy from depths down to about 400 m. Most often, closed or ground-coupled systems such as ground source heat pump (GSHP) systems are used (Lund et al., 2010). Depending on the heating demand, one or several vertical borehole exchangers (BHEs) are typically installed in the ground. The system is operated by circulating a heat carrier fluid in the BHEs, which exchanges heat with the ground and feeds an indoor heat pump. Even if shallow subsurface energy resources are enormous, local extraction causes temperature anomalies (Philippe et al., 2009; Hecht-Méndez et al., 2010). Natural heat conduction automatically balances these anomalies (Signorelli et al., 2004). However, replenishment needs time and hence the ground temperature should not be altered significantly. Ideally GSHP systems are run in seasonal mode, so that summer break is available for progressive replenishment of the energy deficit (Rybach and Eugster, 2010).

In order to ensure a lifetime of decades, it is crucial to configure the BHEs appropriately. This means that during the heating period the commonly rather low temperature of the ground should only be decreased by a few degrees. This condition is also necessary to maximize the performance of the heat pump, which is most efficient when the temperature increment between heat source and receiver is diminutive (e.g., Esen et al., 2008). In addition to technical issues environmental concerns might play a role such as the leakage of anti-freeze liquids used in BHEs (Klotzbücher et al., 2007; Saner et al., 2010) or the impact on the groundwater ecosystem by temperature changes (Brielmann et al., 2009, 2011). Sometimes

artificial temperature changes are also regulated (Haehnlein et al. 2010). For example, in the state capital of Stuttgart in South Germany, the impact on the groundwater temperature in a distance of 50 m from a ground heat exchanger should be ≤ 2 K and for larger GSHP systems (> 10 BHEs) a temperature monitoring is often required by the environmental authorities (Amt für Umweltschutz, 2005). Hence, it is desirable to mitigate the thermal impact of such systems on the subsurface and groundwater.

Appropriate configuration of single and multiple BHEs usually follows standardized recipes and apposite planning software such as Earth Energy Designer (EED), Transient System Simulation Program with the Duct Ground Storage model (TRNSYS-DST) and other programs are available (Schmidt and Hellström, 2005; Nagano et al., 2006). For technical or legal reasons, BHEs commonly are not implemented deeper than a few hundreds of meters (Haehnlein et al., 2010). If a single BHE is not sufficient to supply the energy required for a specific case, BHE fields are constructed, and the total BHE length is oriented at the total energy demand. Depending on the specific case and available space, simple geometric arrangements such as square or longitudinal lattices are commonly selected (Fujii et al., 2005; Katsura et al., 2008; Katsura et al., 2009). Usually, a distance of a few meters is considered sufficient to minimize mutual interference of adjacent BHEs, for example, from 3 m in China and up to 10 m in Germany (Kavanaugh and Rafferty, 1997; Signorelli et al., 2004, Haehnlein et al. 2010). BHE fields cause regional temperature anomalies, and projected to the surface these large scale temperature anomalies are composed of an array of tens to hundreds of concentric or elliptic temperature plumes that evolve around the BHEs. The larger the BHE field is the less effective the natural lateral conductive heat supply is, so that often the temperature within the field successively declines (Signorelli et al., 2004; Lazzari et al., 2010). Seasonal energy use in heating dominated operation is then reflected by periodic temperature variations that have a long-term decreasing trend (Diao et al., 2010).

Accordingly, for a certain expected lifetime of a BHE field the final minimal ground temperature represents a crucial planning criterion. Thus, the aim is to keep the temperature decrease in the subsurface minimal while maximizing the technological performance of the BHEs.

In the present study, we identify thus far unconsidered degrees of freedom when planning BHE fields in conduction dominated media. In order to improve the concerted performance of multiple adjacent BHEs, the task is formulated as a mathematical optimization problem that is based on simulated superimposed BHE fields. Special attention is set on the heat transfer rates between the underground and the multiple BHEs that supply seasonal energy demands. Temperature changes in the underground exerted by multiple adjacent BHEs that operate with variable energy loads in heating mode are simulated. The temperature distribution in the underground can be predicted by numerical modeling (e.g., Bauer et al. 2011) or by spatial superposition of the infinite line source analytical solution (Carslaw and Jaeger, 1959). The time-dependent BHE-specific workloads are subdivided into step pulses and also superimposed (temporal superposition). An ideal energy extraction strategy is sought that takes into account the temperature changes in the underground and the time dependent heating demand. The optimal strategy supplies an effective input temperature to the heat pump and, therefore, is expected to improve the overall technical efficiency of the system compared to standard practice. Furthermore, the ideal solution should also guarantee lowest environmental impacts in the underground, i.e. aquifer temperatures should not be changed according to a pre-defined criterion or defined temperature limits and thresholds (Haehnlein et al., 2010).

Similar to previous work (e.g. Li et al., 2006; Katsura et al., 2008; Li et al., 2009; Lazzari et al., 2010), we focus on optimization of BHE workloads (i.e., heat extraction rates). For example, Gao et al. (2010) present an operational strategy based on intermittent control of two

BHEs; similarly, Cui et al. (2001) use discontinuous loads for the long-term operation of BHEs. While BHE specific loads can easily be simulated with the line source model, they do not exactly represent the real conditions in practice. In order to achieve a pre-defined load by an operating BHE, a control system that could, for example, adjust the flow rates of the heat carrier fluid would be necessary. Therefore, it is more common in practical applications to use equal flow rates for all BHEs, and by this, to indirectly obtain apposite BHE-specific energy extraction rates. Local low-temperature anomalies in the BHE field automatically lead to a smaller local energy extraction. Accordingly, in the well-established BHE designing tools EED (Hellström and Sanner, 1997), and GLHEPRO (Spitler, 2000) the volumetric flow rate per borehole is uniformly distributed by the number of BHEs. A constant volumetric flow rate of the heat carrier can also be found in analytical and numerical simulation studies or performance investigations of multiple BHE (Urchueguía et al., 2008; Katsura et al., 2009).

In the following, we will exploit the attractive properties from the analytical line source equation and, as a surrogate for flow rates, optimize BHE workloads in the field. The optimized solutions obtained by this proxy will be compared to standard practice, operating at equal flows and loads. The question is, even if flow regulation is not implicitly addressed in the mathematical formulation of the optimization problem, can the identified degrees of freedom be used to further improve BHE field design? To answer this question, the optimized results are compared to a BHE field implementation, in which a separate regulation of BHEs is not considered. Simulations by the Superposition Borehole Model (SBM, Eskilson, 1986; Pahud et al., 1996), which is able to compute underground and circulating fluid temperatures using the flow rates within the pipes, serve as a reference for the comparison.

2.2 Mathematical background

Symbol	Variable	Unit
COP	coefficient of performance of the heat pump	[-]
E_l	total energy demand for each time step	[W]
Ei	exponential integral	[-]
EWT	entering water temperature	[K]
i	coordinate in the *x*-direction in field coordinates	[m]
j	coordinate in the *y*-direction in field coordinates	[m]
L	length of the BHE	[m]
q	power demand/load	[W]
R_b	thermal resistance of the borehole	[m K W^{-1}]
T	temperature at the BHE location	[K]
T_b	temperature at the borehole wall	[K]
T_u	undisturbed temperature of the porous media	[K]
t	time	[s]
x_k	coordinate of BHE *k* in the *x*-direction	[m]
y_k	coordinate of BHE *k* in the *y*-direction	[m]
z	virtual variable	[-]
w	weighting factor	[-]
λ	thermal conductivity of the porous media	[W m^{-1} K^{-1}]
α	thermal diffusivity	[m^2 s^{-1}]
ω	response factor	[-]
k	running index of BHEs	[-]
l	running index of timesteps	[-]
m	number of timesteps	[-]
n	number of BHEs	[-]

2.2.1 Conductive heat transport in porous media (superposition principle)

A common approach for calculating two-dimensional (2-D) radial temperature distribution in the underground due to the presence of a vertical BHE is the infinite line source model (Carslaw and Jaeger, 1959). Assuming an infinite homogeneous underground and a given energy transfer rate per unit length of the borehole, the temperature change ($\Delta T = T_u - T$) caused by a single BHE with load q and with T_u as the undisturbed temperature of the underground for a certain time (t) is expressed as:

$$\Delta T(\Delta x, \Delta y, t, q) = \frac{q}{4\pi L \lambda} Ei\left[\frac{\left(\Delta x^2 + \Delta y^2\right)^{0.5}}{4\alpha t}\right] \tag{2-1}$$

Ei is the so-called exponential integral, $\Delta x = (i - x_k)$ and $\Delta y = (j - y_k)$ are the distances to an arbitrary location (i,j) with respect to a BHE centered at (x_k,y_k), α is the thermal diffusivity and λ is the bulk thermal conductivity.

With the assumption that the soil thermal properties do not depend on temperature, i.e., Eq. (2-1) is linear with respect to q and, due to the fact that energy is an extensive and additive variable (Hellström, 1991; Yavuzturk et al., 1999; Diao et al., 2004; Michopoulos and Kyriakis, 2009; Marcotte et al., 2010), the superposition principle can be applied to Eq. (2-1) as:

$$\Delta T_{i,j}(t, q_{k=1\ldots n}) = \sum_{k=1}^{n} \Delta T_k \left(i - x_k, j - y_k, t, q_k\right) \tag{2-2}$$

where n is the number of BHEs and T_k is the temperature change at (i,j) due to BHE k with an energy transfer rate q_k located at (x_k,y_k). When the workload q varies over time, it can be considered as a series of heating pulses (temporal superposition). This superposition of heat pulses has already been used in various previous works (Eskilson, 1987; Bernier et al., 2004; Marcotte and Pasquier, 2008; Michopoulos and Kyriakis, 2009; Marcotte et al., 2010). The variable energy extraction is subdivided into m time steps with constant load:

$$\Delta T(\Delta x, \Delta y, t, q_{l=1\ldots m}) = \sum_{l=1}^{m} \frac{q_l - q_{l-1}}{4\pi L\lambda} Ei\left[\frac{\left(\Delta x^2 + \Delta y^2\right)^{0.5}}{4\alpha\left(t_m - t_l\right)}\right] \tag{2-3}$$

where m is the total number of time steps and q_l is the load during time step l which runs from t_{l-1} to t_l, with $q_0 = 0$ and $t_0 = 0$.

By combining Eq.s (2-2) and (2-3), the temperature change at any arbitrary location in the subsurface exerted by multiple BHEs each with different time variable energy loads can be estimated through:

$$\Delta T_{i,j}(t, q_{k\ldots n,1\ldots m}) = \sum_{l=1}^{m}\sum_{k=1}^{n} q_{k,l}\,\omega_{k,l}^{t,i,j}(i - x_k, j - y_k) \tag{2-4}$$

With:

$$\omega_{k,l}^{t,i,j}(\Delta x,\Delta y)=\frac{1}{4\pi L\lambda}\left(Ei\left[\frac{\left(\Delta x^2+\Delta y^2\right)^{0.5}}{4\alpha(t-t_{l-1})}\right]-Ei\left[\frac{\left(\Delta x^2+\Delta y^2\right)^{0.5}}{4\alpha(t-t_l)}\right]\right) \quad (2\text{-}5)$$

as the response factor of BHE k on a position (i,j) within the BHE field at time step $l \in \{1,\ldots,m\}$ with reference to the current time step $t \in \{1,\ldots,m\}$ and $l \leq t$ and $\Delta x = (i - x_k)$ and $\Delta y = (j - y_k)$.

By merging $q_{k,l}$ and $\omega_{k,l}^{t,i,j}$ into vectors of the form $\vec{q}=(q_{1,1},\ldots,q_{n,1},\ldots,q_{n,m})$ and $\vec{\omega}^{t,i,j}=(\omega_{1,1}^{t,i,j},\ldots,\omega_{n,1}^{t,i,j},\ldots,\omega_{n,m}^{t,i,j})$ Eq. 2-4 can be written as:

$$\Delta\vec{T}_{i,j}(t,\vec{q})=\vec{q}(\vec{\omega}^{t,i,j})^T \quad (2\text{-}6)$$

where $\Delta\vec{T}_{i,j}(t,\vec{q})$ is the actual temperature change in the underground on the position (i,j) at time step t caused by the superposition of all BHEs in the field with the temporal load pattern $\vec{q}$.

2.2.2 Optimization objectives and constraints

The efficiency of the heat pump of a geothermal installation is mainly influenced by the fluid temperature coming from the BHE field which itself hugely depends on the temperature of the underground T. Therefore in the heating case, it is reasonable to keep $\min(T)$ as high as possible to keep the maximum observed cooling of the underground $\max(\Delta\vec{T}_{i,j})$ caused by the heat extraction through the BHEs as small as possible. As a result, extreme local cooling is avoided, the temperature distribution is smoothed, and potential ecological impacts from substantial local temperature gradients are mitigated. This leads to the primary objective of the proposed load assignment optimization

$$\text{minimize}(\max(\Delta\vec{T}_{i,j})) \quad (2\text{-}7)$$

Depending on the field thermal parameters and the given load pattern the maximum overall temperature change may not be influenced by the load assignment for certain time steps. For

these cases, which are otherwise not captured by the primary objective, we minimize the maximum temperature change within each time step as a secondary objective which is given a much lower weight than the primary objective.

In order to fulfill the energy demand required from the BHE field, the sum of the loads $q_{k,l}$ for each time step l has to equal to the required energy E_l for the given time step. This reads:

$$E_l = \sum_{k=1}^{n} q_{k,l} \qquad l = 1 \ldots m \tag{2-8}$$

2.2.3 Linear optimization procedure

Based on the definition of $\Delta\vec{T}_{i,j}(t,\vec{q})$ given in Eq. 2-6, the primary objective of minimization of the maximum overall temperature change for the entire considered time span given in Eq. 2-7 can be expressed as:

$$\arg\min\left(\max(\Delta\vec{T}_{i,j}(t,\vec{q}))\right) \qquad \forall(i,\, j,t) \in S \tag{2-9}$$

where $\vec{q}$ is the decision variable and S is a set of all spatial and temporal reference points defined by 3-tuples $(i,\, j,t)$.

In a similar manner the secondary objective of minimizing the temperature change within each single time step l can be written as:

$$\arg\min\left(\sum_{l=1}^{m}\max(\Delta\vec{T}_{i,j}(l,\vec{q}))\right) \qquad \forall(i,\, j,t) \in S \quad t = l \tag{2-10}$$

In order to obtain a single objective function suitable for minimization, we combine the objective functions given in Eq.s 2-7 and 2-8 to:

$$\arg\min\left(w \cdot \max(\Delta\vec{T}_{i,j}(t,\vec{q})) + \sum_{l=1}^{m} \max(\Delta\vec{T}_{i,j}(l,\vec{q})) \right) \qquad \forall(i,j,t) \in S \tag{2-11}$$

where w is a weighting factor which should be set to a large value to ensure the priority of the primary objective over the secondary objectives. w was set to 100 in this study.

Through the introduction of additional virtual variables $z_{0\ldots m}$ the max-norm terms of the objective function can then be rewritten as m+1 linear programs which minimize $z_{0\ldots m}$ and for every z reads:

$$\begin{aligned} &\min(z) \\ &\Delta\vec{T}_{i,j}(l,\vec{q}) - z\vec{e} \quad \prec 0 \\ &-\Delta\vec{T}_{i,j}(l,\vec{q}) - z\vec{e} \quad \prec 0 \end{aligned} \tag{2-12}$$

with $\vec{e}$ as the unity vector (Boyd and Vandenderghe, 2004).

Since the relationship between $\Delta\vec{T}$ and q is linear and between $\Delta\vec{T}_{i,j}$ and $\vec{q}$ is also linear, the energy load assignment problem can therefore be posed as a linear program:

$$\min\left(w \cdot z_0 + \sum_{l=1}^{m} z_l \right) \tag{2-13}$$

subject to the constraints:

$$\begin{aligned} &\Delta\vec{T}_{i,j}(t,\vec{q}) - z_0 \quad \prec 0 \\ &-\Delta\vec{T}_{i,j}(t,\vec{q}) - z_0 \quad \prec 0 \\ &\Delta\vec{T}_{i,j}(l,\vec{q}) - z_l \quad \prec 0 \\ &-\Delta\vec{T}_{i,j}(l,\vec{q}) - z_l \quad \prec 0 \end{aligned} \qquad \begin{aligned} &\forall(i,j,t) \in S \\ &\forall(i,j,l) \in S \qquad l = 1\ldots m \end{aligned} \tag{2-14}$$

where $z_{0\ldots m}$ and $\vec{q}$ are optimization variables.

The linear program is additionally constrained by the power demand for each time step which can be expressed as the equality constraint given in Eq. 2-8.

This is the monthly workload in case of a constant step size of one month between subsequent steps *l*. Since in our case we only consider heating, the load for each BHE for all time steps has to be positive. This results in the inequality constraint given by:

$$q_{k,l} \geq 0 \qquad l = 1 \ldots m, k = 1 \ldots n \tag{2-15}$$

Based on the formulation of the linear program given in the Eqs. 2-11 to 2-14, the load assignment problem can be solved using standard linear program solvers such as CPLEX.

2.3 Model set up

In the present study a hypothetical BHE field scenario of 25 square lattice-like arranged BHEs with 10 m spacing (δx = δy = 10 m) and 100 m length each, which is similar to the study by Katsura et al. (2009), is considered as demonstration case for optimization of individual energy extractions (Figure 2-1a). The subsurface geology is approximated as homogeneous and isotropic media. It is water-saturated and in this study no groundwater flow is considered, thus only conductive heat transport is addressed. Analytical simulation is performed for an operation period of thirty years with time variable BHE-specific energy loads. The geothermal system is optimized only for heating application, and no cooling is accounted for. As common for low-enthalpy geothermal simulations, temperature dependency of hydraulic (density and viscosity of the water) as well as of thermal parameters (thermal conductivity and volumetric heat capacity) is neglected (Hecht-Mendez et al. 2010).

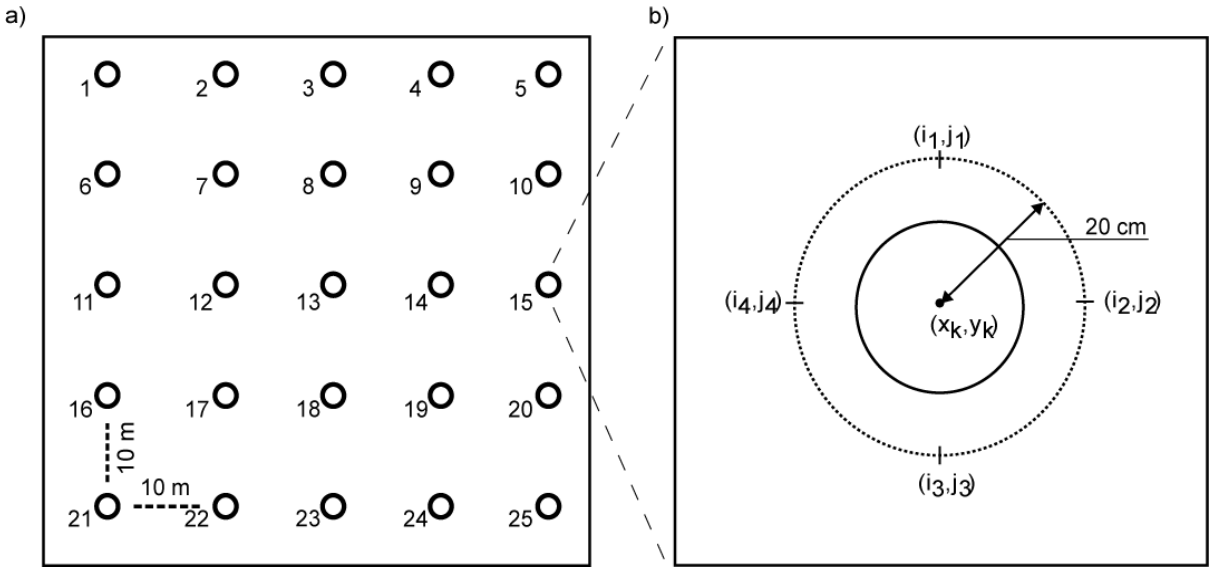

Figure 2-1. a) Top view of geothermal field with 25 BHEs used for applying the simulation-optimization procedure, b) extended view of one BHE showing the reference points located around each BHE used for calculating a representative average borehole wall temperature.

As shown in Figure 2-1b, four reference points for each BHE k are defined. These reference points are evenly distributed on a circle with a radius of 20 cm around the BHE position (x_k, y_k), which approximates the dimensions of the BHE. In order to estimate a single average subsurface temperature at the borehole wall for each BHE, we averaged $\Delta T_{i_{1\ldots4},j_{1\ldots4}}$ of the corresponding four reference points at each time step l. This results in n effective reference points in S for each time step l, respectively in $m \cdot n$ reference points for the whole optimization process. Thus for the considered time span (360 months) and the given BHE field (25 BHEs), the corresponding linear program then consists of 9,361 optimization variables, which can be subdivided into 361 virtual variables z and 9,000 actual loads $q_{k,l}$. The number of constraints is 45,361. Assuming a subsurface composed of silts and clays, typical thermal parameters for groundwater saturated material are selected for the demonstration case (Table 2-1). The thermal parameters represent reference values for specific energy extraction of BHEs given by the German Engineer Association guideline for thermal use of the underground (VDI, 2001).

Table 2-1. Parameter specifications for demonstration case used for application of the simulation-optimization procedure.

Parameter	Unit	Value
thermal conductivity (λ)*	W m^{-1} K^{-1}	1.70
thermal diffusivity (α)*	m^2 s^{-1}	$7 \cdot 10^{-7}$
length of the borehole (L)	m	100

* Values taken from VDI (2001)

Considering a heat transfer rate of 24 W m^{-1} (VDI, 2001) and an annual runtime of 1,800 hours, the entire energy extraction of the BHE field is 108 MWh per year. The total energy extraction of one year is divided into 12 uneven intervals according to a monthly and individual heating demand typical for a GSHP system in Central Europe. Accordingly, an energy load profile for one year is defined, which is shown in Figure 2-2. This profile approximates conditions applied in southern Germany by BHE-field designers, when no additional heat is required during the summer months. This profile is similar to the base load default profile of the EED software (version 3.15).

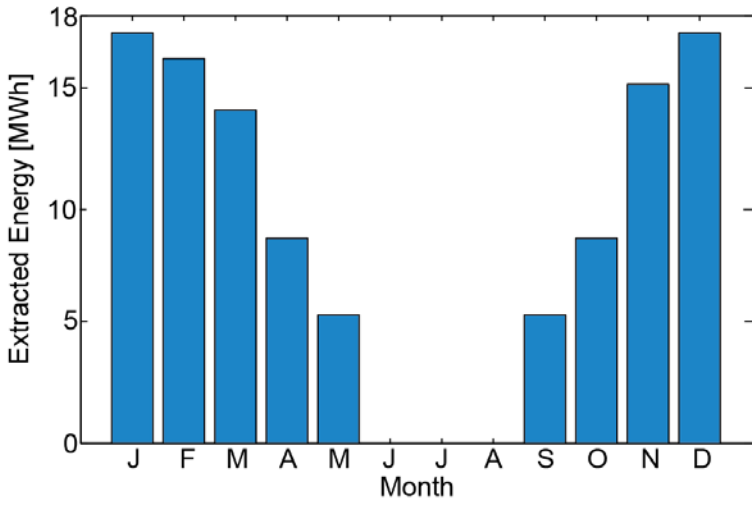

Figure 2-2. Extracted energy per month of a GSHP system using 25 BHEs with a specific energy extraction of 24 W m-1 and 1,800 operating hours per year.

In the following sections, we will distinguish three cases: (i) the load optimized case, as described in the methodology section, (ii) the equal load case, which represents a non-optimized variant, assuming the same energy extraction for all BHEs, and (iii) the equal flow case, which corresponds to typical conditions of BHE fields in practice. The first two cases are simulated by the line source equation (Eq. 2-3), whereas for the last case, equal volumetric

flow rates of the circulating heat carrier fluid are obtained from the SBM model. The latter was applied to all (non-)optimized cases to visualize the temperatures at 50 m depth and to compute the mixed outflow temperatures for all BHEs of the field, which enters the heat pump. SBM specific settings, which are used additionally to the values in Table 2-1, are listed in Table 2-2. These include fluid properties of water and assumed borehole resistances.

Table 2-2. Parameters specified in SBM.

Parameter	Unit	Value
fluid viscosity (15°C)	kg m^{-1} s^{-1}	1.14 ·10^{-3}
fluid density	kg m^{-3}	1,000
fluid vol. heat capacity	J m^{-3} K^{-1}	4.1912 ·10^{6}
fluid thermal conductivity	W m^{-1} K^{-1}	0.6
borehole thermal resistance R_b	K W^{-1} m^{-1}	0.0723
borehole internal thermal resistance R_a	K $W^{-1}m^{-1}$	0.2514

2.4 Results and discussion

Figures 2-3, 2-4 and 2-5 depict the BHE loads and the resulting temperature distribution in the subsurface for the non-optimized BHE fields with equal flow and equal loads and the load-optimized field, respectively. All three figures are divided into 16 subplots as follows: Each subplot shows a combined load/temperature profile of the simulated BHE field for a defined time step *t* within 30 years of simulation time. The twelve subplots in the upper three rows visualize the month-wise development at half-time, that is, during the 15^{th} operating year starting with January. The four lowermost subplots represent the temperature and load distributions for January of the 1^{st}, 8^{th}, 22^{th} and 29^{th} years of operation and thus illustrate the long-term temperature trends of the installed BHE field. January is selected as the month with highest energy extraction and the largest temperature changes. BHEs are shown as grey shaded circles, where darker color shades denote higher BHE loads. Hence, switched-off BHEs are colored white and black BHEs are driven with the highest load possible during the

actual time step. The subsurface temperature distribution (depth of 50 m) is illustrated by colors, where high absolute temperatures appear in red and lower temperatures in blue.

The three BHE field operation modes are simulated with the load profile depicted in Figure 2-2. Thus, at each month all three fields extract the same amount of energy. For the optimized case (Figure 2-5), the BHE loads are optimized individually for each BHE. In contrast, for the non-optimized cases (Figure 2-3 and 2-4), the loads of all BHEs within the field are assigned the same loads, respectively the same heat carrier flow velocities.

As anticipated, optimized and equal loading of BHEs, as well as equal flow, result in symmetric temperature anomalies that develop in the ground. Further, as illustrated by the bottom plots in Figures 2-3, 2-4 and 2-5, the January records of the 1st, 8th, 22th and 29th years reveal a continuous cooling of the BHE field. Apparently, the regeneration time during the summer period is too short to balance the deficit by conductive lateral heat supply in all three cases, which is a well-known long-term behavior of such GSHP systems (Eugster, 2000). This is also reflected by the small changes that can be observed during the small or no energy extraction phase in the summer season between May and August.

Figures 2-3 to 2-5 reveal that long-term BHE operations can generate substantially decreased temperatures that locally fall below 2.5°C. The relatively high observed temperature changes, ΔT, correspond to the results of recent investigations, for instance by Priarone et al. (2009), who obtained even higher values for heating dominated cases with large BHE fields. Rybach and Eugster (2010) observed similar values close to the borehole wall of a single BHE application at the Elgg site in Switzerland. Since the relationship between ΔT and the loads $\vec{q}$ is linear, ΔT can easily be limited to a desired value of ΔT by scaling the $\vec{q}$ obtained from the optimizer with the ratio between the desired ΔT and the actual ΔT. In other words, the relative difference between optimized and non-optimized BHE fields remains the same even

if much smaller total specific heat extraction rates are assumed and/or a stricter ΔT constraint has to be obeyed.

At first sight, the differences between the three cases do not appear significant. While equal flows and workloads tend to generate local anomalies in the BHE field, the optimized system yields more smoothed temperature contours. The temperature anomalies successively develop for all operation modes, but are most concentrated in the equal load case. This reflects that, in particular, the interior BHEs in the field are insulated by the outer BHEs, which averts sufficient conductive energy supply from the ambient ground. Even in the equal flow case, which represents a self-regulated system, where heat transfer is automatically smaller in low-temperature regions, a similar trend can be observed. Central BHEs cool the ground much more than the outer BHEs. Still, this case, represents standard practice, performs better than the more hypothetical equal load case: The low temperature extremes are less pronounced after the full operation period of thirty years (Figures 2-3, 2-4 and 2-5).

Figures 2-3 and 2-5 show that the load distribution does not exhibit equal extraction rates for all BHEs during equal flow and optimized load operation modes. In fact, the individual BHE loads crucially differ depending on the position of the individual BHE within the field and at a certain time-step. While for equal flow this is self-regulated according to the temperature gradients at each BHE, load optimization yields a system-specific strategy. It turns out that it is beneficial to deactivate the BHEs with the largest influence on neighboring BHEs, starting at the months with lowest energy demand, and to reactivate them when the energy demand rises again. Thus, the global optimum for the used load profile suggests deactivating first the BHEs in the centre of the field in April of each year (BHEs: 8, 12, 13, 14 and 18). In September, when energy extraction starts again after the summer months, first the BHEs at the outer edge of the field (BHEs: 1 to 6, 10, 11, 15, 16, 20 to 25) should be reactivated. As a

result, local temperature anomalies are mitigated, and a more balanced lateral cooling of the ground is achieved.

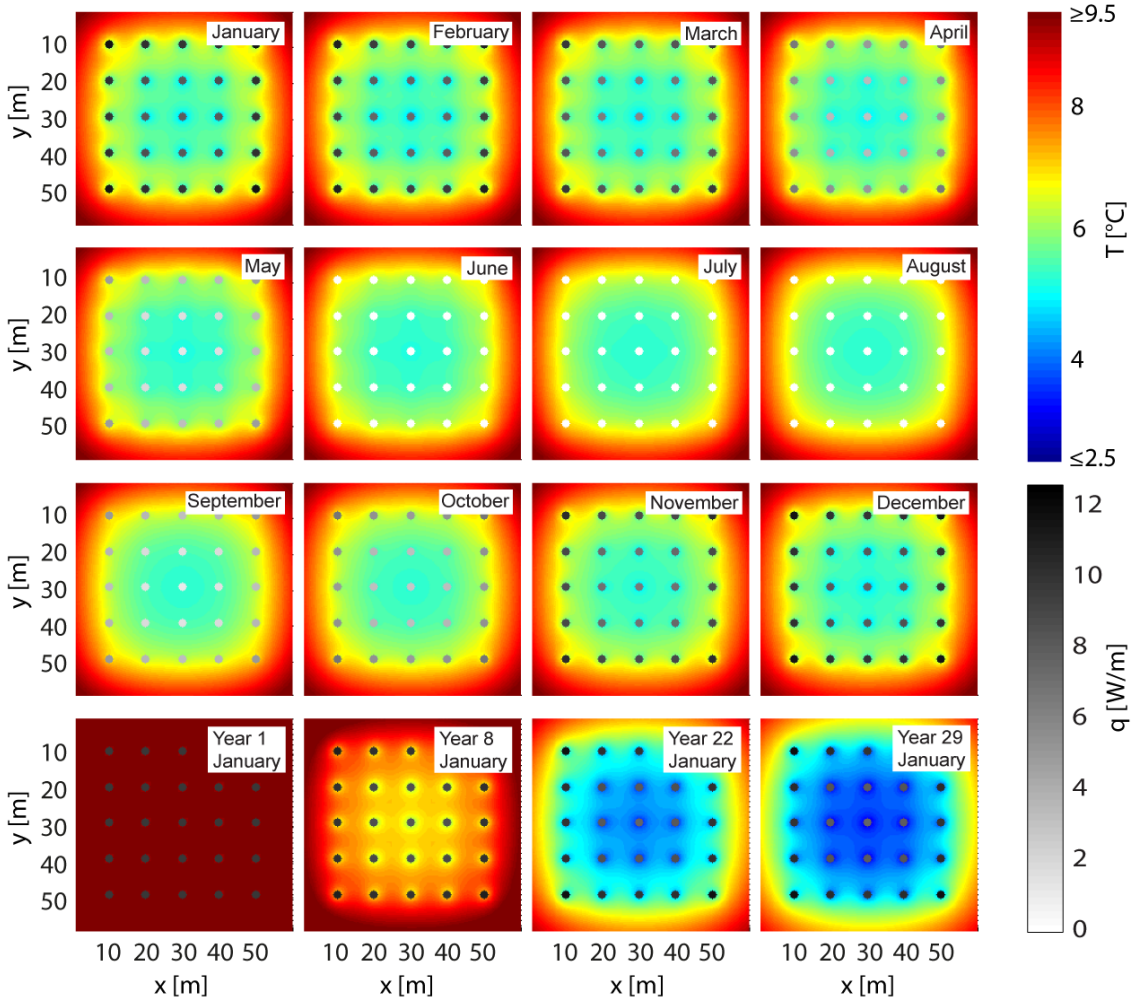

Figure 2-3. Temperature distribution and BHE workloads for the non-optimized equal flow case. Each circle represents a BHE with its corresponding load in grayscale. Darker color shades denote higher BHE loads. The subsurface temperature distribution at a depth of 50 m is illustrated by colors, where high absolute temperatures appear in red and lower temperatures in blue.

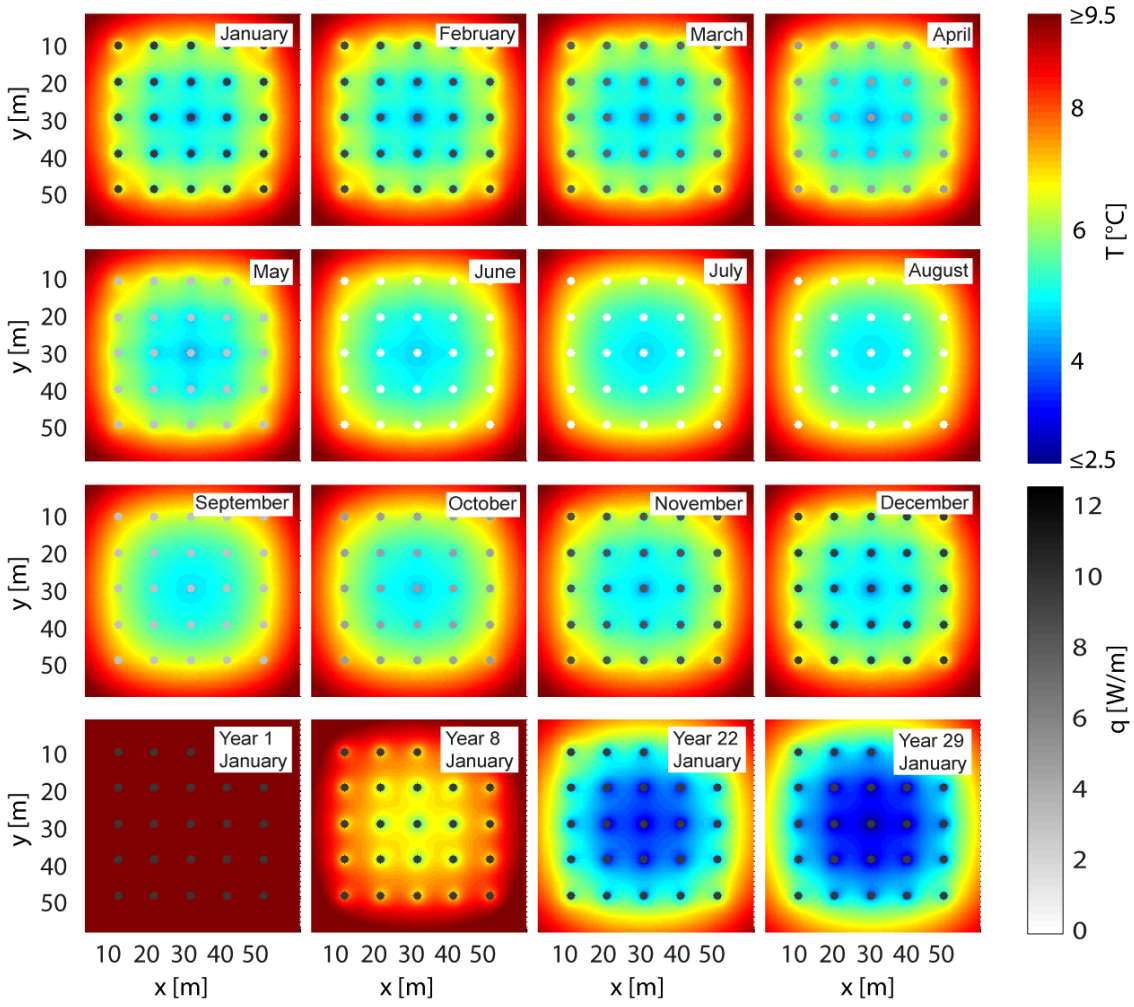

Figure 2-4. Temperature distribution and BHE workloads for the non-optimized equal load case. Each circle represents a BHE with its corresponding load in grayscale. Darker color shades denote higher BHE loads. The subsurface temperature distribution at a depth of 50 m is illustrated by colors, where high absolute temperatures appear in red and lower temperatures in blue. Please note: For a given month all BHE have equal load. The impression of slightly varying shades of grey is an optical illusion caused by differing background coloring.

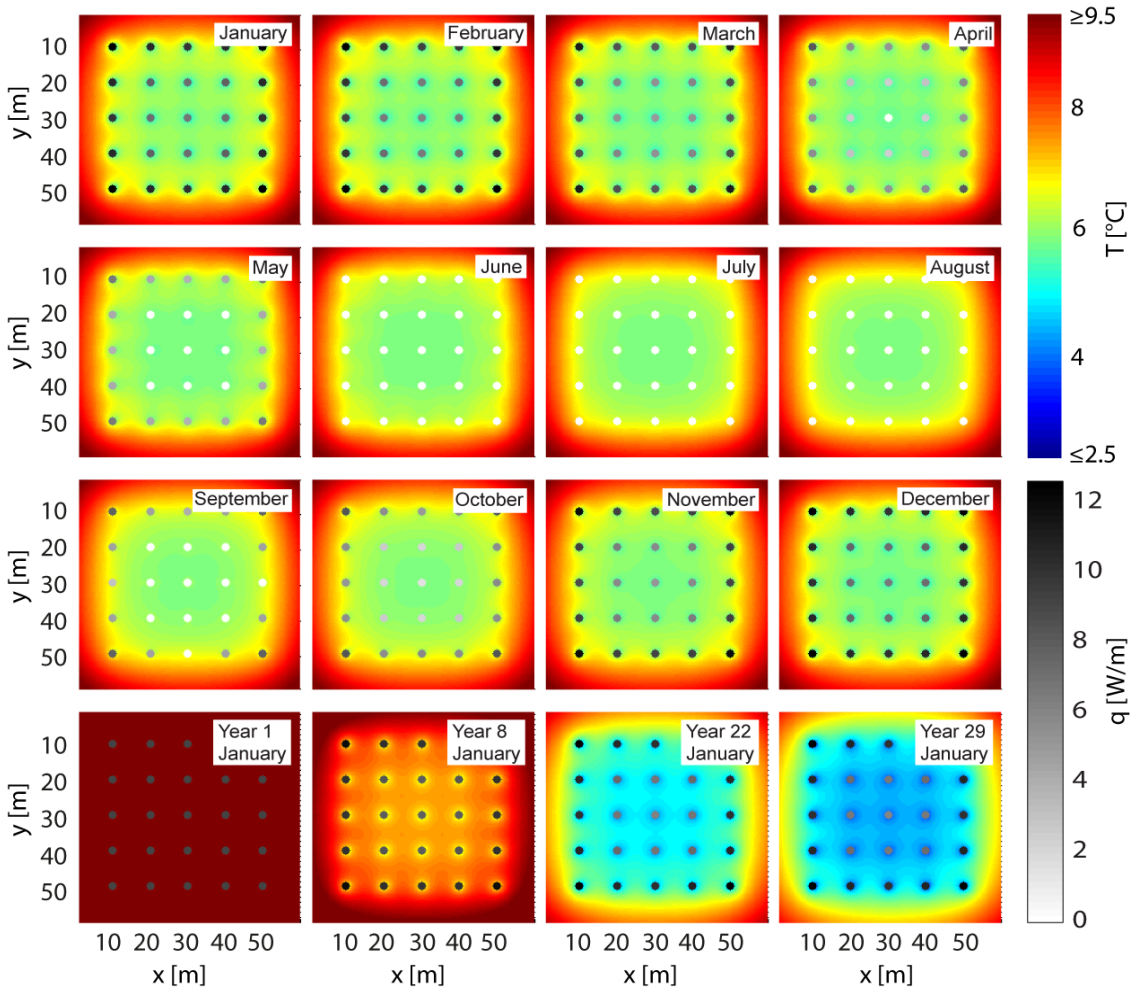

Figure 2-5. Temperature distribution and BHE workloads for the optimized case. Each circle represents a BHE with its corresponding load in grayscale. Darker color shades denote higher BHE loads. The subsurface temperature distribution at a depth of 50 m is illustrated by colors, where high absolute temperatures appear in red and lower temperatures in blue.

This is illustrated in more detail in Figure 2-6, which inspects the underground temperature after the heating period in the final year. Figure 2-6a shows the areal temperature difference in 50 m depth between both cases. Additionally, a cross section of the temperature change along the dashed line is depicted in Figure 2-6b. The differences in Figure 2-6a reach up to 1.25°C (i.e., 18%), which represents the strongest cooling at the central BHE. By load optimization, the lower central heat extraction is compensated by relatively higher loads at the BHE field boundary. This is reflected by the areas (dark blue) at the fringe with negative temperature differences, and shown in Figure 2-6b when comparing the temperatures of the BHEs at a distance of 10 m and then 50 m from the corner of the field. Another aspect that can be

extracted from the plots in Figure 2-6 is that even if the optimized system does not manage to generate equal temperatures, the variability is much less pronounced. The positive differences in the center of the field demarcate relative higher cooling by the equal flow case when compared to the optimized case. These are considerably more severe than the negative differences which are located at the fringe of the field.

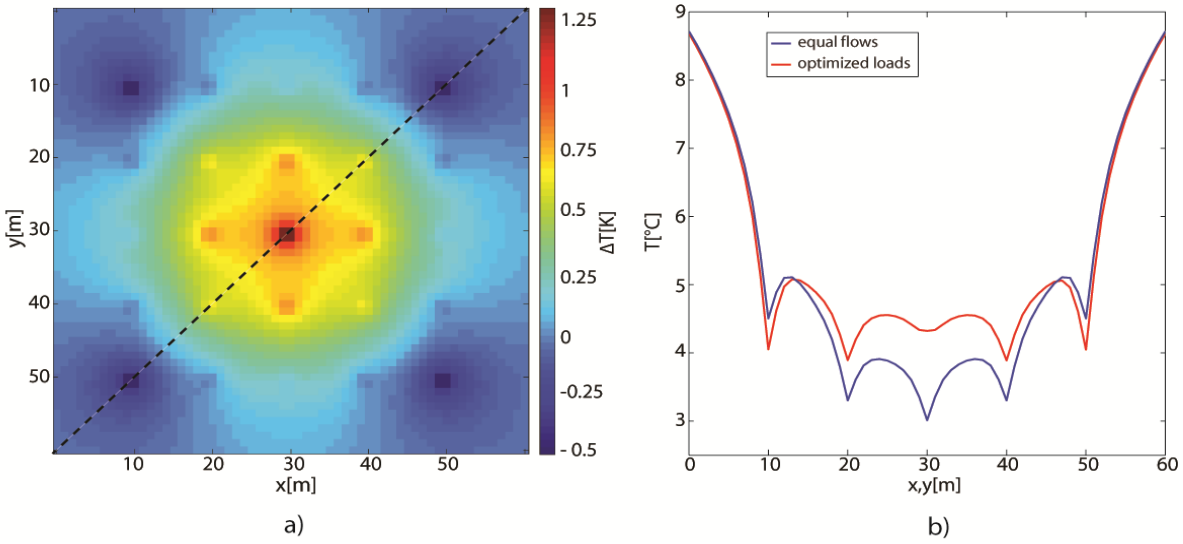

Figure 2-6. Temperature differences in the subsurface between the optimized and the equal flow case at the end of the heating period (March) of the final year (30) of the simulated time frame. 2-6a shows the areal temperature difference at 50 m depth between both cases. 2-6b depicts a cross section of the temperature change from one corner of the BHE field to the opposed one (dotted line in 2-6a).

Of special interest is the temperature that arrives at the heat pump, which can also be used to compare the three different operation modes. The lower this temperature is, the smaller the expected seasonal performance factor and thus the worse the efficiency of the entire geothermal heating system. Figure 2-7 reports the mixed outflow temperature evolution of the working fluid of all BHEs of the non-optimized equal flow case and the load optimized case in the field. These are obtained by averaging the monthly BHE-specific outflow temperatures simulated by SBM. Similar to the findings from previous studies (e.g. Signorelli 2004), sinusoidal oscillation reflects alternating use phases and regeneration phases. Since the subsurface is not able to regenerate during the course of the year, annual mean temperatures decline with progressing use. Due to averaging, the differences between the two cases are

only very small. Obviously, mixing rules out the extremes as observed when comparing the in-situ temperature distribution (Figures 2-3 to 2-6). Even so, as highlighted in the zoomed section in Figure 2-7, the optimized load case yields slightly higher temperatures than the alternative cases. This demonstrates that even if loads are used as proxy for the combined simulation-optimization, better strategies can be found than standard practice. Since the difference is rather small, however, in practice slight performance improvement potential may not be sufficient for justifying the application of additional control systems. In fact, the advantage of an optimized system is the possibility to extract a higher amount of energy while complying with given temperature thresholds or environmental constraints.

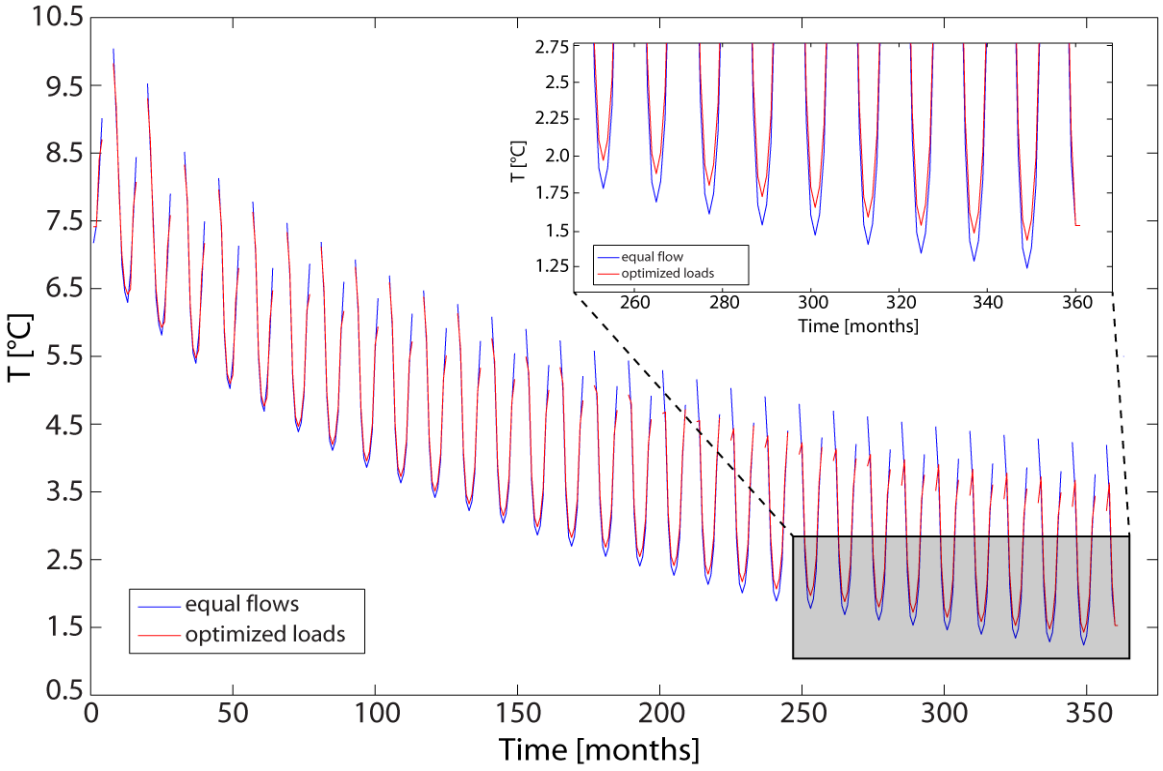

Figure 2-7. Mixed temperature evolution of the working fluid of all BHEs in the field. The mixed outflow temperature is depicted in blue for the equal flow case and in red for the optimized case. The zoomed section highlights the permanently higher temperatures of the optimized case.

2.5 Conclusions

A new approach for the optimization of scheduled energy extraction of closed shallow geothermal systems based on linear programming is presented. In this work flow, regulation

is not implicitly addressed in the mathematical formulation of the optimization problem, thus BHE workloads will be optimized as a surrogate for flow rates. Combined spatial and temporal superposition of the infinite line source analytical solution is used to simulate temperature changes in the underground caused by multiple adjacent borehole heat exchangers (BHEs), which operate with variable energy loads. By exploiting the linear relationship between the individual loads of the BHEs and the temperature changes in the underground we are able to formulate a linear optimization problem for assigning globally optimal loads for each BHE for each time step. The optimization objective is to minimize the ground temperature changes and therefore maximize heat pump performance, comply with regulative thresholds for induced temperature changes and mitigate environmental impacts. To determine if the workload optimization allows for improvement of BHE field design even without considering flow regulation, the optimized solutions obtained by this proxy were compared to a BHE field implementation, which operates at equal flows and loads. Except for the optimization step, all simulations were accomplished by the SBM code (Eskilson, 1986; Pahud et al., 1996).

The procedure is demonstrated for a simplified hypothetical case with 25 BHEs that are operated for 30 years to accomplish seasonally variable heating energy requirements typical for larger office buildings, schools or district heating systems. In the current study only heat conduction, i.e. no significant groundwater flow is considered in a homogeneous ground. The optimized BHE fields result in a mitigation of long-term temperature decrease and local temperature anomalies, and a more balanced, more lateral cooling of the ground is achieved. Current practical applications using equal flow rates for all BHEs achieve acceptable mixed outflow temperatures, but the absolute temperature decrease in the subsurface can additionally be diminished up to 18% if optimization is incorporated. This instance allows for significantly higher energy extraction rates without increasing environmental impacts and respectively a

better compliance with statutory provisions. Since the developed optimization method does not distinguish between any assumptions regarding the geometry of the field and the geological, hydrogeological and thermal parameters of the ground, it can be easily transferred to other cases and be readily implemented in planning software. Depending on the specific problem, the selected monthly resolution of the load profile can also be replaced by a coarser or finer resolution. As an extension, cooling can be accounted for. Almost any given BHE field geometry can be inspected, if the underlying superposition assumptions hold. However, since the mutual impact factors of the BHEs in the field are calculated using the infinite line source model, the presented method can currently only be used for conductive cases without groundwater flow. Alternative BHE simulation would therefore be necessary, if convective heat transport in the ground is significant. Likewise, the optimization procedure can also be extended for additional analytical solutions, as for instance the finite line source model (Zeng et al., 2002) or finite moving line source model (Molina-Giraldo et al., 2011).

Large matrices are utilized to represent the mutual influence coefficients between the BHEs for all time steps. Implemented in a computer, they easily grow to several gigabytes in size. This sets an upper limit on the number of BHEs and of time steps depending on the platform used. The computational time was approximately 30 minutes for the calculation of the coefficients ω and three hours for solving the linear program on a 3.6 GHz quad-core CPU utilizing 6 GB of RAM. In view of the growing computational power, however this is not considered to be a severe shortcoming in the future. As a remedy, it is often desirable to search for close-optimal solutions that can be obtained by separation of the full operation problem into sub-problems, e.g. by successively optimized separate operation intervals.

2.6 References

Amt für Umweltschutz Landeshauptstadt Stuttgart, 2005. Nutzung der Geothermie in Stuttgart. Schriftreihe des Amtes für Umweltschutz, Heft 1/2005, 89 pp.

Bauer, D., Heidemanna,W., Diersch, H.-J.G., 2011. Transient 3D analysis of borehole heat exchanger modeling. Geothermics 40(4), 250-260.

Bayer, P., Saner, D., Bolay, S., Rybach, L., Blum, P., 2012. Greenhouse Gas Emission Savings of Ground Source Heat Pump Systems in Europe: A Review. Renewable and Sustainable Energy Reviews, doi:10.1016/j.rser.2011.09.027, in press.

Bernier, M.A., Pinel, P., Labib, R., Paillot, R., 2004. A Multiple Load Aggregation Algorithm for Annual Hourly Simulations of GCHP Systems. HVAC & R Research Journal 10(4), 471-488.

Blum, P., Campillo, G., Münch, W., Kölbel, T., 2010. CO2 savings of ground source heat pump systems - A regional analysis. Renewable Energy 35, 122-127.

Boyd, S., Vandenderghe, L., 2004. Convex Optimization, Cambridge University Press, Cambridge, 697 pp.

Brielmann, H., Griebler, C., Schmidt, S.I., Michel, R., Lueders, T., 2009. Effects of thermal energy discharge on shallow groundwater ecosystems. FEMS Microbiology Ecology 68(3), 273-286.

Brielmann, H., Lueders, T., Schreglmann, K., Ferraro, F., Blum, P., Bayer, P., Hammerl, V., Griebler, C., 2011. Oberflächennahe Geothermie und ihre potentiellen Auswirkungen auf die Grundwasserökologie, Grundwasser, 16(2), 77-91.

Carslaw, H.S., Jaeger, J.C., 1959. Conduction of Heat in Solids, Oxford University Press, New York, NY, USA, 510 pp.

Cui, P., Diao, N.R., Fang, Z.H., 2001. Analysis on discontinuous operation of geothermal heat exchangers of the ground-source heat pump systems. Journal of Shandong Institute of Architecture and Engineering 16, 52-57.

Diao, N., Cui, P., Liu, J., Fang, Z., 2010. R&D of the ground-coupled heat pump technology in China. Frontiers of Energy and Power Engineering in China 4, 47-54.

Diao, N., Li, Q., Fang, Z., 2004. Heat transfer in ground heat exchangers with groundwater advection. International Journal of Thermal Sciences 43, 1203-1211.

Esen, H., Inalli, M., Sengur, A., Esen, M., 2008. Predicting performance of a groundsource heat pump system using fuzzy weighted pre-processing-based ANFIS. Building and Environment 43(12), 2178-2187.

Eskilson, P., 1986. Superposition Borehole Model. Manual for computer code, Department of Mathematical Physics, University of Lund, Lund, Sweden, 95 pp.

Eskilson, P., 1987. Thermal Analysis of Heat Extraction Boreholes, Department of Mathematical Physics, University of Lund, Lund, 222 pp.

Eugster, W.J., Rybach, L., 2000. Sustainable production from borehole heat exchanger systems. Proceedings World Geothermal Congress, Kyushu-Tohoku, Japan, pp. 825-830.

Fujii, H., Itoi, R., Fujii, J., Uchida, Y., 2005. Optimizing the design of large-scale ground-coupled heat pump systems using groundwater and heat transport modeling. Geothermics 34, 347-364.

Gao, Q., Li, M., Yu, M., 2010. Experiment and simulation of temperature characteristics of intermittently-controlled ground heat exchanges. Renewable Energy 35, 1169-1174.

Haehnlein, S., Bayer, P., Blum, P., 2010. International legal status of the use of shallow geothermal energy. Renewable and Sustainable Energy Reviews 14, 2611-2625.

Hecht-Méndez, J., Molina-Giraldo, N., Blum, P., Bayer, P., 2010. Evaluating MT3DMS for heat transport simulation of closed geothermal systems. Ground Water 48, 741-756.

Hellström, G., 1991. Ground heat storage: Thermal Analysis of Duct Storage Systems, I. Theory. Department of Mathematical Physics, University of Lund, Lund, 262 pp.

Hellström, G., Sanner, B., 1997. EED – Earth Energy Designer, Version 1.0, User's Manual, Wetzlar, Germany, 43 pp.

Katsura, T., Nagano, K., Narita, S., Takeda, S., Nakamura, Y., Okamoto, A., 2009. Calculation algorithm of the temperatures for pipe arrangement of multiple ground heat exchangers. Applied Thermal Engineering 29, 906-919.

Katsura, T., Nagano, K., Takeda, S., 2008. Method of calculation of the ground temperature for multiple ground heat exchangers. Applied Thermal Engineering 28, 1995-2004.

Kavanaugh, S.P., Rafferty, K.D., 1997. Ground Source Heat Pumps: Design of Geothermal Systems for Commercial and Institutional Buildings, ASHRAE, Atlanta, 167 pp.

Klotzbücher, T., Kappler, A., Straub, K.L., Haderlein, S.B., 2007. Biodegradability and groundwater pollutant potential of organic anti-freeze liquids used in borehole heat exchangers. Geothermics 36, 348-361.

Lazzari, S., Priarone, A., Zanchini, E., 2010. Long-term performance of BHE (borehole heat exchanger) fields with negligible groundwater movement. Energy 35, 4966-4974.

Li, S., Yang, W., Zhang, X., 2009. Soil temperature distribution around a U-tube heat exchanger in a multi-function ground source heat pump system. Applied Thermal Engineering 29, 3679-3686.

Li, X.., Chen, Z., Zhao, J., 2006. Simulation and experiment on the thermal performance of U-vertical ground coupled heat exchanger. Applied Thermal Engineering 26, 1564-1571.

Lund, J.W., Freeston, D.H., Boyd, T.L., 2010. Direct Utilization of Geothermal Energy 2010 Worldwide Review. In: Proceedings 2010 World Geothermal Congress. Bali, Indonesia, 25-29 April, 23 pp.

Marcotte, D., Pasquier, P., 2008. Fast Fluid and Ground Temperature Computation for Geothermal Ground-Loop Heat Exchanger Systems. Geothermics 37(6), 651-665.

Marcotte, D., Pasquier, P., Sheriff, F., Bernier, M., 2010. The Importance of Axial Effects for Borehole Design of Geothermal Heat-Pump Systems. Renewable Energy 35(4), 763-770.

Metzger, T., Didierjean, S., Maillet, D., 2004. Optimal experimental estimation of thermal dispersion coefficients in porous media. International Journal of Heat and Mass Transfer 47, 3341-53.

Michopoulos, A., Kyriakis, N., 2009. A New Energy Analysis Tool for Ground Source Heat Pump Systems. Energy and Buildings 41, 937-941.

Molina-Giraldo, N., Bayer, P., Blum, P., 2011a. Evaluating the influence of thermal dispersion on temperature plumes from geothermal systems using analytical solutions. International Journal of Thermal Sciences 50, 1223-31.

Molina-Giraldo, N., Blum, P., Zhu, K., Bayer, P., Fang, Z., 2011b. A moving finite line source model to simulate borehole heat exchangers with groundwater advection. International Journal of Thermal Sciences 50, 2506-13.

Nagano, K., Katsura, T., Takeda, S., 2006. Development of a design and performance prediction tool for the ground source heat pump system. Applied Thermal Engineering 26, 1578-1592.

Pahud, D., A., F., Hadorn, J.C., The superposition borehole model for TRNSYS (TRNSBM). User manual for the November 1996 version. Internal Report, in, LASEN -DGC-EPFL, Switzerland, 1996, 6 pp.

Philippe, M., Bernier, M., Marchio, D., 2009. Validity ranges of three analytical solutions to heat transfer in the vicinity of single boreholes. Geothermics 38, 407-413.

Priarone, A., Lazzari, S., Zanchini, E., 2009. Numerical Evaluation of Long-Term Performance of Borehole Heat Exchanger Fields. In: Proceedings of the COMSOL Conference, Milano, 6 pp.

Rybach, L., Eugster, W.J., 2010. Sustainability aspects of geothermal heat pump operation, with experience from Switzerland. Geothermics 39, 365-369.

Rybach, L., Mongillo, M., 2006. Geothermal sustainability - A review with identified research needs. Geothermal Resource Council Transactions 30, pp. 1083 - 1090.

Saner, D., Juraske, R., Kübert, M., Blum, P., Hellweg, S., Bayer, P., 2010. Is it only CO2 that matters? A life cycle perspective on shallow geothermal systems. Renewable and Sustainable Energy Reviews 14, 1798-1813.

Schmidt, T., Hellström, G., Ground source cooling - Working paper on usable tools and methods, in, EU Commission SAVE program and Nordic Energy research, 2005, 21 pp.

Signorelli, S., Kohl, T., Rybach, L., 2004. Sustainability of production from borehole heat exchanger fields. In: (Ed.), Proceeding Twenty-Ninth Workshop on Geothermal Reservoir Engineering. Stanford, January 26-28, 2004, 6 pp.

Spitler, J.D.; 2000. GLHEPRO - A Design Tool For Comercial Building Ground Loop Heat Exchangers. In: (Ed.), Proceedings of the Fourth International Conference of Heat Pumps in Cold Climates, Aylmer, Québec, 17–18 August 2000, pp. 1–15.

Sutton, M.G., Nutter, D.W., Couvillion, R.J., 2003. A ground resistance for vertical bore heat exchangers with groundwater flow. Journal of Energy Resources Technology 125, 183-9.

Urchueguía, J.F., Zacarés, M., Corberán, J.M., Montero, Á., Martos, J., Witte, H., 2008. Comparison between the energy performance of a ground coupled water to water heat pump system and an air to water heat pump system for heating and cooling in typical conditions of the European Mediterranean coast. Energy Conversion and Management 49, 2917-2923.

VDI, 2001. Thermal use of the underground, part 2: geothermal heat pump systems, VDI-Verlag, VDI 4640, Düsseldorf, 43 pp.

Yavuzturk, C., Spitler, J.D., Rees, S.J., 1999. A Transient Two-dimensional Finite Volume Model for the Simulation of Vertical U-tube Ground Heat Exchangers. ASHRAE Transactions 105(2), 465-474.

Zeng, H.Y., Diao, N.R., Fang, Z.H., 2002. A finite line-source model for boreholes in geothermal heat exchangers. Heat Transfer − Asian Research 31, 558-567.

3. Optimization of energy extraction for vertical closed-loop geothermal systems considering groundwater flow[2]

Abstract: A combined simulation-optimization procedure is presented to regulate the operation of borehole heat extractors (BHEs) in a multiple BHE field when groundwater flow exists. Such fields are of increasing interest for large-scale geothermal heating energy supply of buildings, but so far strategic adjustment of energy extraction rates (loads) of the individual BHEs has not been considered in practice. Groundwater flow means an additional convective energy supply, which is advantageous but also complicates proper BHE adjustment. In the presented procedure, the field is simulated by temporally and spatially superimposed moving line source equations. The optimization goal is formulated in an objective function to minimize the thermal impact in the ground, to avoid extreme temperature anomalies, and by this, ultimately improve heat pump performance. For a given seasonal energy demand and total operation time, linear programming efficiently delivers optimized BHE operation patterns. For an examined square lattice of 25 BHEs, the optimized radial load patterns characteristic for conduction dominated conditions change to patterns that are oriented at the groundwater flow when convection dominates. Through this, optimization always levels the temperature distribution in the ground. Also, in comparison to standard practice, mean BHE outlet temperatures can be increased. For the small study case, numerical simulation reveals that already more than 1 K can be achieved, given a seasonal energy demand oriented at common conditions in central Europe. However, for a fixed energy demand, convective heat supply towards the BHEs increases with groundwater flow velocity and thus mitigates the benefits from optimization.

[2] Reproduced from: Hecht-Méndez, J., de Paly, M., Beck, M., Bayer, P., Optimization of energy extraction for vertical closed-loop geothermal systems considering groundwater flow. Energy Conversion and Management, submitted.

3.1 Introduction

Vertical ground source heat pumps (GSHPs) are standardized devices of shallow geothermal energy use. In the most common case, they are employed for space heating of buildings. The prevalent variants, such as in the dominating markets of Europe, are mini-systems that supply individual residential houses with an installed power ranging between 10 kW and 12 kW [1-3]. One, or a small number of adjacent boreholes are drilled down to a depth of typically 50-150 m, and by continuous circulation of a carrier fluid, heat is collected from the ambient underground. The heat is transported to a heat pump in the building to feed the space and/or hot water heating unit, and then is returned to the ground loop. This ground loop most often represents a piped circuit system installed within the borehole, the borehole heat exchanger (BHE), which is separated from the ground and extracts heat solely by conduction. Meanwhile, large-scale applications to supply hotels, schools, big office buildings or district heating systems are growing in number [4,5]. A higher energy demand is supplied by extraction of heat from larger volumes of the subsurface. This is achieved by running galleries of multiple BHEs. In contrast to the design of single BHE systems, such multiple neighbouring BHEs can interact and influence each other. This could have an effect on the overall system's performance and hence, should be either avoided or integrated in the operation strategy [6,7]. Proficient operation of BHE fields often also has to account for the effects of seasonal use. This means that the ground chilled in the cold seasons needs intermittent summer periods to slowly recover and at least partly recharge the battery. In fact, the lower the temperature in the ground, the less efficient the GSHP is. In order to guarantee sustainable use, i.e. at lower than maximum possible production level but with satisfactory performance [8], the intensity of local temperature anomalies in the BHE field needs to be minimized while recharge during the recovery period is maximized.

Identifying an optimal BHE field design for given subsurface conditions and specific annual energy requirements is challenging, considering the degrees of freedom in design and operation mode. Available design software such as EED, GLHEPRO or TRNSYS-DST [9-11], provide solutions with simplifying assumptions. For example, the underlying concepts ignore the potential of individually adjusting BHE operation. In de Paly et al. [12], we demonstrate for a hypothetical case that temporally and spatially variable energy extraction of BHEs can improve the overall system's performance and mitigate long-term temperature decline. Temperature changes in the underground are simulated by superimposed line source equations. For a given configuration, the optimal operation mode is searched for by linear programming. The present study builds up on this work, and extends it to those conditions where groundwater flow in the subsurface cannot be neglected. The particular questions are: How does groundwater flow influence optimal BHE field design, and can the efficiency be improved if the effect of convective heat transport by moving groundwater is pro-actively included in the developed operation strategy? A real-case oriented synthetic setup is used to derive general conclusions on optimal individual BHE operation depending on the location of BHEs and hydrogeological conditions. In the following, related works are shortly reviewed, which particularly discuss the role of groundwater flow for shallow geothermal systems.

In one of the first studies on the influence of heat convection for BHEs, Eskilson [13] concluded that the effect of groundwater flow is negligible. For a simple example, the borehole wall temperature is estimated using a groundwater flow velocity (specific discharge) of 1.5×10^{-8} m s^{-1}, showing a change of 2% in comparison to a pure conductive scenario (no flow). The used flow velocity is considered a representative average value for rocks. However, flow velocities in porous media can vary among several orders of magnitude. Recently, others have shown that the presence of groundwater flow indeed can be relevant for the heat transport around BHEs. Sutton et al. [14], Diao et al. [6] and Molina-Giraldo et al.

[15,16] developed a transient analytical solution based on the moving line source theory [17] that accounts for conductive and convective heat transport. A common conclusion is that temperature distribution obtained by simulating conduction only produces errors that substantially rise with increasing groundwater flow velocity.

The modelling studies by Chiasson et al. [18] and Hähnlein et al. [19] show that when groundwater flow is present, the temperature changes in the underground surrounding the BHE are invariant after shorter operation time (i.e. steady state is reached faster). Chiasson et al. [18] also compare the performance of a BHE field adjusted by convection-free BHE design software to that simulated by the numerical model with groundwater flow. Their results indicate large differences among the predicted ground temperatures. Fan et al. [20] evaluate the performance of multiple BHEs connected to a hybrid GSHP system, using a finite volume simulation method. They find that the influences of the groundwater on the heat transfer between the BHE and the surrounding soil depends on the system operation mode and the flow velocity. The numerical modelling study by Lee and Lam [21] is dedicated to the influence of groundwater flow direction on BHE fields. They conclude that square BHE configurations are likely to be less affected than non-square setups. Wang et al. [22] quantifies the heat transfer enhancement due to the presence of groundwater flow in an in-situ BHE field experiment. Average fluid temperatures within the BHE were measured for two heat extraction and two heat injection operation conditions. Comparisons with numerical results of a conductive scenario show a heat transfer rate improvement by 12.9% and 9.8% for energy extraction and injection, respectively.

In contrast to these previous, mostly process-based studies, our purpose is on integrating the potentially beneficial effects of natural groundwater flow, in order to optimize the performance of GSHP systems. Only one study, by Fujii et al [4], is found that similarly focuses on optimization of GSHP systems, including groundwater flow. In their work, four

different heat extraction and storage schemes are examined to optimize the performance of a field of 75 BHEs installed in Akita, Japan. Ground temperatures are simulated for a period of 50 years. Although the prevalent groundwater flow velocity is insufficient to remarkably enhance the heat transfer to the geothermal system, it influences the temperature distribution and the heat extraction rate of the BHEs. Depending on operation scheme and BHE spacing, BHEs located upstream of the flow direction show higher energy extraction rates than those at downstream locations.

As shown, for instance, in Fujii et al. [4] and de Paly et al. [12], ground temperature changes in BHE fields are spatially variable, and may become significant in the long term. Control and minimization of the overall underground temperature change is in favour of the entire GSHP system performance (e.g. Bernier et al., [23]). At the same time, regulations often constrict the maximum allowed temperature changes, in order to keep the induced temperature variations within a range that is not of environmental concern [24,25]. Groundwater flow adds complexity to simulation and control of the ground thermal regime. The heat supplied by natural convection is an attractive additional source, which, if used strategically, may enhance the overall system's efficiency and regeneration. In the present work, the optimization procedure developed by de Paly et al. [12] is extended for considering the effects of the groundwater flow. A two-dimensional transient analytical approach, which describes conductive-dispersive heat transport in porous media, is included in a simulation-optimization procedure. Based on the superposition principle, temperature changes in the underground due to multiple BHEs are evaluated using monthly variable energy loads. As objective we define the minimization of the maximal underground temperature change for given total operation time. Concurrently, the BHE field has to fulfil a given annual and monthly variable heating energy demand. Equivalent to de Paly et al. [12], the optimization procedure is applied to a

case with 25 BHEs. For this case, optimized solutions are investigated for a range of different groundwater flow velocities.

3.2 Mathematical background

symbol	variable	unit
C	volumetric heat capacity	[J m^{-3} K^{-1}]
c	specific heat capacity	[J kg^{-1} K^{-1}]
d	borehole diameter	[m]
E_l	total energy demand for each time step	[W]
k	running index of BHEs	[-]
L	length of the BHE	[m]
L'	characteristic length	[m]
l	running index of time steps	[-]
m	number of time steps	[-]
n	porosity	[-]
Pe	Péclet number	[-]
p	number of BHEs	[-]
Q	volumetric flow rate	[m^3 s^{-1}]
q	power demand/load	[W]
q'	heat extraction rate per unit length	[W m^{-1}]
R_a	internal thermal resistance of the borehole	[m K W^{-1}]
R_b	thermal resistance of the borehole	[m K W^{-1}]
T	temperature	[K]
T_u	undisturbed temperature	[°C]
$\Delta\overline{T}$	mean temperature change	[K]
$Tout$	temperature at the BHE outlet	[°C]
$\overline{T}out$	mean mixed outlet temperature for all BHEs	[°C]
t	time	[s]
u	specific discharge (Darcy velocity)	[m s^{-1}]
v_a	seepage velocity	[m s^{-1}]
w	weighting factor	[-]
x_k	coordinate of BHE k in the x-direction	[m]
y_k	coordinate of BHE k in the y-direction	[m]
z	coordinate in the z-direction	[m]
ρ	density	[kg m^{-3}]
μ	dynamic fluid viscosity	[kg m^{-1} s^{-1}]
λ	thermal conductivity	[W m^{-1} K^{-1}]
α	dispersivity	[m^2 s^{-1}]
ω	response factor	[-]

subscripts	
s	solid
w	water
m	porous media
l	longitudinal
t	transversal

3.2.1 Heat transport in porous media

The governing equation for transient heat conductive and convective transport in porous media, based on the principle of heat conservation, is [26]:

$$\left(\frac{\rho_m c_m}{n\rho_w c_w}\right)\frac{\partial T}{\partial t} - div\left[\left(\frac{\lambda_m}{n\rho_w c_w} + \alpha v_a\right) grad T\right] + div(v_a T) \pm \frac{q}{n\rho_w c_w} = 0 \qquad (3\text{-}1)$$

The first term represents the thermal equilibrium between the solid and fluid phases, and the second term describes heat conduction and dispersion, with an added convective component that represents heat transported at seepage velocity, v_a. The last term accounts for the energy source given as a heat flux or thermal load, q.

Assuming an infinite homogeneous porous media at a constant uniform initial temperature, T_u, Metzger et al. [27] introduced a two-dimensional transient analytical solution for Eq. 3-1, based on the line source model. By this, the transversal temperature distribution, due to an infinite line source aligned with the z-axis can be estimated. At the source a constant heat flux per unit length q is assigned. Molina et al. [15] applied this equation to simulate the thermal anomaly from single BHE operation. The temperature difference ($\Delta T = T - T_o$) for a time t is:

$$\Delta T(\Delta x, \Delta y, t) = \frac{q}{4\pi L\sqrt{\lambda_l \lambda_t}} \exp\left(\frac{\rho_w c_w n v_a \Delta x}{2\lambda_l}\right) \times \int_0^{\frac{(\rho_w c_w n v_a)^2 t}{4\rho_m c_m \lambda_l}} \exp\left[-\left(\frac{\Delta x^2}{\lambda_l} + \frac{\Delta y^2}{\lambda_t}\right) \times \frac{(\rho_w c_w n v_a)^2}{16\lambda_l \theta} - \theta\right] \frac{d\theta}{\theta} \qquad (3\text{-}2)$$

where $\Delta x = (i - x_k)$ and $\Delta y = (j - y_k)$ are the distances to an arbitrary location (i,j) with respect to a BHE centred at (x_k,y_k). Further parameters are:

$$\lambda_l = \lambda_m + \alpha_l \rho_w c_w n v_a \tag{3-3}$$

$$\lambda_t = \lambda_m + \alpha_t \rho_w c_w n v_a \tag{3-4}$$

as the effective thermal conductivity in the (l) longitudinal and (t) transverse direction, respectively [15,28]. Since Eq. 3-2 is linear with respect to q, and assuming that the soils thermal properties do not depend on temperature, this equation can be spatially and temporally superimposed, similar to the approach in [12] for the infinite line source analytical solution without groundwater flow. This allows flexible simulation of multiple BHE fields at temporally variable loads:

$$\Delta T_{i,j}(t, q_{1\dots p,1\dots m}) = \sum_{l=1}^{m}\sum_{k=1}^{p} q_{k,l} \left(\frac{1}{4\pi L\sqrt{\lambda_l \lambda_t}} \exp\left(\frac{\rho_w c_w u x}{2\lambda_l}\right) \times \left(\int_0^{\frac{(\rho_w c_w)^2 u^2 (t-t_{l-1})}{4\rho_m c_m \lambda_l}} \exp\left[-\left(\frac{x^2}{\lambda_l} + \frac{y^2}{\lambda_t}\right) \times \frac{(\rho_w c_w)^2 u^2}{16\lambda_l} \frac{1}{\theta} - \theta \right] \frac{d\theta}{\theta} - \int_0^{\frac{(\rho_w c_w)^2 u^2 (t-t_l)}{4\rho_m c_m \lambda_l}} \exp\left[-\left(\frac{x^2}{\lambda_l} + \frac{y^2}{\lambda_t}\right) \times \frac{(\rho_w c_w)^2 u^2}{16\lambda_l} \frac{1}{\theta} - \theta \right] \frac{d\theta}{\theta} \right) \right) =$$

$$\sum_{l=1}^{m}\sum_{k=1}^{p} q_{k,l}\, \omega_{k,l}^{t,i,j} \tag{3-5}$$

where p is the number of BHEs and m is the number of time steps. The temperature difference at a location (i,j) is obtained by the sum of the temperature differences exerted by each individual BHE k, with load q_l applied during time step l. Using Eq. 3-5, the ground temperature change from multiple BHEs, each with different time variable energy loads, including convective heat transport, can be estimated.

The term $\omega_{k,l}^{t,i,j}$ represents the response factor of BHE *k* at a position (*i,j*) within the BHE field at time step $l \in \{1,\ldots,m\}$, with reference to the current time step $t \in \{1,\ldots,m\}$ and $l \leq t$, given $\Delta x = (i - x_k)$ and $\Delta y = (j - y_k)$. By merging $q_{k,l}$ and $\omega_{k,l}^{t,i,j}$ into vectors of the form $\vec{q} = (q_{1,1},\ldots,q_{p,1},\ldots,q_{p,m})$ and $\vec{\omega}^{t,i,j} = (\omega_{1,1}^{t,i,j},\ldots,\omega_{p,1}^{t,i,j},\ldots,\omega_{p,m}^{t,i,j})$, Eq. 3-5 is rewritten as:

$$\Delta\vec{T}_{i,j}(t,\vec{q}) = \vec{q}(\vec{\omega}^{t,i,j})^T \tag{3-6}$$

where $\Delta\vec{T}_{i,j}(t,\vec{q})$ is the actual temperature change in the underground at position (*i,j*) and time step *t*, derived from the superposition of all BHEs in the field with the temporal load pattern $\vec{q}$.

3.2.2 Linear optimization procedure

The prime objective is to keep the maximum observed cooling of the underground $\max(\Delta\vec{T}_{i,j})$, caused by heat extraction through BHEs, as small as possible for the entire time span *t*. If extreme local cooling is avoided, the temperature distribution in the subsurface becomes smoother. This ideally results in a better efficiency of the heat pump, which is heavily influenced by the heat carrier fluid temperature of the BHE field, and consequently is controlled by the subsurface temperature. Another goal is the mitigation of the environmental impact of the system, which can play a role in case of environmental constraints for the design of BHE fields. Thus the objective function of the proposed load assignment optimization reads:

$$\text{minimize}(\max(\Delta\vec{T}_{i,j})) \tag{3-7}$$

With reference to the definition of $\Delta\vec{T}_{i,j}(t,\vec{q})$ given in Eq. 3-6, the objective function can also be expressed as:

$$\arg\min\left(\max(\Delta\vec{T}_{i,j}(t,\vec{q}))\right) \qquad \forall(i,j,t)\in S \tag{3-8}$$

where $\vec{q}$ is the decision variable and S is a set of all spatial and temporal reference points defined by 3-tuples (i,j,t).

In some cases the maximum overall temperature change in the subsurface may not be influenced by the load assignment for certain time steps, depending on the field thermal parameters, the given load pattern and the inertia of the system. To capture these special cases, a secondary objective is introduced, which additionally minimizes the maximum temperature change within every single time step l of the defined load pattern:

$$\arg\min\left(\sum_{l=1}^{m}\max(\Delta\vec{T}_{i,j}(l,\vec{q}))\right) \qquad \forall(i,j,t)\in S \quad t=l \tag{3-9}$$

To obtain a single objective function, which is sufficient for the given optimization problem, both Eqs. 3-8 and 3-9 are combined to:

$$\arg\min\left(w\cdot\max(\Delta\vec{T}_{i,j}(t,\vec{q}))+\sum_{l=1}^{m}\max(\Delta\vec{T}_{i,j}(l,\vec{q}))\right) \qquad \forall(i,j,t)\in S \tag{3-10}$$

where the second objective is only subsidiary and thus the primary objective is assigned a higher weight w than the secondary objective. In this study, w is set to 100.

To fulfill the energy demand required from the BHE field and to bar the optimizer from converging to the trivial solution, which is simply a complete switch-off of the BHE field, the adherence to the given energy demand is defined as a constraint. The sum of the loads $q_{k,l}$ for each time step l has to equal to the required energy E_l for the given time step:

$$E_l=\sum_{k=1}^{n}q_{k,l} \qquad l=1\ldots m \tag{3-11}$$

A more detailed explanation of the structure of the resulting equation system can be found in [12].

3.3 Application case

3.3.1 Parameter settings and analytical model set-up

In our case-study, 25 BHEs are arranged in a square lattice that is analytically simulated by the superposition of Eq. 3-5 (Figure 3-1). The distance between the BHEs is 10 m ($\Delta x = \Delta y =$ 10 m) and the installation depth is 100 m. The subsurface is approximated as homogeneous isotropic media, with given properties as listed in Table 3-2, and a constant groundwater flow velocity is assumed in the *x*-direction (W-E). The annual energy load pattern, which has to be fulfilled, is given in Figure 3-2. It was elaborated assuming a heat transfer rate of 50 W m^{-1} [29], with an annual runtime of 1,800 hours, which results in a total energy extraction of 225 MWh per year. The total energy extraction is subdivided into twelve monthly energy demands that reflect a seasonal operation mode in Central Europe, with exaggerated BHE use during the winter. The load pattern is repeated throughout the ten years of simulation. The optimization procedure distributes the monthly loads among the individual BHEs while minimizing the relative temperature changes in the ground as estimated by the analytical solution.

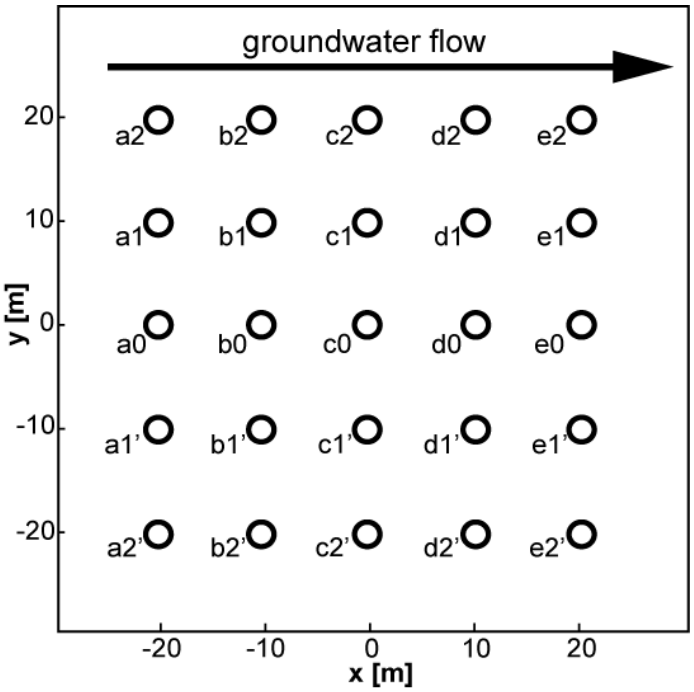

Figure 3-1. Geometric arrangement and indices of simulated and optimized 25 BHEs.

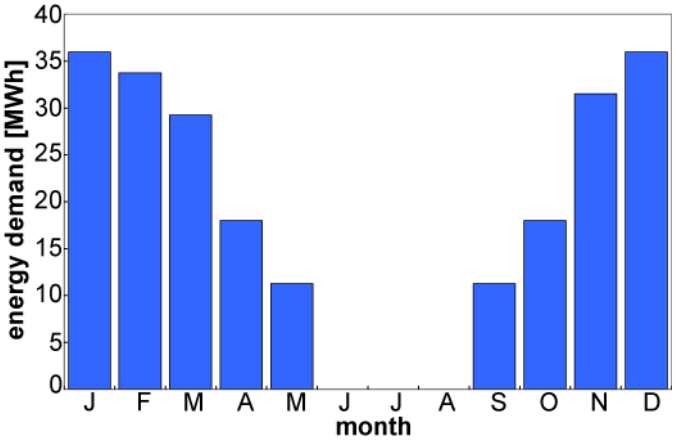

Figure 3-2. Monthly energy demand of the BHE field assuming a specific energy extraction of 50 W m^{-1} and 1,800 operating hours per year.

Table 3-1. Scenario-specific groundwater seepage velocities, v_a, and corresponding Péclet numbers, *Pe*.

scenario	v_a (m s^{-1})	*Pe* [-]
1	6.7×10^{-8}	0.4
2	1.0×10^{-7}	0.5
3	1.3×10^{-7}	0.7
4	1.7×10^{-7}	0.9
5	2.0×10^{-7}	1.1
6	2.3×10^{-7}	1.2
7	2.5×10^{-7}	1.3
8	2.7×10^{-7}	1.4
9	3.0×10^{-7}	1.6
10	3.3×10^{-7}	1.8
11	3.8×10^{-7}	2.0
12	4.3×10^{-7}	2.3
13	5.3×10^{-7}	2.8
14	6.7×10^{-7}	3.5
15	8.7×10^{-7}	4.5

hydraulic gradient $i=1\times10^{-2}$

The Péclet number, *Pe*, for heat transport [30], as listed in Table 3-1, is a measure for the intensity of convection. It is calculated by:

$$Pe = \frac{v_a n L' \rho_w C_w}{\lambda_m} \tag{3-12}$$

with *L'* as the characteristic length, which, in this work, is set to the grid distance between the BHEs (10 m). Based on this definition, the Péclet number indicates the ratio between the heat transported by the moving groundwater and the heat solely transported by conduction.

Table 3-2. Parameter specifications for application case.

parameter	value
porosity (n)	0.26
density of solid (ρ_s)	2.65×10^3 kg m^{-3}
density of water (ρ_w)	1.00×10^3 kg m^{-3}
volumetric heat capacity of solid (C_s)[1]	2.40×10^6 J m^{-3} K^{-1}
volumetric heat capacity of water (C_w)	4.19×10^6 J m^{-3} K^{-1}
thermal conductivity of solid (λ_s) [1]	2.4 W m^{-1} K^{-1}
thermal conductivity of water (λ_w)	0.6 W m^{-1} K^{-1}
longitudinal dispersivity (α_l)	1.0 m
transverse dispersivity (α_t)	0.1 m
length of the borehole (L)	100 m
only used for the numerical model:	
undisturbed temperature (T_u)	12°C
borehole diameter (d)	0.15 m
volumetric flow rate[2] (Q)	4×10^{-4} m^3 s^{-1}
dynamic fluid viscosity[3] (μ)	1.14×10^{-3} kg m^{-1} s^{-1}
density of circulating fluid[2] (ρ_w)	1,000 kg m^{-3}
borehole thermal resistance (R_b)	0.07 K W^{-1} m^{-1}
borehole internal thermal resistance (R_a)	0.25 K W^{-1} m^{-1}

[1] [26]; [2]circulating fluid is water [31]; [3]at 15 °C

3.3.2 Numerical simulation

Even if line-source-based simulation of BHE is standard, it is based on several simplifying assumptions. Among these are ideal, homogeneous conditions in the ground, which often do not exist. A relevant assumption for BHE field simulation is that the energy loads assigned to each BHE is known. In reality, however, energy extraction is achieved by circulating a cold heat carrier fluid, and the established temperature gradient forces conductive heat transfer from the ground. This means that the ground temperature in a BHE field is self-regulatory, and substantial local temperature anomalies thus are mitigated by smaller heat extraction from cold regions. In contrast, our approach is based on computationally efficient simulation and the optimization of loads. This presumes that working loads can be adjusted directly, e.g. by controlling the temperature of the heat carrier fluid. Showing that this control is reasonable depends on the benefit in comparison to standard practice, which means that all BHE in a

field are operated similarly. To examine this in more detail, numerical simulations are carried out that compare the load-optimized strategies to non-optimized BHE operation.

Transient heat transport simulations for the fifteen scenarios are performed using the finite element code FEFLOW (version 6) [32]. A three-dimensional model with 100 layers of 1 m thickness (200 m × 200 m × 100 m), representing a homogeneous confined aquifer with steady flow, is set up. Twenty-five BHEs, each with a length of 100 m, are implemented. An initial uniform undisturbed temperature of 12°C is assigned to the model, and further settings are given in Table 3-2. We chose the implemented analytical method of Claesson and Eskilson [33] for simulating the local heat transport processes within single U-type BHEs. The BHEs are operated using the single-load model [34,35]. Monthly loads are entered by scheduling operative hours of each borehole per month. For the non-optimized case, the operative hours per BHE are uniformly assigned. In contrast, for the optimized scenarios, we iteratively adjusted the operative hours for each BHE to achieve the determined optimal loads. All scenarios are simulated for 10 years and temperatures of the entire field are recorded at the end of each month. Additionally, the detailed numerical model allows for the monitoring of temperatures at the inlet and outlet of each BHE.

3.3.3 Simulation time and steady state condition considerations

The convective heat flow, in addition to conduction, further compensates the deficit from permanent energy extraction. The higher the groundwater flow velocity is, the less pronounced the temperature changes close to BHEs are. As a result, the time to reach steady state is shorter at high velocity [6,18] This is also relevant for the 15 scenarios inspected in our study. Due to the different groundwater flow velocities, some scenarios reach steady-state condition at early times, while others show a transient temperature change until the end of the examined total operation time of 10 years. This is visualized in Figure 3-3, where the evolution of mean temperature changes for all scenarios is compared.

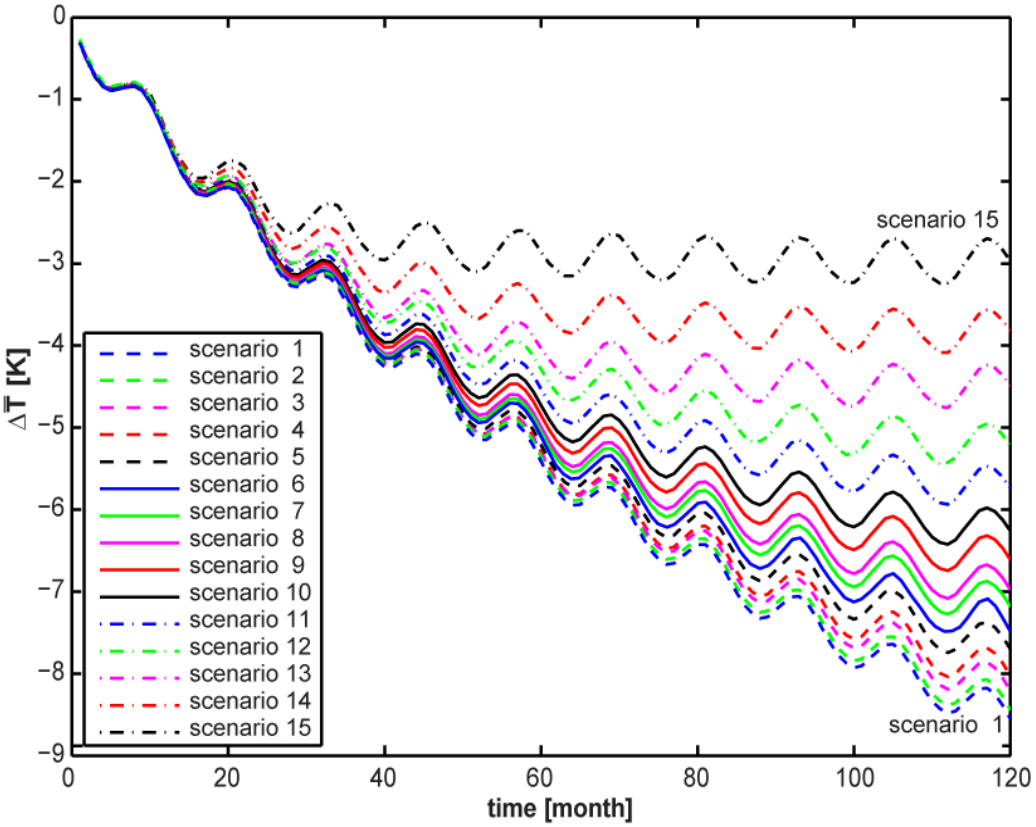

Figure 3-3. Time-dependent mean temperature changes $\Delta\overline{T}$ within non-optimized BHE field (area of 40 m x 40 m) at a depth of 50 m. Dashed lines correspond to sc. 1 to 5, solid lines to sc. 6 to 10 and dash-dotted lines to sc. 11 to 15.

The mean temperature change is estimated by:

$$\Delta\overline{T} = (m \times n)^{-1}\left(\sum_{i=1}^{m}\sum_{j=1}^{n}\Delta T_{ij}\right) \tag{3-13}$$

where ΔT is the temperature change at each location (i,j) within the area $m \times n$ where the BHEs are located. All the undulating time series in Figure 3-3 reflect the seasonal energy extraction, but those scenarios with high velocity are less affected. Temperature decrease is less pronounced and, in particular for sc. 12-15, the trends stabilize, which indicates that a steady state is (nearly) reached. We compared the maximum difference of $\Delta\overline{T}$ at the end of the last two successive years. For these scenarios, this difference is smaller than 1% after 72 (sc. 15), 84 (sc. 14), and 96 (sc. 13) months. With a criterion of 2%, scenario 12 takes 108 months to reach a steady state. In summary, high flow velocities (Pe > 2.3) allow for a (quasi) steady-state condition before the end of the considered period of 10 years is reached, whereas

conduction in scenarios 1 to 11 (Pe < 2.3) is significant enough so that transient conditions prevail.

3.4 Results and discussion

3.4.1 Temperature fields and profiles

From the 15 scenarios, four are sampled that span the range of inspected groundwater flow velocities: the two extremes with the lowest (sc. 1, Pe = 0.4) and highest velocity (sc. 15, Pe = 4.5), as well as intermediate cases sc. 5 (Pe = 1.1) and sc. 10 (Pe = 1.8). Figure 3-4 depicts the central (z = 50 m depth) temperature distribution from numerical simulation for the optimized and non-optimized cases. A total operation time of 10 years is simulated, and the plotted temperatures reflect the conditions in December, that is, in the middle of the heating season. All BHE fields supply the given seasonal energy demand (Figure 3-2), and accordingly, extract the same amount of energy each month.

As expected, the temperature anomaly that is induced from operating the BHE field is influenced by groundwater flow. At very small velocity, the most pronounced ground cooling is observed within the field, and it nearly symmetrically diminishes outside the field. The temperature plume moves downgradient at increasing velocity, is displaced from the centre of the BHE field, and appears significantly elongated for the most convection dominated sc. 15. For each scenario, the plumes have a comparable shape independent of the operation mode. However, strongest cooling is observed for the non-optimized cases. The optimization regulates individual BHE operation in order to avoid local cooling in favour of smoother temperature changes. This is most beneficial for conduction-dominated conditions.

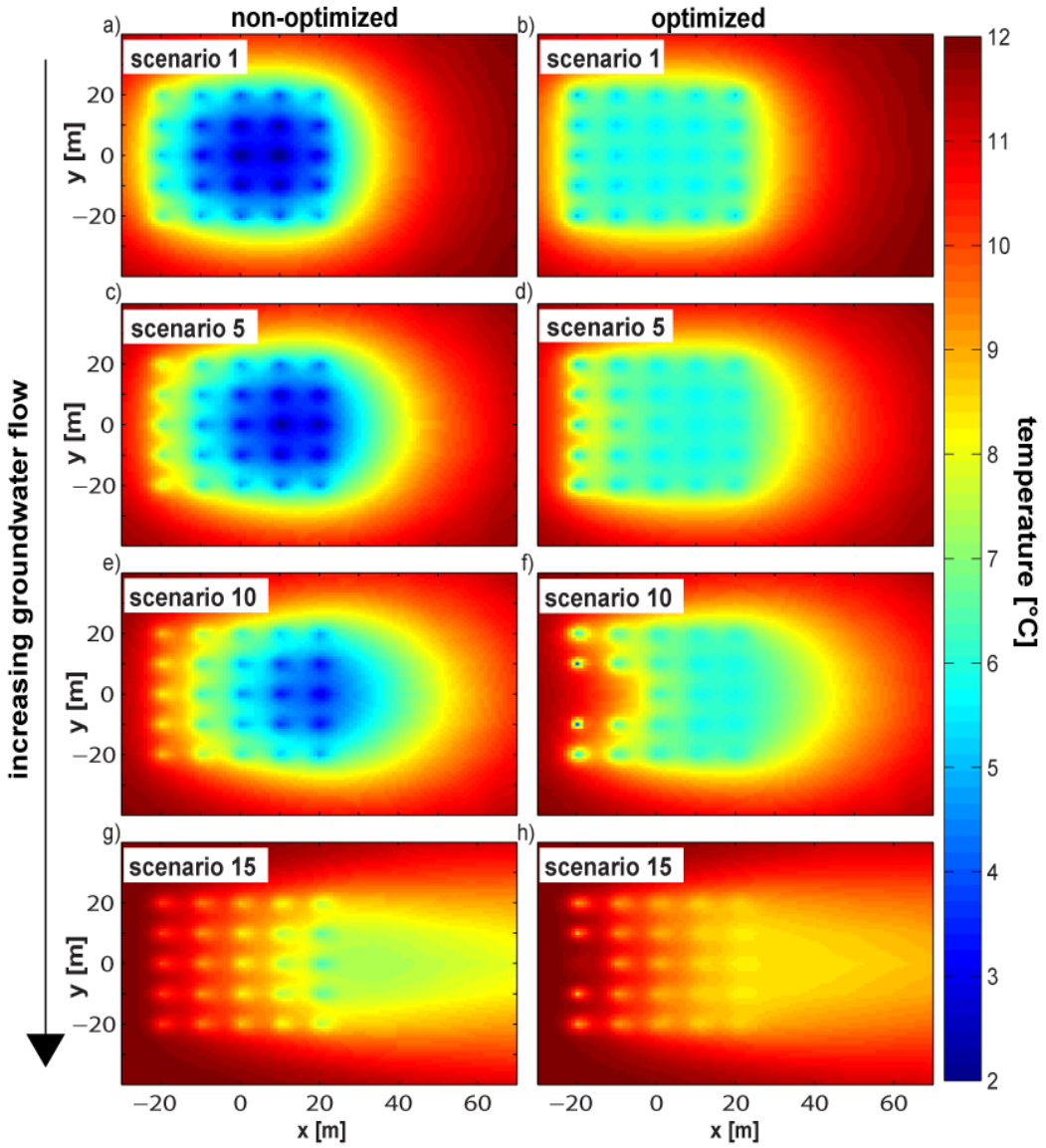

Figure 3-4. Spatial temperature distribution for the non-optimized (subplots a, c, e and g) and optimized cases (subplots b, d, f and h) for selected scenarios (sc. 1, 5, 10 and 15) after ten years (31st December). The depicted fields correspond to the temperature distribution at the 50th layer (z = 50 m).

For instance, in sc. 1, the temperature maximally decreases by 10.4 K without and by only 7.3 K with optimization, which means a difference of more than 3 K. This difference in max ΔT, as well as overall cooling, becomes smaller the more groundwater flow balances the mounting energy deficits by convection. For the conditions with highest velocity, sc. 15, max ΔT reaches 5.7 K without and 3.7 K with optimization. In this non-optimized scenario, the centre of the cold plume is found around the last downgradient column (‘e’, Figure 3-1) of the BHE array. This centre is smoothed when the BHEs are individually regulated, and also shifted further downgradient, that is, if possible outside of the BHE field.

A closer insight is provided by Figure 3-5, which inspects the differences in max ΔT for the selected four scenarios in the *x*-direction of groundwater flow and perpendicular to it, both along the centreline of the BHE array. Negative values indicate that the temperature at a given location of the non-optimized scenarios is lower than for the optimized ones and vice versa.

As expected, the temperature differences perpendicular to the regionally uniform groundwater flow are symmetric (Figure 3-5a). Since optimization especially mitigates the energy extraction by the BHEs in the centre of the field, differences are most significant at BHEs 'c0' and 'c1'. The higher the groundwater flow velocity, the more convective heat is supplied and thus the smaller the differences between optimized and non-optimized scenarios. For sc. 15, convection is exploited more by the optimized lateral BHEs, 'c2', which is reflected by the slightly stronger cooling at these positions of the temperature difference curves.

Along the horizontal centreline (Figure 3-5b), each trend is specific for the simulated conditions with highest differences at the locations of the BHEs. The simulated cooling with optimal loads of sc. 1, 10 and 15 is always minor. Sc. 5 is special – it shows a stronger cooling (difference > 1 K) at the location of the first BHE ('a0', Figure 3-1). Apparently, this is compensated by the higher temperatures at the other downgradient BHE locations (difference of nearly -4 K). The energy extraction rate of BHE 'a0' for this month is 32.66 W m^{-1}, while for the downgradient BHEs 'b0'–'e0' have optimized rates of 25.18 W m^{-1}, 15.68 W m^{-1}, 11.33 W m^{-1} and 11.45 W m^{-1}. The energy extraction rates for the same BHEs in the non-optimized case are 22.88 W m^{-1}, 22.88 W m^{-1}, 22.96 W m^{-1}, 22.88 W m^{-1} and 22.96 W m^{-1} ('a0'–'e0'). Obviously, the concerted BHE array takes advantage of the energy carried by the groundwater more efficiently. This exemplarily shows that for a given month in the optimal load pattern, each BHE is adjusted depending on position, groundwater flow velocity and the current time step.

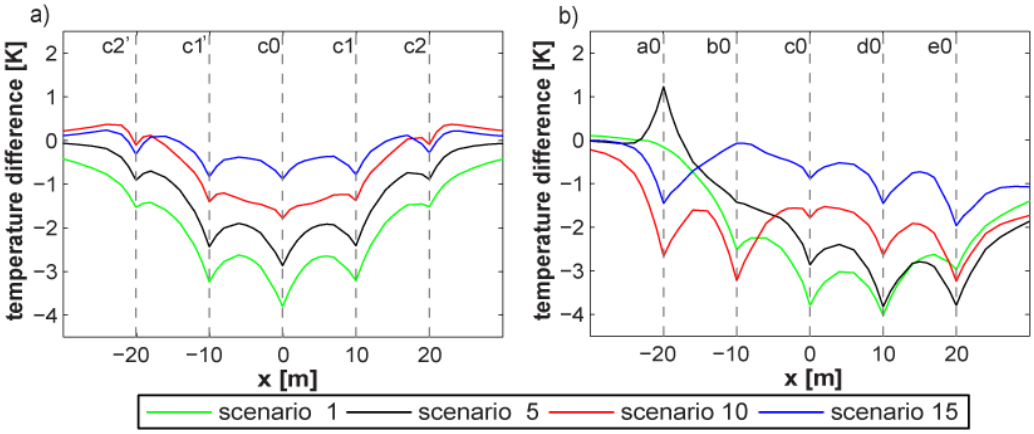

Figure 3-5. Temperature difference between non-optimized and optimized cases for selected scenarios: a) central column ('c', Figure 1) perpendicular to flow, and b) central row (a0 – e0, Figure 1) in direction of groundwater flow.

An important feature of Figure 3-5, particularly in the direction of groundwater flow (Figure 3-5b), is the occurrence of four different curve shapes. These four are also characteristic for the other scenarios. Similar curves are observed for sc. 1 to 2 ($Pe \leq 0.5$), sc. 3 to 6 ($Pe = 0.7 - 1.2$), sc. 7 to 12 ($Pe = 1.3 - 2.3$), and sc. 13 to 15 ($Pe \geq 2.8$). They, apparently, reflect that a small number of optimized load patterns exists, which is selected and adjusted depending on the groundwater flow velocity and supplied energy demand.

3.4.2 Optimized load patterns

In Figure 3-6, the spatial temperature distributions during the last entire heating season (9th year) of the selected optimized scenarios are shown. The relative contribution (i.e. monthly normalized load) of each BHE is visualized by the grey scale of the circle marker. The figures show the initial stage of the heating season (in September), the month with highest demand (in January) and the last month of the heating season (in May). At the beginning of the heating season, for the scenarios with higher groundwater flow velocity (sc. 10 and 15), the BHEs located downgradient (columns c, d, e; Figure 3-1) are activated first. In order to maximize energy extraction from outside the BHE field, the BHEs at the fringe provide most of the energy demand.

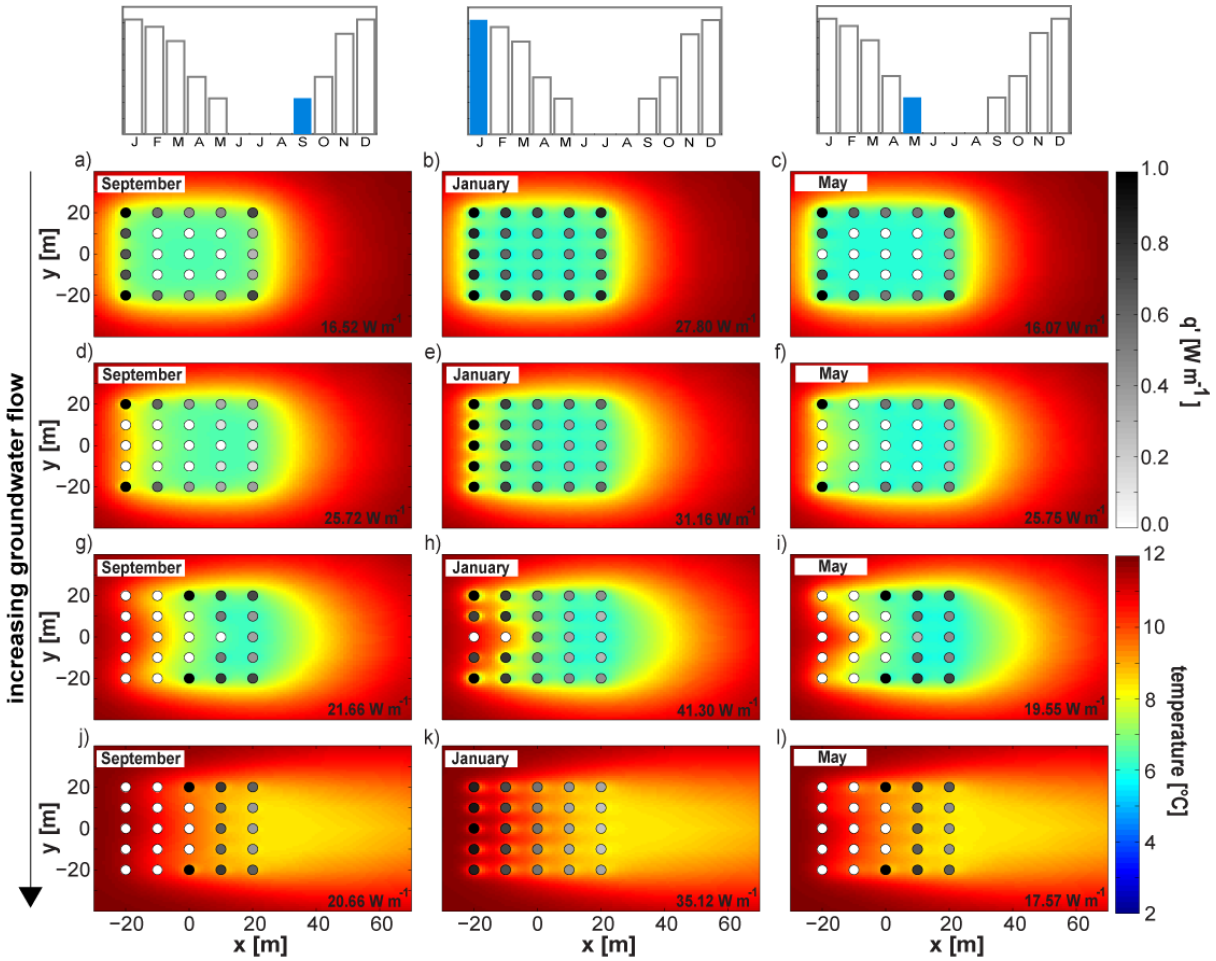

Figure 3-6. Temperature distribution and BHE extraction rates for the optimized selected scenarios (scenarios 1, 5, 10 and 15, from top to bottom) for three months of the entire last heating period (9th year). Each circle represents a BHE, with its corresponding normalized load in greyscale (maximal load is shown in each plot). Darker colour shades denote higher BHE loads. The subsurface temperature distribution at a depth of 50 m is illustrated with colours.

The upgradient BHEs, as well as the central BHEs in the columns ‘c’ and ‘d’, are shut off. An attractive strategy, evidently, is keeping the temperature highest in the centre and preparing the system for the higher energy demand scheduled for the next months. The energy demand reaches its maximum in January, all BHEs in sc. 15 are on and almost all (23 of 25 BHEs) are activated in sc. 10. At this stage, the upgradient BHEs in column ‘a’ have the highest energy extraction rates. This way, the system takes advantage of the surplus energy brought by the moving groundwater. The extraction rates successively decrease downgradient. Then, at the end of the heating season in May, the load pattern of the BHEs is similar to that in September.

For the scenarios with lower groundwater flow velocity (sc. 1 and 5), the operation strategy is different. At the beginning of the heating season, again the BHEs in the centre are off.

However, now, all BHEs at the lateral rows are activated. In sc. 1, the highest loads are assigned to the BHEs in the upgradient corners (position ‘a2’) and they continuously shrink downgradient. In sc. 1 groundwater flow is minimal, and the optimal load pattern accentuates all corner BHEs (‘a2’, ‘e2’). This scheme is also kept for the peak of the heating season in January. Both scenarios show a similar use of the BHEs, with more upgradient energy extraction. In the more conductive scenario (sc. 1), the highest energy extraction rates are still in the corners and decrease towards the centre. Again, at the end of the heating season, a similar operation of the BHEs is observed as in the beginning.

In general, two operation patterns for the 25 examined BHE fields are identified. For high groundwater flow velocities, the operation of the BHE follows a column-wise strategy. In all scenarios 12 to 15, the optimal tactic for seasonal energy extraction is to start with the downgradient BHEs, and then activate increasingly the upgradient ones, while reducing the loads downgradient. The downgradient movement of the cooled zones is strategically integrated in the optimized load pattern. The optimal usage of a column thus depends on the energy demand of each consecutive month. For lower groundwater velocities, conduction comes more into the fore and hence, a more radial pattern is observed. BHEs at the corners are turned on first and run permanently, with a higher emphasis on the downgradient ones depending on the role of convection. Under low-convection conditions, these BHEs have least interaction with neighbouring BHEs. In contrast, central BHEs mean strongest competition for conductive heat supply. Accordingly, the interior BHEs are activated or deactivated in a radial way. For the inspected total simulation time of 10 years, this radial pattern is most apparent for the high conduction end members, sc. 1, 2 and 3. In particular, for sc. 4-11, a mixed pattern with column-wise and radial scheme is found.

3.4.3 Mean temperature in BHE field and heat carrier fluid

In order to compare optimized to standard operation mode, Eq. 3-13 is applied for the three months of the final heating season. Depending on the scenario-specific *Pe*, the induced mean temperature changes $\Delta\overline{T}$ for January is shown in Figure 3-7a. In addition, the difference of $\Delta\overline{T}$ between optimized and non-optimized conditions for September, January and May is depicted. This difference appears to be always positive, it reaches between 0.37 K and 1.96 K, and it is nearly the same for the different months. This means that BHE field optimization does not only mitigate local cooling but also the average temperatures in the field are less altered. Since groundwater flow compensates, to some extent, the deficits from energy extraction, the difference shrinks in the more convection-dominated scenarios. A nearly linear trend is observed, whereas for the most extreme cases, sc. 14, 15 ($Pe \geq 3.5$), this difference becomes very small and stabilizes.

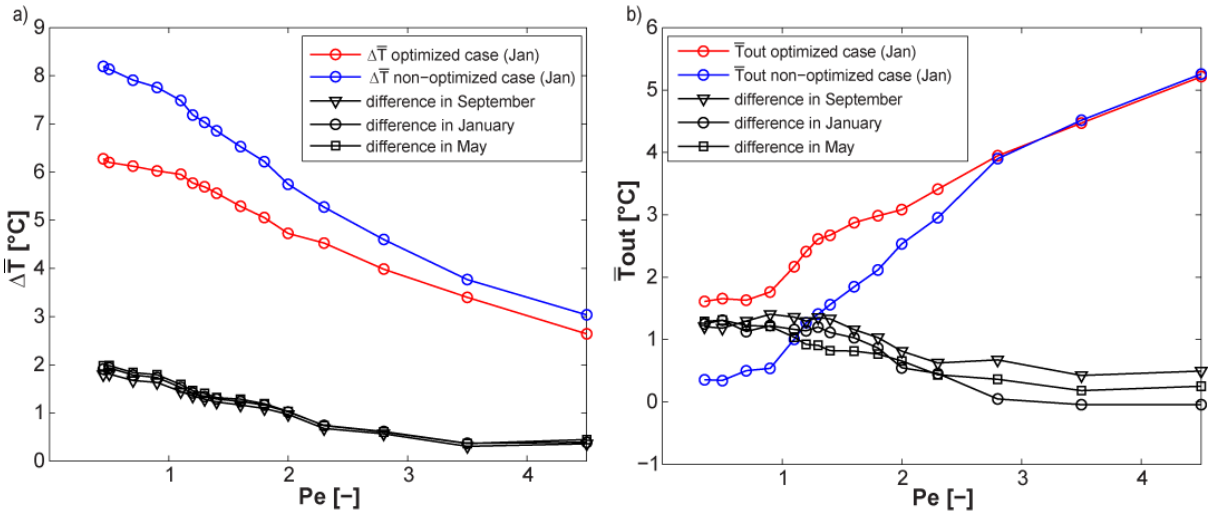

Figure 3-7. a) Mean temperature change $\Delta\overline{T}$ in the BHE field at a depth of 50 m for all scenarios (optimized and non-optimized); b) monthly mean temperature $\overline{Tout}$ of the BHE working fluid. The trends are shown only for January (red and blue lines with circles for optimized and non-optimized, respectively), the black curves show the difference between optimized and non-optimized cases in September, January and May.

The efficiency of a heat pump in GSHP systems strongly depends on the temperature of the heat carrier fluid circulating through the BHE (e.g. Bernier [23]). If aboveground thermal losses are negligible, this temperature equals the temperature at the outlet of a BHE (*Tout*).

Figure 3-7b compares the mean (mixed) temperatures for all BHEs $\overline{T}out$ for the optimized and non-optimized cases in January of the 10th year. Also, similar to Figure 3-7a, the differences between both cases in January, as well as in September and May, are shown. These temperatures are obtained by averaging the monthly BHE outflow temperature predicted by the numerical model. Slight numerical inaccuracies are reflected in the non-uniform curves in Figure 3-7b. The finite element mesh for this study was developed following the direct estimation of the nodal distance for BHE nodes [36]. However, in order to keep the computational burden at a minimum, the mesh was discretized in two different sections, one very dense around the BHE field and a coarser mesh outside of the BHE field. The slightly non-symmetrical distribution of the elements probably causes small variations in the borehole wall temperatures, which are used to calculate $\overline{T}out$.

Optimized configurations result, although not explicitly included in the optimization problem formulation, generally in higher output temperatures $\overline{T}out$ of the heat carrier fluid. The January values show that the difference between optimized and non-optimized depend on the groundwater flow velocity. Roughly, three characteristic ranges for *Pe* can be distinguished: For $Pe < 1$ (sc. 1-4), conduction dominates, the output temperatures are independent of the flow velocity, and benefit from optimization is maximal. Here, the heat carrier fluid is more than 1 K higher. Between $Pe = 1.1$ (sc. 5) and 2.3 (sc. 12), as observed for the average ground temperatures in Fig. 3-7a, the impact from convection comes more into the fore, and cooling of the ground is mitigated. Since, for the study case, the seasonal energy demand is kept constant, differences between optimized and non-optimized operation mode decline. For very high velocities, sc. 13-15 ($Pe \geq 2.8$), we observe no difference or the difference remains constant on a small value as shown for September and May. However, note that the averaging method used for estimating $\overline{T}out$ disregards local variations at individual BHEs, which may be of relevance in practice when more than one heat pump is operated.

3.5 Conclusions

Low enthalpy geothermal technologies are established and, once installed, supply space heat and domestic hot water for decades. Fields of multiple adjacent BHEs, which in the long run, cool the ground over large volumes, often accomplish high-energy demand. Often, aquifers exist, which are affected by the cooling, while convective heat transport from flowing groundwater additionally balances the deficits. Integrating the convection into the planning of BHE fields is not common yet, and it is only done indirectly by introducing an effective thermal conductivity that is higher than the actual one (e.g. Wagner et al. [37]). The study here demonstrates that for a given BHE field, case-specific individual BHE operation mode offers benefits to standard applications, where BHEs are all operated the same. As an objective, we chose to avoid extreme local cooling of the ground while guaranteeing a given seasonally variable energy demand. An efficient linear-programming based solution procedure that combines superimposed moving line source equations is developed, and the performance of optimized solutions is inspected by post-optimization high-resolution numerical models.

The major findings are that ideal adjustment of BHE-specific, monthly energy extraction rates (loads) produces typical load patterns that depend on time and groundwater flow velocity. The patterns change from the beginning of the heating season to the peak demand month, and those at the end are similar to those at the beginning of the season. Formulating the optimization problem for the entire operation period (in our study case 10 years) enables pro-active management where, for example, the BHE active in the early season prepares efficient operation in the peak time. Also, long-term transient conditions, which exist in the low groundwater flow velocity scenarios of our study, provoke a slight change in the patterns from year to year. If groundwater flow is small (here $Pe < 1$), radial patterns are suggested, where most energy is extracted by the BHEs at the borders. Increase of flow velocity

generates optimized patterns that, advantageously, are oriented at the flow direction. For example, in the lattice BHE field in the study case, a column-wise pattern is found, where the season starts and ends, with downgradient BHE operation.

We inspected the role of increasing convection for a fixed energy demand, and as a result, benefits from optimization decrease with flow velocity. In practice, however, higher velocity may be accounted for by a higher effective thermal conductivity, and thus the specific energy extraction in standard applications is augmented. Therefore, due to the assumptions particular for the study case in this work, potential benefits from optimized BHE operation patterns have to be clarified based on the individual conditions. Even so, it is shown that improvements could always be achieved by automatic optimization, with more balanced ground cooling and mostly higher temperatures in the heat carrier fluid. These may be further improved by also considering the positioning of the BHE in the optimization framework, and if energy injection for cooling of buildings during the summer is included.

3.6 References

[1] L. Ozgener, A. Hepbasli, I. Dincer, A key review on performance improvement aspects of geothermal district heating systems and applications, Renewable and Sustainable Energy Reviews 11 (2007) 1675-97.

[2] J.W. Lund, D.H. Freeston, T.L. Boyd, Direct Utilization of Geothermal Energy 2010 Worldwide Review, In: Proceeding of the 2010 World Geothermal Congress, 2010.

[3] P. Bayer, D. Saner, S. Bolay, L. Rybach, P. Blum, Greenhouse Gas Emission Savings of Ground Source Heat Pump Systems in Europe: A Review, Renewable and Sustainable Energy Reviews 16 (2012) 1256-1267.

[4] H. Fujii, R. Itoi, J. Fujii, Y. Uchida, Optimizing the design of large-scale ground-coupled heat pump systems using groundwater and heat transport modeling, Geothermics 34 (2005) 347-64.

[5] Q. Gao, M. Li, M. Yu, J.D. Spitler, Y.Y. Yan, Review of development from GSHP to UTES in China and other countries, Renewable & Sustainable Energy Reviews 13 (2009) 1383-94.

[6] N. Diao, Q. Li, Z. Fang, Heat transfer in ground heat exchangers with groundwater advection, International Journal of Thermal Sciences 43 (2004) 1203-11.

[7] T. Katsura, K. Nagano, S. Narita, S. Takeda, Y. Nakamura, A. Okamoto, Calculation algorithm of the temperatures for pipe arrangement of multiple ground heat exchangers, Applied Thermal Engineering 29 (2009) 906-19.

[8] L. Rybach, W.J. Eugster, Sustainability aspects of geothermal heat pump operation, with experience from Switzerland, Geothermics 39 (2010) 365-9.

[9] G. Hellström, B. Sanner, EED – Earth Energy Designer, Version 1.0, User's Manual. Prof. Dr. Knoblich & Partner GmbH, Wetzlar, 1997.

[10] J.D. Spitler, GLHEPRO: a design tool for commercial building ground loop heat exchangers, In: Fourth International Heat Pumps in Cold Climates Conference, 2000.

[11] G. Hellström, L. Mazzarella, D. Pahud, Duct Ground Storage Model – TRNSYS version. Department of Mathematical Physics, University of Lund, Lund, 1996.

[12] M. de Paly, J. Hecht-Méndez, M. Beck, P. Blum, A. Zell, P. Bayer, Optimization of energy extraction for closed shallow geothermal systems using linear programming, Geothermics, in press.

[13] P. Eskilson. Thermal Analysis of Heat Extraction Boreholes. Department of Mathematical Physics. University of Lund, Lund, 1987.

[14] M.G. Sutton, D.W. Nutter, R.J. Couvillion, A ground resistance for vertical bore heat exchangers with groundwater flow, Journal of Energy Resources Technology 125 (2003) 183-9.

[15] N. Molina-Giraldo, P. Bayer, P. Blum, Evaluating the influence of thermal dispersion on temperature plumes from geothermal systems using analytical solutions, International Journal of Thermal Sciences 50 (2011) 1223-31.

[16] N. Molina-Giraldo, P. Blum, K. Zhu, P. Bayer, Z. Fang, A moving finite line source model to simulate borehole heat exchangers with groundwater advection, International Journal of Thermal Sciences 50 (2011) 2506-13.

[17] H.S. Carslaw, J.C. Jaeger, Conduction of Heat in Solids. Oxford University Press, New York, 1959.

[18] A.C. Chiasson, S.J. Rees, J.D. Spliter, A preliminary assessment of the effects of ground-water flow on closed-loop ground-source heat pump systems, ASHRAE Transactions 106 (2000) 380-93.

[19] S. Hähnlein, N. Molina-Giraldo, P. Blum, P. Bayer, P. Grathwohl, Cold plumes in groundwater for ground source heat pump systems (in German), Grundwasser 15 (2010) 123-33.

[20] R. Fan, Y.Q. Jiang, Y. Yao, D. Shiming, Z.L. Ma, A study on the performance of a geothermal heat exchanger under coupled heat conduction and groundwater advection, Energy 32 (2007) 2199-209.

[21] C.K. Lee, H.N. Lam, Effects of groundwater flow direction on performance of ground heat exchanger borefield in geothermal heat pump system using 3-D finite difference method, In: 10th IBPSA Building Simulation Conference, 2007.

[22] H. Wang, C. Qi, H. Du, J. Gu, Thermal performance of borehole heat exchanger under groundwater flow: A case study from Baoding, Energy and Buildings 41 (2009) 1368-73.

[23] M. Bernier, Closed-loop ground-coupled heat pump systems, ASHRAE Journal 48 (2006) 12-9.

[24] S. Haehnlein, P. Bayer, P. Blum, International legal status of the use of shallow geothermal energy, Renewable and Sustainable Energy Reviews 14 (2010) 2611-25.

[25] C. Butscher, P. Huggenberger, A. Auckenthaler, D. Baenninger, Risk-oriented approval of borehole heat exchangers (in German), Grundwasser 16 (2011) 13-24.

[26] G. de Marsily, Quantitative Hydrogeology. Academic Press, Orlando, 1986.

[27] T. Metzger, S. Didierjean, D. Maillet, Optimal experimental estimation of thermal dispersion coefficients in porous media, International Journal of Heat and Mass Transfer 47 (2004) 3341-53.

[28] A. Chiasson, A. O'Connell, New analytical solution for sizing vertical borehole ground heat exchangers in environments with significant groundwater flow: Parameter estimation from thermal response test data, Hvac&R Research 17 (2011) 1000-11.

[29] VDI-Richtlinie. Thermal Use of the Underground, Part 2 (in German) in: V.D. Ingenieure, (Ed.). VDI-Verlag, Düsseldorf, 2001.

[30] P.A. Domenico, F.W. Schwartz, Physical and Chemical Hydrogeology, 2nd ed., John Wiley & Sons Inc., New York, 1990.

[31] R. Al-Khoury, T. Kolbel, R. Schramedei, Efficient finite element modeling of shallow geothermal systems, Computers & Geosciences 36 (2010) 1301-15.

[32] H.J.G. Diersch, FEFLOW 6- User's Manual. Wasy GmbH, Berlin, 2010.

[33] J. Claesson, P. Eskilson, Conductive heat extraction to a deep borehole: Thermal analyses and dimensioning rules, Energy 13 (1988) 509-27.

[34] S. Signorelli, T. Kohl, L. Rybach, Sustainability of production from borehole heat exchanger fields, In: Proceeding of the 29th Workshop on Geothermal Reservoir Engineering, 2004.

[35] L. Rybach, W.J. Eugster, Sustainability aspects of geothermal heat pumps, In: Proceedings 27th Workshop on Geothermal Reservoir Engineering, 2002.

[36] Wasy, White Papers Vol. 5. DHI-Wasy GmbH, Berlin, 2010.

[37] V. Wagner, P. Bayer, M. Kuebert, P. Blum, Numerical sensitivity study of thermal response tests, Renewable Energy 41 (2012) 245-253.

4. Evaluating MT3DMS for heat transport simulation of closed geothermal system[3]

Abstract: Due to the mathematical similarities between heat and mass transport, the multi-species transport model MT3DMS should be able to simulate heat transport if the effects of buoyancy and changes in viscosity are small. Although in several studies solute models have been successfully applied to simulate heat transport, these studies failed to provide any rigorous test of this approach. In the current study we carefully evaluate simulations of a single borehole Ground Source Heat Pump (GSHP) system in three scenarios: a pure conduction situation, an intermediate case, and a convection-dominated case. Two evaluation approaches are employed: first, MT3DMS heat transport results are compared with analytical solutions. Second, simulations by MT3DMS, which is finite difference, are compared with those by the finite element code FEFLOW and the finite difference code SEAWAT. Both FEFLOW and SEAWAT are designed to simulate heat flow. For each comparison, the computed results are examined based on residual errors. MT3DMS and the analytical solutions compare satisfactorily. MT3DMS and SEAWAT results show very good agreement for all cases. MT3DMS and FEFLOW 2D and 3D results show good to very good agreement, except that in 3D there is somewhat deteriorated agreement close to the heat source where the difference in numerical methods is thought to influence the solution. The results suggest that MT3DMS can be successfully applied to simulate GSHP systems, and likely other systems with similar temperature ranges and gradients in saturated porous media.

[3] Reproduced from: Hecht-Méndez, J., Molina-Giraldo, N., Blum, P., Bayer, P., 2010. Evaluating MT3DMS for heat transport simulation of closed geothermal systems. Ground Water 48, 741-756.

4.1 Introduction

MT3DMS (Zheng and Wang 1999) is a widely used program for simulation of solute transport in porous media. Since the governing equations for solute transport are mathematically identical to those for heat transport, this program appears also applicable to simulation of thermal transport phenomena in saturated aquifers. This is demonstrated in recent case studies. Martin et al. (2001) used MT3DMS to simulate heat transport on Grand Cayman Island. Cathomen (2002) and Cathomen et al. (2002) applied MT3DMS to assess the ground water temperature distribution in an urban area of the Altach Municipality (Austria) under the influence of several ground source heat pump (GSHP) systems.

Using MT3DMS for heat transport in aquifers has limitations, because it is decoupled from the flow model. MT3DMS uses the flow regime predicted by flow simulators such as MODFLOW (Harbaugh et al. 2000) without feedback. However, in principle this is necessary, because temperature variation affects water viscosity and density, which effect hydraulic conductivity. Temperature variations in the shallow subsurface commonly are small, so simulation errors produced from using constant viscosity and density often are small and acceptable. Shallow geothermal systems produce conditions for which such errors are likely to be inconsequential. Evaluating the utility of MT3DMS for shallow geothermal systems is the topic of the presented study.

Geothermal energy is the form of energy stored as heat in the soil, rocks, and fluids below the surface of the solid earth. It is available almost everywhere and it represents an enormous source of energy which can be applied in, for example, electricity generation, process heating, and space heating (e.g. Clauser, 2006). Geothermal energy usage has shown a continuous and rapid development within the last decades. Considering the trends in global annual energy production of the different applications (Bertani 2005, Lund et al. 2005), for the period from 2000 to 2005, an annual growth rate of 10 % can be estimated. The use of this energy has

become attractive due to inherent savings of fossil fuels and relatively low CO_2 emissions. Blum et al. (2009) provide values for CO_2 savings when using ground source heat pump systems for heating or cooling of buildings. For instance, by using a ground source heat pump system for heating a single family house in central Europe, at least 35 % of additional CO_2 emissions can be avoided in comparison to conventional heating systems.

Geothermal systems for heating/cooling of building and facilities use heat available in the upper part of the subsurface (down to 400 m). This is often done via GSHP systems, which are installed underground, usually down to depths of 150 m. Two types of shallow geothermal systems can be generally distinguished, closed and open systems (Figure 4-1); the latter is defined as a groundwater heat pump (GWHP) system. In the current study closed shallow geothermal systems are considered and are referred to as GSHP. Closed systems employ one or more pipes or borehole heat exchangers (BHEs). The heat stored in the ground is mined through a segregate heat carrier fluid inside the BHE and extracted by a heat pump on the surface. In contrast, open systems operate with ground water production and injection wells; ground water at a certain temperature is directly brought to the surface. A comprehensive review of these systems is provided by Florides and Kalogirou (2007).

Depending on the use mode (heating or cooling), energy can be extracted or injected. Thus, the ambient aquifer temperature is disturbed and cold or warm plumes develop. These disturbances are compensated by lateral conductive heat transport and by convection due to moving water. The efficiency of geothermal technologies depends on the prevalent hydrogeological and thermal conditions. Proper installation and efficient maintenance requires an appropriate characterization of the heat transport processes, conduction and convection, in the subsurface.

Among others, Eskilson (1987), Chiasson et al. (2000), Diao et al. (2004), Fan et al. (2007), and Guimera et al. (2007) simulated the effects of ground water flow on the heat transfer into

the borehole heat exchangers (BHE) in vertical closed systems. A common conclusion is that, for material with high hydraulic conductivity and thus high discharge rates, ground water flow enhances heat transfer between BHEs and the surrounding aquifer. Therefore, it is essential to have tools that allow for the evaluation not only of technical aspects of GSHP systems but also the effects of ground water flow on the system efficiency and, further, the temperature changes in the aquifer exerted by the energy extraction or injection rates. Indeed, as recently mentioned by Ferguson (2009), this last aspect is closely related to the environmental impact and sustainability of such systems, and to the temperature propagation of one or several GSHP systems.

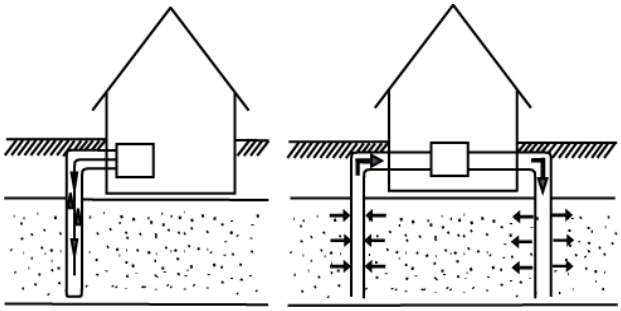

Figure 4-1. Scheme of shallow geothermal systems that are closed (left, ground source heat pump system) and open (right, groundwater heat pump system).

Numerical heat transport models are widely used, such as for design of BHEs, regional heat transport modeling, seasonal aquifer thermal energy storage and technico-economic system design (Tsang 1981, Chiasson 2000, Hellström and Schmidt 2005). The development of numerical codes for heat and solute transport has been closely related to the advent of more powerful computers. In an early stage of numerical simulation, only simple one-dimensional problems were conducted while, today, more complicated problems with complex boundary conditions can be efficiently handled (Anderson 2005). Heat simulation codes allow for simulating one, two, and three dimensional problems. Table 4-1 offers a comprehensive list of models that have been used or are potentially suitable for both convective and conductive heat transport simulations of shallow GSHP systems. Anderson (2005) provided a similar table;

Table 4-1 lists some additional codes not considered by Anderson (2005), but is still not considered to be exhaustive.

In these models the coupling of the ground water flow simulation and the heat transport calculation is done by means of Darcy´s velocity. Codes such as: AST/WOW, TRADIKON3D, and VS2H feature one-way coupling between flow and transport, i.e. the flow field is calculated once at the beginning of the overall simulation and then used as an input for the transport simulation without there being any feedback to the flow simulation. The remaining codes can be classified as fully coupled and can handle temperature dependencies of density and viscosity. Some codes (e.g. FEFLOW, FRACHEM and SHEMAT) couple hydraulic, thermal, and chemical processes. Such processes are common in deep environments with high temperatures; therefore these codes are also suitable for deep geothermal assessment (e.g. Hot Dry Rock, HDR). Others have specialized routines which allow for simulation of mechanical deformation processes (BASIN2, FRACHEM, FRACture, ROCKFLOW/GeoSys). Some routines were originally developed for assessing shallow geothermal systems, such as GSHPs or energy storage systems (e.g. HEATFLOW, THETA), and others specifically for GSHP simulations (e.g. AST/WOW, TRADIKON 3D). In addition to these numerical codes, there are other advanced routines such as HydroGeoSphere (finite elements, Therrien et al. 2006) and ParFlowE (finite differences, Kollet et al. 2009), which both allow for fully coupled simulations of surface flow, subsurface flow, and energy transport processes.

Table 4-1. Numerical codes suitable for heat transport simulations of shallow geothermal systems considering ground water flow (not meant to be exhaustive or complete).

Code Name	Numerical Method	Processes*	Coupling of Processes**	Availability	Comments	Reference
AST/TWOW***	FD	H, T	H → T	Commercial	3D, calculates near-field heat transport around BHEs	Schmidt and Hellström (2005)
BASIN2	FD	H,T, C	H ↔ T, M, CH	Free code	2D, simulates sedimentary basin development. Cross sectional view.	Bethke et al. (2007)
COMSOL***	FE	H, T, C	H ↔ T	Commercial	3D, multi-physics (more processes can be coupled)	Holzbecher and Kohfahl (2008)
FEFLOW***	FE	H, T , C	H ↔ T, M, C	Commercial	2D, 3D	Diersch (2002)
FRACHEM	FE	H, T, C	H ↔ T, M, C	Scientific	3D, used for Hot Dry Rock modeling.	Bächler (2003)
FRACture***	FE	H, T	H ↔ T, M	Scientific	3D, developed for Hot Dry Rock modeling	Kohl and Hopkirk (1995)
ROCKFLOW/GeoSys	FE	H, T , C	H ↔ T, C	Scientific	3D, fracture systems can be included. Allows for multi-phase flow	Kolditz et al. (2001)
HEATFLOW***	FE	H, T	H ↔ T	Free code	1D, 2D, 3D,	Molson and Frind (2002)
HST2D/3D	FD	H, T, C	H ↔ T, M, CH	Free code	2D, 3D	Kipp (1986)
HydroTherm	FD	H, T	H ↔ T	Free code	2D, 3D, two-phase model. Can simulate 0 to 1,200 °C	Kipp et al. 2008
HYDRUS-2D	FE	H, T, C	H → T	Commercial	2D, unsaturated zone, plant water uptake is considered	Šimůnek et al. (1999)
SEAWAT	FD	H, T, C	H ↔ T, C	Free code	3D	Langevin et al. (2008)
SHEMAT***	FD	H, T, C	H ↔ T, C	Commercial	3D	Clauser (2003)
SUTRA	FE/FD	H, T, C	H ↔ T	Free code	2D, 3D	Voss and Provost (2002)
THETA***	FD	H, T, C	H ↔ T, CH	Scientific	3D	Kangas (1996)
TOUGH2	FD	H, T, C	H ↔ T, C, CH	Commercial	1D, 2D and 3D, one of the most widely used code in geothermal energy technologies. Allows for multi-phase flow	Pruess et al. (1996)
TRADIKON 3D***	FD	H, T	H → T	Free code	3D, specially designed for BHEs assessments	Brehm (1989)
VS2DH	FD	H, T	H → T	Free code	2D	Healy and Ronan (1996)

*H: Hydraulic, T: Temperature and C: Contaminant (solute)
** H → T: fluid flow is independent of T; H ↔ T: fluid flow depends on T, M: mechanical deformation (pore deformation), CH: chemical reaction
*** Already used for GSHP simulations

Aside from MT3DMS, other solute transport codes have also been used for heat transport simulations. For example, Chiasson (2000) evaluated the effect of ground water flow on a borehole heat exchanger using AQUAD3D, software developed for contaminant transport. Guimera et al. (2007) used the solute transport model TRANSIN (Medina et al. 1996) to simulate heat transport of open systems near Barcelona, Spain. In their work, the thermal impact of several production wells on ground water is predicted. Thorne et al. (2006) added heat transport (including temperature dependency of the fluid density and viscosity) to the USGS density variable fluid code SEAWAT (Langevin et al. 2003) and solved the classic Henry-Hilleke problem, which involves a saltwater intrusion in coastal areas. SEAWAT is based on the well-known codes MODFLOW and MT3DMS. In their approach, heat is introduced as a single contaminant species.

Although in several studies solute transport models were successfully applied for simulating heat transport, a rigorous test of this transfer is missing, and consequently simulations of GSHP systems with such codes do not have a credible background. The presented study provides a comprehensive evaluation of MT3DMS version 5.2 for its application in two-dimensional (2D) and three-dimensional (3D) heat transport simulations of closed GSHP systems. These systems are considered for various generic scenarios that are distinguished by the Péclet number. Two types of tests are employed. First, numerical results are compared with standard solute and heat transport analytical solutions. For 2D scenarios, line-source analytical solutions for heat transport simulation are applied (Carslaw and Jäger 1959, Diao et al. 2004, Metzger et al. 2004). For 3D scenarios, planar-source analytical solutions based on classical solute transport equations are considered (Fried et al. 1979, Domenico and Robbins 1985, Hähnlein et al. 2009). Note that the selected analytical solutions do not consider temperature dependency of ground water density and viscosity. Second, MT3DMS results are compared with simulations by the finite element code FEFLOW version 5.3 (Diersch 2002,

Table 4-1) and numerical results computed by the SEAWAT code version 4.0 (Langevin et al. 2008). The fore commercial software package has already been used in numerous studies for simulating heat transport of GSHP systems (e.g. Nam et al. 2008, Rühaak et al. 2008, Kupfersberger 2009).

MT3DMS is very attractive for heat transport modeling. It is probably the most popular finite difference code used for 3D simulation of multi-species solute transport in ground water systems. A major advantage of using MT3DMS for heat transport simulation is that it integrates five different advection solver methods, which are suitable for solving problems in a broad range of hydrogeological and transport conditions. It also allows the user to flexibly enter crucial transport parameters such as diffusivity and dispersivity in form of arrays. Last but not least, as an open source code, it can be modified, extended, and adjusted to specific modeling requirements and individual application cases.

4.2 Implementation of the model

Symbol	Variable	Unit
K_d	Distribution coefficient	[$m^3\ kg^{-1}$]
C^k	Dissolved mass concentration	[$kg\ m^{-3}$]
q_{ss}	Volumetric flow rate per unit volume of aquifer representing sources and sinks	[$m^3\ s^{-1} m^{-3}$]
q_h	Heat injection/extraction	[$W\ m^{-3}$]
C_{ss}	Concentration of the sources or sinks	[$kg\ m^{-3}$]
F_o	Energy extraction (point source)	[W]
F_L	Energy extraction per unit length of the borehole (line source)	[$W\ m^{-1}$]
F_A	Energy extraction per area of the source (planar source)	[$W\ m^{-2}$]
l	Characteristic length (grid spacing)	[m]
λ_m	Effective thermal conductivity of the porous media	[$W\ m^{-1}\ K^{-1}$]
λ_w	Water thermal conductivity	[$W\ m^{-1}\ K^{-1}$]
λ_s	Solid thermal conductivity	[$W\ m^{-1}\ K^{-1}$]
n	Porosity	[-]
ρ_w	Density of water	[$kg\ m^{-3}$]
c_w	Specific heat capacity of the water	[$J\ kg^{-1} K^{-1}$]
$\rho_w\ c_w$	Volumetric heat capacity of the water	[$J\ m^{-3} K^{-1}$]
ρ_s	Density of the solid material (= minerals)	[$kg\ m^{-3}$]

c_s	Specific heat capacity of the solid	[J $kg^{-1}K^{-1}$]
$\rho_s c_s$	Volumetric heat capacity of the solid	[J $m^{-3}K^{-1}$]
ρ_b	Dry bulk density $\rho_b = (1-n)\,\rho_s$	[kg m^{-3}]
α, α_l	Dispersivity, longitudinal dispersivity	[m]
α_{th}	Transversal horizontal dispersivity	[m]
α_{tv}	Transversal vertical dispersivity	[m]
$q=v_f$	Darcy velocity	[m s^{-1}]
v_a	Seepage velocity	[m s^{-1}]
D_m, D_h	Molecular diffusion, thermal diffusivity	[$m^2 s^{-1}$]
D_l	Longitudinal heat dispersion coefficient	[m^2 s^{-1}]
D_{th}	Transversal horizontal heat dispersion coefficient	[m^2 s^{-1}]
D_{tv}	Transversal vertical heat dispersion coefficient	[m^2 s^{-1}]
x, y, z	Cartesian coordinates	[m]
r	Radial coordinate	[m]
Y	Dimension (length) of the source in *y* direction	[m]
Z	Dimension (length) of the source in *z* direction	[m]
ΔT	Temperature difference	[K]
ΔT_o	Temperature difference at the source	[K]
t	Time	[s]
T, T_s	Temperature, Temperature of the solid	[K]
T_u	Undisturbed temperature of the underground	[K]
R	Retardation factor	[-]
E_i	Exponential integral function	[-]
η	Integration parameter	[-]
K_o	Modified Bessel function of second kind and order zero	[-]

4.2.1 Governing equations

Due to the analogies between solute and heat transport processes, the governing equations for transport in the subsurface can be represented by similar differential equations. The partial differential equation for solute transport in transient ground water flow systems solved by MT3DMS can be written as follows (Zheng and Wang 1999):

$$\left(1+\frac{\rho_b K_d}{n}\right)\frac{\partial C^k}{\partial t} = div\left[\left(D_m+\alpha v_a\right)gradC^k\right] - div(v_a C^k) + \frac{q_{ss}C_{ss}}{n} \qquad (4\text{-}1)$$

The left side represents the transient term multiplied by the retardation factor *R*. This dimensionless factor denotes the ratio between the total solute concentration and the mobile solute concentration given by the distribution of the contaminant in the fluid and solid phase. The first term in the right side of Equation (4-1) is the hydrodynamic dispersion term, including pure molecular diffusion (D_m) and mechanical dispersion ($\alpha\ v_a$). The second term describes advection and the third term represents source and sinks.

Analogously, the heat transport equation can be characterized by the principle of heat conservation, including conduction and convection (de Marsily 1986):

$$n\rho_w c_w \frac{\partial T}{\partial t} + (1-n)\rho_s c_s \frac{\partial T_s}{\partial t} = div\left[\left(\lambda_m + n\rho_w c_w \alpha v_a\right) grad T\right] - div(n\rho_w c_w v_a T) + q_h \qquad (4\text{-}2)$$

Assuming that the temperature of water and soil are the same, and that there is no net transfer from one phase to another, i.e. thermal equilibrium (Nield and Bejan 2006), the term on the left side of the heat transport equation can be expressed as follows:

$$n\rho_w c_w \frac{\partial T}{\partial t} + (1-n)\rho_s c_s \frac{\partial T_s}{\partial t} = \rho_m c_m \frac{\partial T}{\partial t} \qquad (4\text{-}3)$$

in which $\rho_m c_m$ denotes the volumetric heat capacity of the porous medium. It can be computed as the weighted arithmetic mean of solid rock and pore fluid (Hsu 2005, Anderson 2005, Hoehn 2006):

$$\rho_m c_m = n\rho_w c_w + (1-n)\rho_s c_s = n\rho_w c_w + \rho_b c_s \qquad (4\text{-}4)$$

Using Equations (4-2) and (4-3), and rearranging them, Equation (4-2) simplifies to:

$$\left(\frac{\rho_m c_m}{n\rho_w c_w}\right)\frac{\partial T}{\partial t} = div\left[\left(\frac{\lambda_m}{n\rho_w c_w} + \alpha v_a\right) gradT\right] - div(v_a T) + \frac{q_h}{n\rho_w c_w} \qquad (4\text{-}5)$$

4.2.2 Conforming coefficients

In order to relate Equations (4-1) and (4-5), the coefficients are compared as follows and each term and its implementation in MT3DMS is described in more detail:

1. Retardation factor and distribution coefficient (thermal equilibrium)

The retardation factor (R) and the distribution coefficient (K_d) represented in the solute transport equation as solute sorption can be equivalently expressed in the heat transport equation as the heat exchange between the solid and the water. The retardation factor for heat is given as the ratio between volumetric heat capacity of the porous medium (total phase) and volumetric heat capacity of the water (mobile phase) (Shook 2001). The distribution coefficient is expressed as the ratio between the specific heat capacity of the solids and the volumetric heat capacity of the water:

$$R = \frac{\rho_m c_m}{n\rho_w c_w} \qquad [-] \qquad (4\text{-}6)$$

$$K_d = \frac{c_s}{\rho_w c_w} \qquad [\mathrm{m^3\,kg^{-1}}] \qquad (4\text{-}7)$$

$\Rightarrow$ The new distribution coefficient for heat transport is implemented in MT3DMS in the *Chemical Reaction Package*. The type of sorption must be set to a *linear isotherm* (*ISOTHM=1*) in order to keep the temperature exchange rate between the solid and the water constant independently of changes in temperature.

2. Diffusion and dispersion coefficients

In the diffusion and dispersion term of the partial differential equation for solute transport (Equation 4-1), we identify two parts. The first one is the pure molecular diffusion term (D_m) that represents a process driven only by the concentration gradient. In the heat transport equation, it is equivalent to the thermal diffusivity driven by the temperature gradient:

$$D_h = \frac{\lambda_m}{n\rho_w c_w} \qquad [m^2 s^{-1}] \qquad (4\text{-}8)$$

The second term of Equation (4-1), the hydrodynamic dispersion (αv_a), is a process driven by the differences in flow velocities at pore scale. For the implementation in MT3DMS, the heat dispersivity coefficient is analogously applied as in solute transport (Anderson 2005).

⇒ The new diffusion coefficient and the dispersivity coefficient are set in the *Dispersion Package*.

3. Sources and Sinks

The source and sink term in the solute transport equation represents the mass entering or leaving the domain. In the heat transport equation, this source and sink term indicates energy input or extraction.

$$q_{ss} C_{ss} = \frac{q_h}{\rho_w C_w} \qquad [K\ s^{-1}] \qquad (4\text{-}9)$$

To be consistent with the dimensions relating the contaminant and heat transport, the unit Kelvin [K] is equivalent to the concentration [kg m^{-3}]. Thus energy input/extraction is stated similar as a mass load per unit volume of aquifer.

⇒ The new source and sink term for heat transport is implemented in MT3DMS in the *Sink & Source Mixing Package*, and the type of source must be set to a *mass-loading source* (*ITYPE0=15*).

4.2.3 Limitations

Temperature has an influence on several physical parameters such as density and viscosity of water, and thermal conductivity and heat capacity of the porous medium (Figure 4-2). The principal limitation of the application of MT3DMS for heat transport simulation is that these relationships are not taken into account. Density and viscosity would directly affect the ground water flow calculation and, consequently, affect the heat transport through the hydraulic conductivity. So the question is what role does this limitation play within the temperature spectrum typical for closed GSHP systems? Commonly, ground water temperature changes are restricted by installation guidelines or occasionally by governmental environmental agencies (e.g. Hähnlein et al. 2008). For instance, in Switzerland the maximum allowed temperature difference induced from geothermal energy use is 3 K (GSchV 2001). As a simple example, the physical relationship of hydraulic conductivity with density and viscosity is considered (Bear 1972). The behavior of hydraulic conductivity in regard to temperature is shown in Figure 4-2a, which shows an approximately linear trend in a range from 0°C to 40°C. Computation of the hydraulic conductivity for a usual temperature range disturbance of the ground water under the presence of a ground source heat pump system (from 7°C to 10°C, being 10°C an approximation of the average annual temperature in Central Europe) yields an error of about 8 %. Nevertheless, this inaccuracy seems acceptable in view of the imprecision related to the determination of hydraulic conductivity, which is already reported as 27 % for laboratory conditions (Butters and Duchateau 2002).

Temperature variations can also promote free convection, which is a process driven by density differences as well as salinity concentration (Nield and Bejan 2006). Free convection creates a buoyancy effect, making a denser fluid flow below the lighter one. However, in the absence of brine currents in shallow aquifers, density changes are weak (Kolditz et al. 1998). Buoyancy effects begin to be important for density differences larger than 0.8 kg m^{-3}

(Schincariol and Schwartz 1990). Neglecting salinity effects, a density variation of 0.8 kg m^{-3} implies a temperature change from 0°C to 15°C. Aside from this, it should be noted that ground source heat pump systems usually only operate some hours per day rather than continuously. Therefore, only temperature changes of few degrees are caused in the proximities of the BHE, which are shown to be gradually balanced by the heat carried by the ground water. For systems in which higher temperature changes are expected (>> 10 K), however, heat transport simulation with MODFLOW-MT3DMS should be done with the awareness that substantial errors due to neglected physical temperature dependencies are very likely to occur.

Figures 4-2b and 4-2c show the influence of temperature on heat capacity and thermal conductivity (Holzbecher 1998, Clauser 2003). Maximum differences in thermal conductivities and heat capacities for a usual temperature range disturbance of the ground water under the presence of a GSHP system (from 7°C to 10°C) are less than 2 %. As a simple example, simulations including thermal conductivity and heat capacity depencences on temperature are set up. The corresponding errors in the heat transport simulation are less than 0.5 %. Even for larger differences (up to 60°C), the error in the heat transport simulation is less than 3 %. Based on these observations, the temperature dependency of the thermal parameters is not a real limitation for heat transport simulation of shallow geothermal systems.

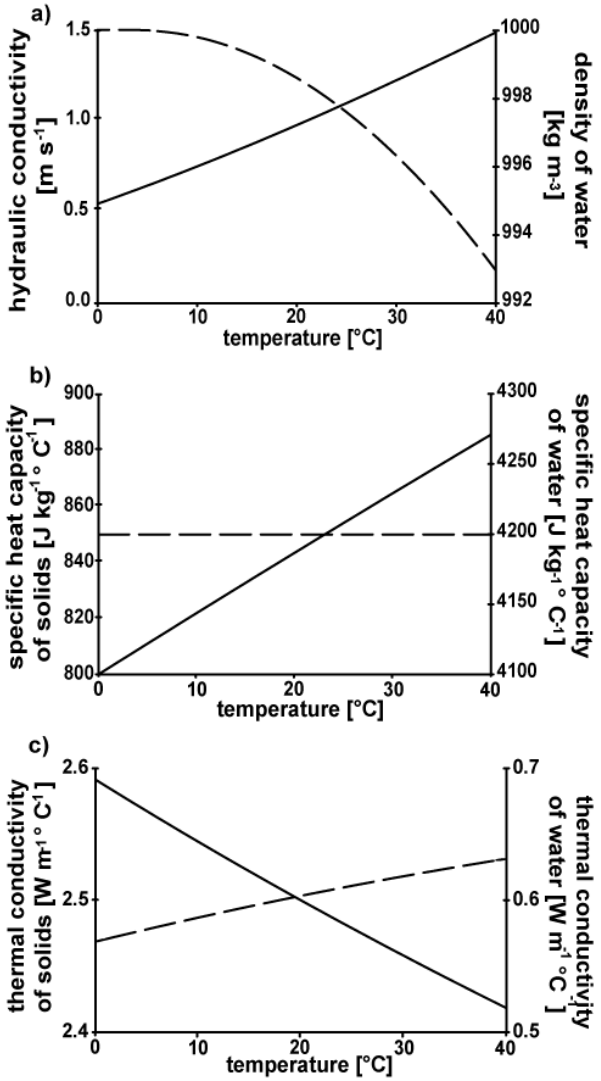

Figure 4-2. Thermal dependencies of: a) hydraulic conductivity and density of the water, b) thermal conductivity of solids and water and, 3) specific heat capacity of solids and water. Left axes are associated with the solid lines; right axes are associated with the dashed lines.

4.2.4 Evaluation procedure

The evaluation procedure is as follows: 1) MT3DMS numerical results are compared with analytical solutions for three scenarios (two- and three-dimensional cases), and 2) for the same scenarios, MT3DMS results are compared with numerical results obtained by two alternative heat and contaminant transport numerical codes. A short description of the analytical solutions is given in the Appendix. The finite element software FEFLOW (version 5.3) and the variable fluid density and viscosity code SEAWAT (version 4.0) are used for the second part of the evaluation.

4.2.5 Comparison metric

Comparison of the simulations is based on residual errors and follows the method of efficiencies (*EF*) described by Loague and Green (1991):

$$EF = \frac{\sum_{i=1}^{n}\left(X_{(i)} - \overline{X} \right)^2 - \sum_{i=1}^{n}\left(X'_{(i)} - X_{(i)} \right)^2}{\sum_{i=1}^{n}\left(X_{(i)} - \overline{X} \right)^2} \qquad (4\text{-}10)$$

$X_{(i)}$ corresponds to the results from the analytical solution or the alternative numerical codes (which we treat as observed or 'true' values), $\overline{X}$ is the mean of the observed values and $X'_{(i)}$ are the values simulated by MT3DMS. The maximum value for *EF* is one, representing no difference between analytical and simulated results. The larger the residual error the closer the value of *EF* is to zero. Computed *EF* values can even be negative; in this case the simulated values are assumed to be wrong. Accordingly to Green and Stephenson (1986) the advantage of the method of efficiencies is that it allows for a dimensionless estimation of goodness-of-fit in contrast to other methods based on dimensional data, such as root mean square error (RMSE) and mean deviation. A disadvantage of the method of efficiencies occurs when values involved vary over many orders of magnitude. However, it should work well for the moderate range of temperatures considered in this work. Efficiency values increase to unity as the agreement between simulated and observed values improves. For the sake of simplicity, we classify the efficiency results as the following: very good, for *EF* values between 0.98 and 1.00; good for *EF* ranging from 0.80 to 0.97; and moderate, for the range from 0.50 to 0.79. Below 0.50 the results are considered unsatisfactory.

The three scenarios are classified according to their respective Péclet number (Table 4-2). For instance, Domenico and Schwartz (1990) define the Péclet number for energy transport as:

$$Pe = \frac{ql\rho_w C_w}{\lambda_m} \qquad \text{with} \qquad \lambda_m = n\lambda_w + (1-n)\lambda_s \tag{4-11}$$

The Péclet number relates the transport of energy by bulk fluid motion to the energy transport by conduction, i.e. it is the ratio between heat conduction and heat convection. Scenarios 1 and 3 represent conduction and convection dominated problems, respectively. In scenario 1, no ground water flow is considered, compared with the relatively high flow velocity of scenario 3. Scenario 2 renders an intermediate case in which the convection and conduction processes have a similar influence (*Pe* = 1).

Table 4-2. Scenarios classified according to the underlying thermal Péclet numbers (*Pe*).

Scenario	*Pe*	Gradient	Seepage velocity (v_a) m s^{-1}
1 (no flow)	0	0	0
2 (*Pe* = 1)	1	1.2×10^{-4}	3.7×10^{-6}
3 (*Pe* = 10)	10	1.2×10^{-3}	3.7×10^{-5}

4.2.6 Model set up

In this section the model configurations used in the numerical codes (MODFLOW, MT3DMS, FEFLOW and SEAWAT) are explained in detail. For the two-dimensional (2D) scenarios, a one-layer rectangular domain representing a confined aquifer is simulated by the finite differences codes (Figure 4-3). The domain size is 300 m × 200 m with a basic regular grid spacing ($\Delta x = \Delta y = 0.5$ m). The BHE is represented by one source cell (positioned at x = 50 m, y = 100 m) of size 0.1 m × 0.1 m, where energy is extracted. For this, close to the source cell, the mesh is gradually refined from 0.5 m (regular grid spacing) to 0.1 m. Vertical heat transfer is ignored for the 2D cases, but included in the 3D simulations. The 3D simulations have 13 identical uniform one-meter layers. The BHE for the 3D scenarios is represented as point source by three cells within the three middle layers (6^{th}, 7^{th} and 8^{th} layer) with the same coordinates as for the 2D case.

MODFLOW-2000 is used for steady state flow field calculations when employing MT3DMS. In all three scenarios, Dirichlet boundary conditions are assigned to the east and west boundaries of the flow model. For scenario 1, equal hydraulic head values are assigned resulting in no background flow. For scenarios 2 and 3, different head values are to produce a uniform flow gradient to the east. Hydraulic conductivity is homogenous and set to 8×10^{-3} m s^{-1}, which is within the range of typical sand aquifers (Spitz and Moreno 1996). An initial uniform density of 999.49 kg m^{-3} is assumed for the whole domain.

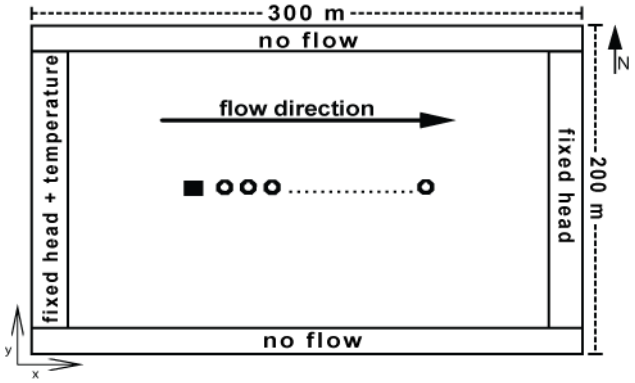

Figure 4-3. Model set up used for all scenarios with fixed head boundary conditions at west and east. Temperature boundary condition: fixed temperature at west border (285.15 K or 12°C). Black square represents the borehole heat exchanger (BHE), circles denote arrangement of observation points. For the 3D model, the source is located in layers 6, 7, and 8, and the observation points are located in the 7^{th} layer.

An initial temperature of 285.15 K is assigned to the entire domain. Constant thermal boundary conditions (Dirichlet) are applied only at the west boundary. At the north and south boundaries, thermal flows are avoided to maintain a solution that can be compared to the analytical solution. At the BHE source cell, a continuous energy extraction of 60 W m^{-1} is set (Equation 4-9). This value is based on reference values from the German Engineer Association guidelines for thermal use of the underground (VDI 2001). Table 4-3 lists the thermal parameters entered in the numerical codes. Simulations are run until steady state conditions are reached. Numerical results are saved at 200 observation points located east of the source cell. For the scenarios with ground water flow, the monitoring points are located on the centerline of the plume.

The third-order TVD (ULTIMATE) scheme is used to solve for the advection term in all scenarios while the Generalized Conjugate Gradient (GCG) solver is employed for the non-advective terms. In order to fulfill the stability criteria related to the third-order TVD scheme, automatic time step estimation was selected.

Table 4-3. MT3DMS specification for all scenarios. Last column indicates the name of the corresponding package within MT3DMS.

Symbol	Variable	Value	Unit	MT3DMS package
n	Porosity	0.26	[-]	BTN
λ_m	Effective thermal conductivity of the porous media	2.0	[W m^{-1} K^{-1}]	-
$\rho_w c_w$	Volumetric heat capacity of the water	$4.18\times10^{+6}$	[J $m^{-3}K^{-1}$]	-
ρ_s	Density of the solid material (= minerals)	2,650	[kg m^{-3}]	-
c_s	Specific heat capacity of the solid	880	[J $kg^{-1}K^{-1}$]	-
ρ_b	Dry bulk density	1,961	[kg m^{-3}]	RCT
K_d	Partition coefficient	2.10×10^{-4}	m^3 kg^{-1}	RCT
α_l	Longitudinal dispersivity	0.5	[m]	DSP
α_{th}	Transversal horizontal dispersivity	0.05	[m]	DSP
α_{tv}	Transversal vertical dispersivity	0.05	[m]	DSP
D_h	Thermal diffusivity	1.86×10^{-6}	[m^2s^{-1}]	DSP
Tu	Undisturbed temperature of the ground	285.15	[K]	BTN
R	Retardation factor	2.59	[-]	RCT

Prior to the final mesh design described above, various domain and source cell sizes were examined for the convection dominated case (scenario 3). This scenario is used due to the extensive spread of the temperature plume downgradient. Numerical simulations were compared with the analytical solution for a line source (Appendix A.3). The discrepancies are measured by model efficiencies and listed in Table 4-4. Figure 4-4 depicts the influence of different sized source cell on the simulated temperature. As expected, smaller source cells improve the agreement, since the referenced analytical model assumes an infinitely small source. This can not be practically implemented in the numerical model, and thus a realistic size of 0.1 m × 0.1 m based on the size of a typical BHE is selected for further analysis.

The domain size of 300 m × 200 m is chosen to avoid boundary effects and because a larger area would extend computational time while only slightly reducing numerical error (Table 4-4). Similar arguments explain the choice to set 13 layers for the 3D case. For the 3D solution, vertical heat transfer across the boundaries may be of concern. No vertical heat flow is selected, to maintain consistency with the analytical solution. In very shallow systems this may not be a valid approach. Temperature gradients at shallow depths can be steep and dynamic, so that a substantial error may be introduced in the simulation by prohibiting heat flow at the top boundary. However, seasonal variability nearly diminishes below a depth of approximately 10 m (Anderson, 2005). In addition, the relatively deep installation of typical GSHP systems of around 100 m or more with clearly dominating lateral heat gradients affirms the assumption to treat the BHE of such systems as a line source.

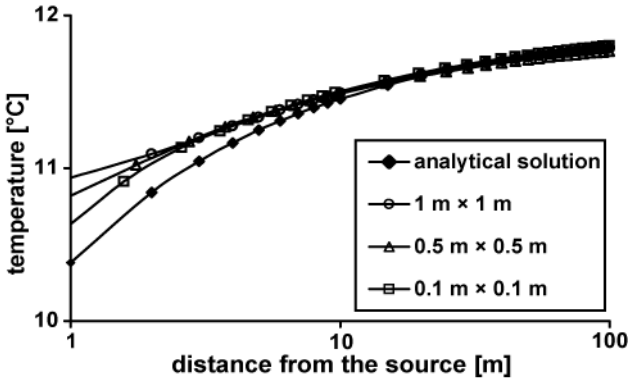

Figure 4-4. Comparison of 2D numerical and analytical solution (Appendix A3) for three source cell sizes in the numerical solution. The values in the legend represent the local discretization Δ*x* and Δ*y* at and around the source cell.

For the FEFLOW model set-up a triangular mesh (about 1 m element size) is chosen with the same type of boundary conditions and flow and thermal input parameters (Table 4-3). The source definition for the 2D cases is represented by a heat flux in one node. This introduces some inconsistency with MT3DMS, in which the energy extraction (expressed as mass loading) is applied to the cell volume (for 2D cases this volume is 0.01 m^3). For 3D cases, in FEFLOW, the source is also defined as heat flux in one node in three layers. In MT3DMS, the source is applied in three cells of total cell volume of 0.03 m^3. Consequently, although the

realized energy extraction is the same (60 W m^{-1}) in both codes, the source definition in FEFLOW differs from MT3DMS, particularly for the 3D scenarios. Additionally, FEFLOW, like SEAWAT, is fully coupled and consequently accounts for temperature dependencies of the flow and thermal parameters. The MT3DMS results lack this capability.

Table 4-4. Preparatory phase: model efficiencies for trial runs with different mesh sizes, numbers of layers, and cell sizes at the source cell. For the 3D analyses, each model layer is 1 m thick. Efficiencies are for comparison between MT3DMS and the analytical results.

2D Case							
Model Size [m × m]	100 × 100	200 × 200	300 × 300	400 × 400	500 × 500	700 × 700	1000 × 1000
Efficiency	-1.00	0.98	0.98	0.98	0.98	0.97	0.97
3D Case (using a 500 m × 500 m model size and 0.10 m × 0.10 m source cell size)							
Number of Layers	3	5	7	9	11	13	15
Efficiency	0.52	0.83	0.87	0.88	0.89	0.89	0.89
Source Cell Size							
Cell Size [m × m]	10 × 10	5 × 5	3 × 3	1 × 1	0.5 × 0.5	0.10 × 0.10	
Efficiency	-2.00	-0.91	-0.24	0.57	0.80	0.98	

Since SEAWAT is based on the MODFLOW and MT3DMS codes, the model set-up described previously for MT3DMS is used. The respective input parameters that account for the temperature dependencies of the fluid density and viscosity are included. The reference fluid density and viscosity are 999.49 kg m^{-3} and 1.2×10^{-3} kg $m^{-1}s^{-1}$, respectively, corresponding to the initial ambient temperature of 12°C. The equation after Pawlowski (1991) relating dynamic viscosity with temperature is used in the viscosity package (Langevin et al. 2008). Since the unique source in the model is a BHE, only temperature changes in the aquifer are expected to occur. Therefore, dependence of fluid density on concentration and pressure are not activated in the density input file within the SEAWAT code.

4.3 Results and discussion

4.3.1 Comparisons with analytical solutions

Simulations of MT3DMS, by analytical methods, FEFLOW and SEAWAT, are compared using the method of efficiencies. Efficiencies are calculated for two sectors: the proximate sector encompasses the observation points near the source (from 1 m to 10 m) and the distant sector, those from 10 m to 100 m. For scenarios 2 and 3, which include convection, observation points are located downgradient of the heat source. Table 4-5 shows the efficiencies for each of the 2D and 3D scenarios. Results for each sector assuming steady state or transient conditions (10 days) are also included.

Table 4-5. Efficiencies of the comparison between MT3DMS and analytical results, steady state and transient conditions. Two sectors are distinguished: proximate, from 1 m to 10 m distance (downgradient) from the source, and distant, from 10 m to 100 m.

Scenario	2D				3D			
	< 10 m		> 10 m		< 10 m		> 10 m	
	Steady State	Transient	Steady State	Transient	Steady State	Transient	Steady State	Transient
1 (no flow)	-	0.98	-	1.00	-	-	-	-
2 (*Pe* = 1)	0.99	1.00	0.99	1.00	0.93	0.96	1.00	1.00
3 (*Pe* = 2)	0.96	0.96	0.96	1.00	0.92	0.84	0.94	1.00

First, MT3DMS simulations without ground water flow (scenario 1) are compared to the corresponding analytical results based on line source theory (Appendix A.1). For the analytical solution, as time tends to infinity, the heat plume extends infinitely (e.g. Diao et al. 2004), i.e. no steady condition is reached. Therefore, results are compared only for transient conditions over a period of 10 days (Figure 4-5a). The calculated efficiency is 0.98 for the first sector, while for larger distances it reaches a value of 1.0, representing a very good agreement between both curves (Table 4-5). The deviation close to the source is mostly due to the limitation of representing an infinitesimal line source numerically. Numerical results from scenarios 2 and 3 (moderate case [*Pe* = 1] and convection-dominated scenario [*Pe* = 10]) are

compared with analytical solutions presented by Metzger et al. (2004, Appendix A.2) and Diao et al. (2004, Appendix A.3); steady state and transient results are shown in Figures 4-5b and 4-5c. The computed efficiencies are listed in Table 4-5. The transient curves (results for 10 days) illustrate a steep temperature gradient for about 2 m from the source for scenario 2 and 15 m for scenario 3; at greater distances, the curves become constant to the ambient temperature (12°C). This trend clearly indicates that these transient temperature disturbances remain fairly close to the source. For steady state conditions, however, the thermal change extends beyond the furthest observation point (located at 100 m approximately). This pattern is observed in both scenarios (Pe = 1 and 10); a similar behavior is also observed in the 3D cases discussed in the next paragraph. Scenario 2 shows a very good agreement between analytical and numerical results. High efficiencies for steady state and transient conditions are obtained. Once again, discrepancies between results close to the source (first two to three observation points) are due to the cell-based representation of the source by the numerical method. A good fit is also obtained for scenario 3; however, the efficiencies in the sectors for steady state conditions are somewhat lower, 0.96. This slight decrease in efficiency may reflect some numerical dispersion when applying the third-order TVD solver for such convection-dominated conditions.

Regarding the absolute temperature differences (ΔT) for each scenario under steady state conditions. For scenario 2 a ΔT = 5 K is computed 1 m downgradient from the source, and ΔT = 1 K for scenario 3. Apparently, the convection-dominated regime brings out a lower absolute temperature change close to the source. This reflects the important role of ground water flow for the energy supply at the borehole.

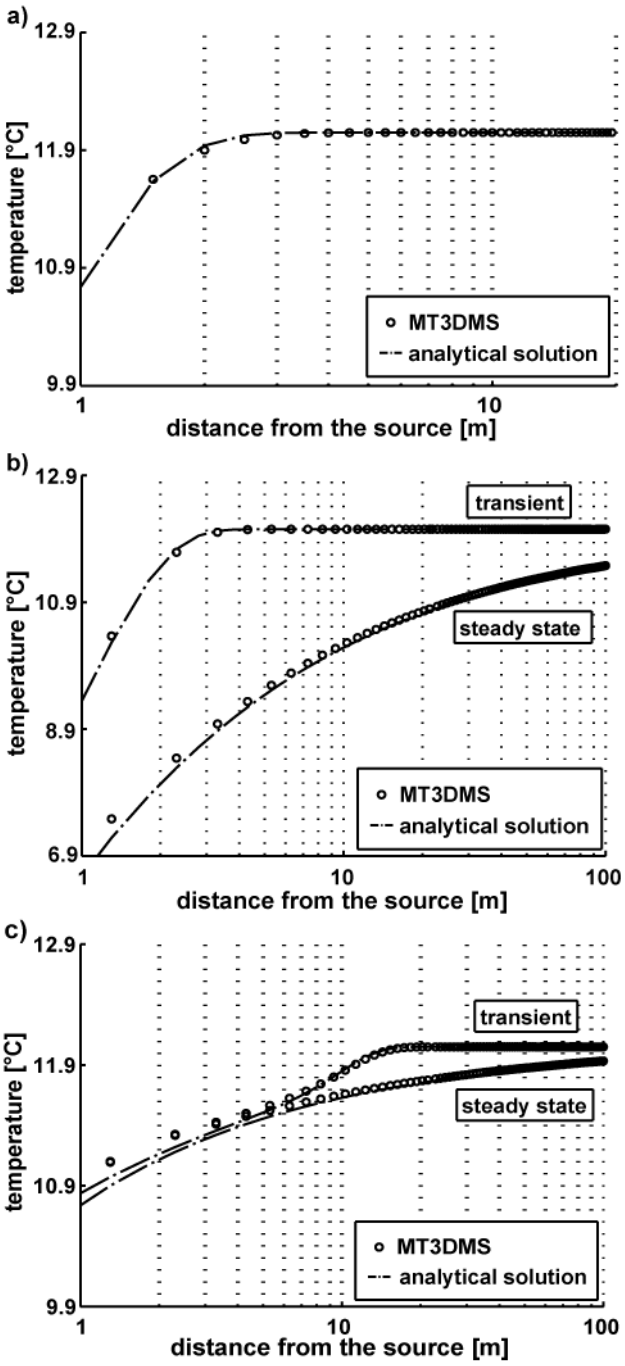

Figure 4-5. Numerical and analytical results for the two-dimensional cases. a) scenario 1 (no flow), b) scenario 2 (Pe=1), and c) scenario 3 (Pe=10). Transient results are shown for ten days.

For the 3D cases, numerical results are compared to an analytical solution with a planar source for heat transport based on classical solute transport equations (Domenico and Robbins 1985; A.5). Scenario 1 (no flow; $Pe = 0$) is not considered due to the lack of a 3D analytical solution for pure conduction. The calculated efficiencies are shown in Table 4-5. Figure 4-6a shows good to very good agreement between steady-state and transient numerical and

analytical results for scenario 2 (Pe = 1) at the proximate sector and the distant sector, respectively. Overall, the discrepancies for scenario 3 (Pe = 10) are small for both steady-state and transient (Figure 4-6b). As for 2D scenario 3, the fit is slightly worse (efficiencies are smaller) close to the source. Again, this is caused by the difference in how the source is represented in the two solutions. The 3D analytical solutions A.4 and A.5 consider a semi-infinite medium and therefore they neglect upgradient spreading. Accordingly, for consistency, thermal conductivity and dispersivity are set to zero in the area upgradient from the source in MT3DMS. Nevertheless, a semi-infinite medium and a planar source cannot be exactly represented in the numerical code. The absolute temperature differences at 1 m distance from the source for the 3D case are the same as for 2D cases, being ΔT = 4 K and ΔT = 1 K.

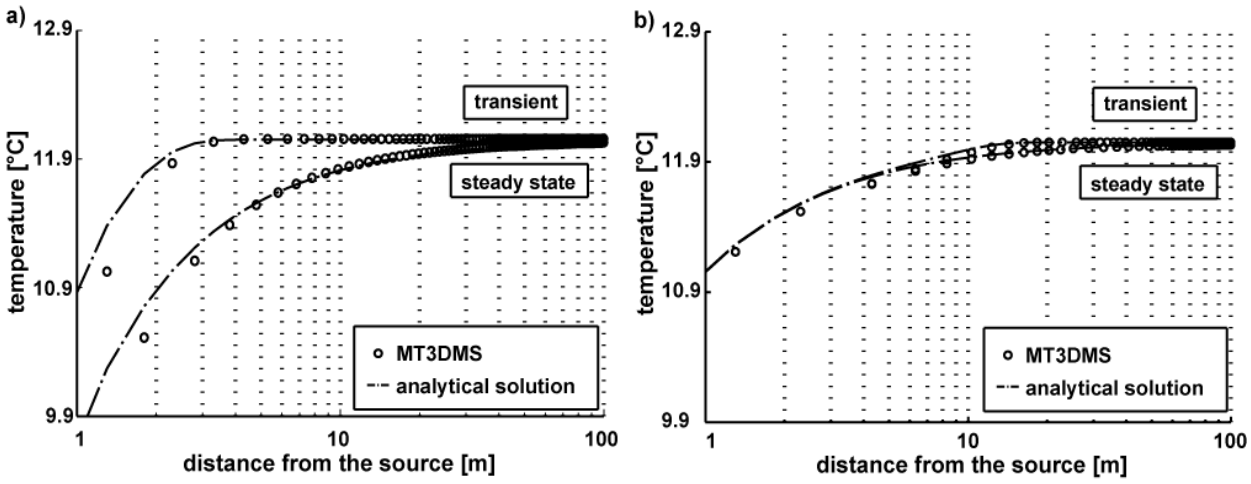

Figure 4-6. Numerical and analytical results for the three-dimensional cases. a) scenario 2 (Pe=1) and b) scenario 3 (Pe=10). Transient results are shown for ten days.

4.3.2 Comparisons with numerical solutions

Figure 4-7 and 4-8 show results from SEAWAT, MT3DMS and FEFLOW for 2D and 3D, respectively. The computed efficiencies for MT3DMS and SEAWAT results are presented in Table 4-6. The close match between MT3DMS and SEAWAT is consistent with the overall efficiency of 1.0 for all cases. Comparison with FEFLOW shows that for 2D there is good to very good agreement, and model efficiencies range between 0.91 and 1.0. Efficiencies are

always lower close to the source and are a little lower away from the source for case 3 (*Pe* = 10). These differences are likely to be dominated by differences in how the source is represented in MT3DMS and FEFLOW.

The very good agreement between the MT3DMS solution and SEAWAT suggests that the influence of fluid density and viscosity changes are minor within the temperature ranges in which GSHP systems usually operate. To further analyze the effect of the temperature dependence of the fluid parameters, scenario 1 (*Pe* = 1), which has the greatest range of temperatures, is additionally tested in FEFLOW with and without the temperature dependency option. Results from these simulations (not shown) display an insignificant difference near the source between both temperature profiles. A minor change in the efficiency value (< 0.01) is computed. This result again demonstrates that temperature dependencies barely influence simulation of the GSHP systems for the specified conditions.

Table 4-6. Model efficiencies of the comparison between MT3DMS-SEAWAT and MT3DMS-FEFLOW results. Two sectors are distinguished: proximate, from 1 m to 10 m distance (downgradient) from the source, and distant, from 10 m to 100 m.

SEAWAT								
Scenario	2D				3D			
	< 10 m		> 10 m		< 10 m		> 10 m	
	Steady State	Transient	Steady State	Transient	Steady State	Transient	Steady State	Transient
1 (no flow)	-	-	-	-	-	-	-	-
2 (*Pe* = 1)	1.00	1.00	1.00	1.00	1.00	1.00	1.00	1.00
3 (*Pe* =10)	1.00	1.00	1.00	1.00	1.00	1.00	1.00	1.00
FEFLOW								
Scenario	2D				3D			
	< 10 m		> 10 m		< 10 m		> 10 m	
	Steady State	Transient	Steady State	Transient	Steady State	Transient	Steady State	Transient
1 (no flow)	-	-	-	-	-	-	-	-
2 (Pe = 1)	0.99	0.99	1.00	1.00	0.64	0.64	0.93	1.00
3 (*Pe* =10)	0.93	0.91	0.95	0.97	0.64	0.64	0.87	1.00

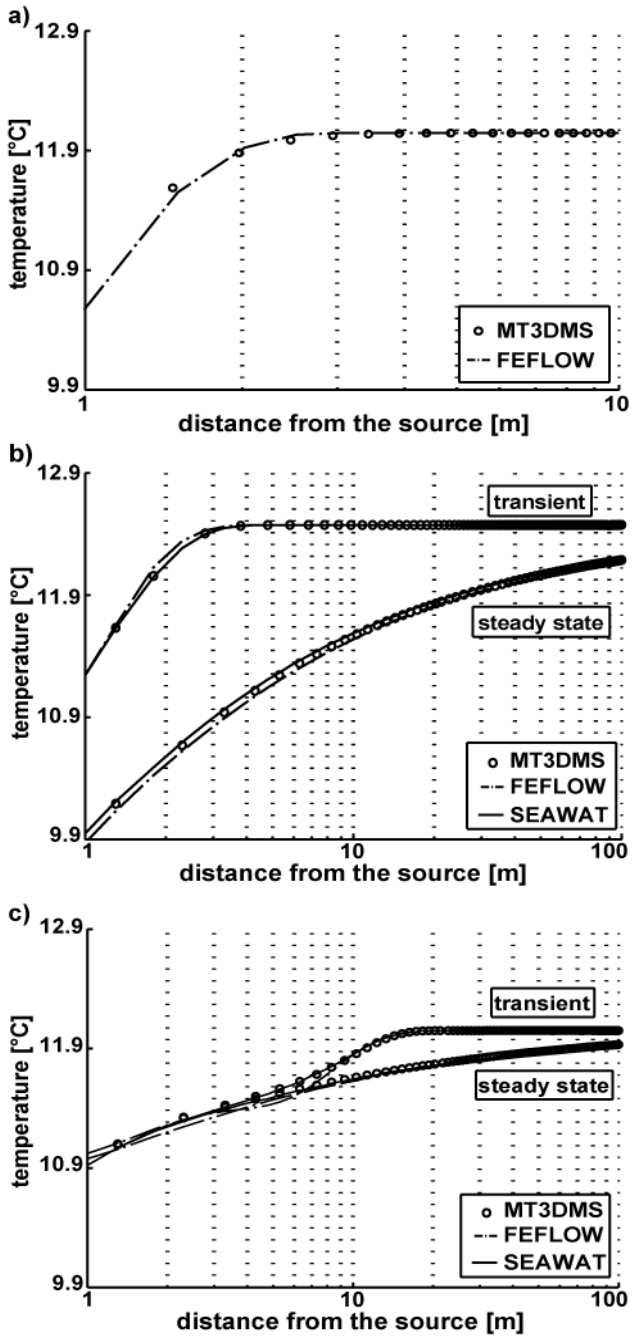

Figure 4-7. Comparison of MT3DMS, FEFLOW and SEAWAT results for the two-dimensional cases. a) scenario 1 (no flow), b) scenario 2 (Pe=1), and c) scenario 3 (Pe=10). Transient results are shown for ten days.

For the 3D scenarios (Figure 4-8), moderate efficiencies are obtained close to the source. This may be attributed to the different source definition. In MT3DMS the energy is extracted from a cell volume, while in the FEFLOW code the energy extraction is assigned to a node. The latter is more similar to a line source than the planar source used in the analytical solution. Therefore the MT3DMS-based results are closer to the analytical solution. However, the difference in these scenarios may also be affected by different influences of numerical

dispersion. The latter is minimized by the transport solution technique used in MT3DMS (TVD method). In FEFLOW the standard Galerkin method (GFEM) is used, which possibly causes more numerical dispersion in the results. For transient conditions, the match between the numerical curves and hence the efficiencies is much better in both sectors.

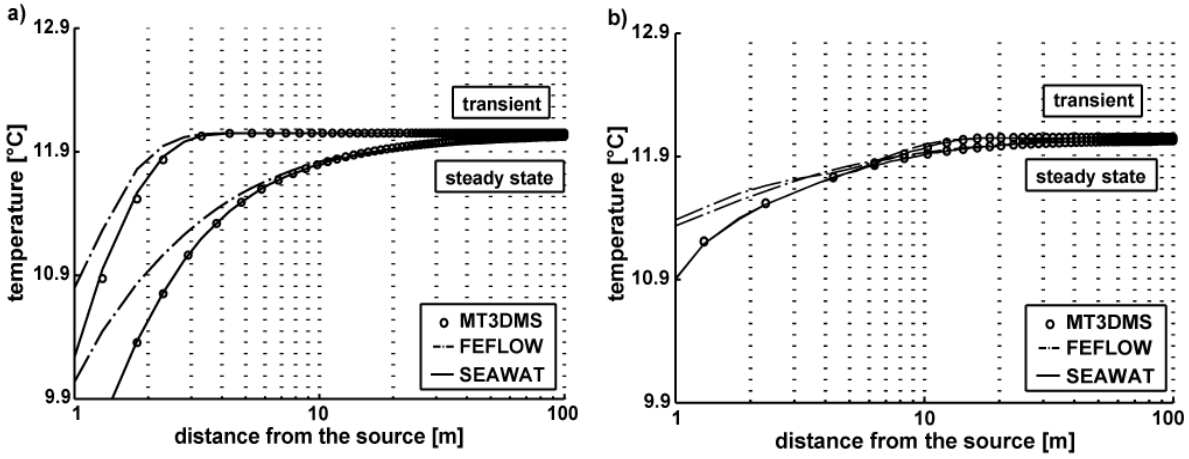

Figure 4-8. Comparison of MT3DMS, SEAWAT and FEFLOW results for the three-dimensional cases. a) scenario 2 (Pe=1) and b) scenario 3 (Pe=10). Transient results are shown for ten days.

Of particular interest are the execution times (computational times necessary to perform a single simulation) of the two finite difference codes. MT3DMS and SEAWAT simulations are performed using the same model setup and solution techniques (with same convergence criterion). Table 4-7 presents run times for scenarios 2 and 3 given in seconds (2D and 3D). Execution times for scenario 1 are not shown since no significant differences are noticeable. Note that the period length used for scenario 2 and 3 are 2000 days and 800 days, respectively. In general, SEAWAT requires longer running times for the same simulated scenarios than MT3DMS. For scenarios 2 (2D and 3D), SEAWAT yields execution times that are approximately 2 times longer than MT3DMS. For scenario 3 (2D and 3D), SEAWAT running times are around 1.5 times longer than MT3DMS. Due to significant differences between the simulation specifications in FEFLOW and those used in the finite differences codes, a comparison with the execution time of the finite element code is not meaningful. However, it should be pointed out that the computational effort with the model setup in

FEFLOW was lower, resulting in shorter execution times for all simulations. For instance, execution times for scenario 2 are 162 s and 645 s for 2D case and 3D case, respectively. This is likely attributed to a lower number of defined nodes, the type of solution techniques for the flow and the transport model and the time step calculation.

Table 4-7. Execution time for the different scenarios.

Code	Execution Time (seconds)			
	2D		3D	
	Scenario 2 (*Pe* = 1)	Scenario 3 (*Pe* = 10)	Scenario 2 (*Pe* = 1)	Scenario 3 (*Pe* = 10)
MT3DMS	238	1,070	5,484	20,051
SEAWAT	507	1,595	11,114	31,737

Hardware specifications: Pentium IV, CPU 3 GHz and 1 GB RAM.

4.4 Conclusions

This work demonstrates the applicability of MT3DMS for heat transport of ground source heat pump (GSHP) systems in a confined aquifer. Although originally developed for solutes, it can be reliably applied for simulation of heat transport in saturated porous media under the influence of closed GSHP systems that result in temperature variations similar to those considered in this work. We utilized three different single borehole scenarios for comparison, which differ with respect to the assumed ground water flow velocities. The overall agreement of MT3DMS with analytical solutions, the SEAWAT code and the finite element model FEFLOW are good to very good. Differences are mostly due to the impossibility of representing the source characteristics (line source, planar source) of the analytical solutions in a numerical model, and the differences ways MT3DMS and the commercial code FEFLOW allow the heat pump well to be represented. Model efficiencies for the pure conduction scenario and the moderate convection scenario are slightly more similar than for the convection-dominated scenario. This is interpreted as an effect of the numerical dispersion for high ground water velocities. Moreover, the different source representations might also result in a discrepancy propagation downgradient.

For these realistic scenarios, highest absolute temperature differences one meter from the source reach 5 K if heat is only transported by conduction and 1 K if convection dominates. MT3DMS does not account for the effects of temperature on density or viscosity. However, for the temperature ranges considered, the influence of the temperature dependencies appear not to be a limitation for simulation of closed loop systems. These findings are corroborated by: 1) the satisfactory agreement with FEFLOW results (fully coupled simulations) even though the two codes differ with respect to definition of the heat source and the transport solution techniques used and, 2) the very good agreement between MT3DMS and SEAWAT (with efficiencies of 1.0 for all scenarios) even though fluid density and viscosity temperature dependencies are represented by SEAWAT. Considering that SEAWAT needs more execution time and the weak effect of the temperature changes on the hydraulic and thermal parameters, the use of MT3DMS is adequate providing the temperature changes exerted by the GSHP system are low (< 5 K). An additional simulation using the moderate seepage velocity case (*Pe* = 1) and an increased energy extraction of 100 W m^{-1} (temperature change = 10 K) also shows a very good agreement between MT3DMS and SEAWAT (overall *EF* of 0.99) and a good agreement between MT3DMS and FEFLOW (*EF* of 0.94 and 0.98 for proximate and distant sector, respectively).

It is recommended to take advantage of the accurate solutions and fast execution times of MT3DMS, but to test the constant-density assumption by running the same model with another code, for example FEFLOW or SEAWAT. For open geothermal systems such as ground water heat pumps and aquifer thermal energy storage (ATES) systems, which might induce higher temperature differences in the aquifer, it may be necessary to use fluid density and viscosity variable codes such as SEAWAT or FEFLOW.

Application of MT3DMS for other shallow geothermal technologies such as open groundwater heat pump systems (GWHP) or aquifer thermal energy storages (ATES) is an

attractive prospect for future work. In addition, testing of the code in field cases is suggested to further explore the potential application range of MT3DMS for geothermal simulations.

Appendix

Two-dimensional analytical solutions:

- Transient conditions, closed system and no ground water flow velocity. It applies for the response of an infinite and constant line-source in a homogeneous, isotropic, infinite medium (Carslaw and Jäger 1959).

$$\Delta T(r,t) = \frac{F_L}{4\ \pi\ \lambda_m} Ei\left[-\frac{r^2}{4(\lambda_m / \rho_m C_m)t} \right] \qquad \text{(A.1)}$$

- Transient conditions, closed system and ground water flow velocity considering heat dispersivity. It applies for the response of an infinite and constant line-source in a homogeneous, isotropic, infinite medium (Metzger et al., 2004).

$$\Delta T(x,t) = \frac{F_L}{4\pi\ n\ \rho_w c_w \sqrt{D_l D_{th}}} \exp\left[\frac{v_a x}{2D_l} \right] \int \frac{1}{\eta} \exp\left[-\eta - \frac{v_a^2 x^2}{16 D_{th}^2 \eta} \right] d\eta \qquad \text{(A.2)}$$

where $D = \frac{\lambda_m}{n\rho_w c_w} + \alpha\ v_a$ is the heat dispersion coefficient (for longitudinal or transversal components).

- Steady state conditions, closed system and ground water flow velocity (Diao et al., 2004). In order to consider heat dispersivity the equation was modified. It applies for the response of an infinite and constant line-source in a homogeneous, isotropic, infinite medium.

$$\Delta T(x) = \frac{F_L}{2\pi\ n\ \rho_w c_w D_{th}} \exp\left[\frac{v_a x}{2D_{th}} \right] K_0\left[\frac{v_a x}{2D_{th}} \right] \qquad \text{(A.3)}$$

Three-dimensional analytical equation

- Transient and steady state conditions, closed system and ground water flow velocity (Hähnlein et al. 2009) based on solute transport analytical solutions (Fried et al. 1979, Domenico and Robbins 1985).

$$\Delta T(x,y) = \frac{F_o}{v_a n\ \rho_w c_w \sqrt{4\pi D_{th} \frac{x}{v_a}}} \exp\left(\frac{-v_a(y^2)}{4D_{th}x}\right) \tag{A.4}$$

$$\Delta T(x,t) = \left(\frac{\Delta T_0}{2}\right) erfc\left[\frac{(Rx - v_a t)}{2\sqrt{D_l Rt}}\right] erf\left[\frac{Y}{4(D_{th}\frac{x}{v_a})^{0,5}}\right] erf\left[\frac{Z}{4(D_{tv}\frac{x}{v_a})^{0,5}}\right] \tag{A.5}$$

4.5 References

Anderson, M.P. 2005. Heat as a ground water tracer. *Ground Water* 43, no. 6: 951−968.

Bächler, D. 2003. Coupled thermal-hydraulic-chemical modelling at the Soultz-sous-Forêts HDR Reservoir (France). Ph.D. diss., Swiss Federal Institute of Technology Zurich.

Bear, J. 1972. *Dynamics of Fluids in Porous Media*. New York: American Elsevier Publishing Company Inc.

Bethke, C., M.-K. Lee, and J. Park. 2007. Basin Modeling with Basin2, Release 5.0.1. Urbana Champaign, Illinois: Hydrogeology Program, University of Illinois.

Bertani, R. 2005. World geothermal generation 2001-2005: State of the art, in: Horne, R.N., and E. Okandan. Conference proceedings: World Geothermal Congress, Reykjavik: Paper 0008.

Blum, P., G. Campillo, W. Münch, and T. Kölbel. 2010. CO_2 savings of ground source heat pump systems - a regional analysis. *Renewable Energy* 35, no. 1:122-127.

Brehm, D. 1989. *Development, Validation and Application of a 3-Dimensional, Coupled Flow and Transport Finite Differences Model*. Giessen: Lenz Verlag.

Butters, G.L., and P. Duchateau. 2002. Continuous flow method for rapid measurement of soil hydraulic properties: I. Experimental considerations. *Vadose Zone Journal* 1, 239–251.

Carslaw, H.S., and J.C. Jäger. 1959. *Conduction of Heat in Solids*, 2nd ed. New York: Oxford University Press.

Cathomen, N. 2002. Wärmetransport im Grundwasser – Auswirkung von Wärmepumpenanlagen auf die Grundwassertemperatur am Beispiel der Gemeinde Altach im Vorarlberger Rheintal. Diploma Thesis. ETH Zürich.

Cathomen, N., F. Stauffer, W. Kinzelbach, and F. Osterkorn. 2002. Thermische Grundwassernutzung. Auswirkung von Wärmepumpenanlagen auf die Grundwassertemperatur. *Gas Wasser Abwasser* 82, no. 12: 901-906.

Chiasson, A.D., S.J. Rees, and J.D. Spitler. 2000. A preliminary assessment of the effects of ground water flow on closed-loop ground-source heat pump systems. ASHRAE Transactions 106, no.1: 380-393.

Clauser, C. 2003. *Numerical Simulation of Reactive Flow in Hot Aquifers, SHEMAT and Processing SHEMAT*. Berlin: Springer Verlag.

Clauser, C. 2006. *Geothermal Energy*, In: K. Heinloth (Ed), Landolt-Börnstein – *Numerical Data and Functional Relationships*, new series, vol. 8: Energy Technologies, Subvolume 3: Renewable Energies. Berlin: Springer Verlag.

de Marsily, G. 1986. *Quantitative Hydrogeology*. Orlando: Academic Press.

Detwiler, R.L., S. Mehl, H. Rajaram, and W.W. Cheung. 2002. Comparison of an algebraic multigrid algorithm to two iterative solvers used for modeling ground water flow and transport. *Ground Water* 40, no. 3: 267-272.

Diao, N, Q. Li, and Z. Fang. 2004. Heat transfer in ground heat exchangers with groundwater advection. *International Journal of Thermal Sciences* 43, no. 12: 1203-1211.

Diersch, H.J.G. 2002. *FEFLOW 5- User's Manual*. Berlin: WASY GmbH.

Domenico, P.A., and G.A. Robbins. 1985. A new method of contaminant plume analysis, *Ground Water* 23, no. 4: 476-485.

Domenico, P.A., and F.W. Schwartz. 1990. *Physical and Chemical Hydrogeology*, 2nd ed. New York: John Wiley & Sons Inc.

Eskilson, P. 1987. Thermal analysis of heat extraction boreholes. Ph.D. diss., Department of Mathematical Physics, Lund Institute of Technology.

Fan, R., Y. Jiang, Y. Yao, and Z. Ma. 2007. Theoretical study on the performance of an integrated ground-source heat pump system in a whole year. *Energy* 32, no. 11: 2199-2209.

Ferguson, G. 2009. Unfinished business in geothermal energy. *Ground Water* 47, no. 2:167-167.

Florides, G., and S. Kalogirou. 2006. Ground heat exchangers - A review of systems, models and applications. *Renewable Energy* 32, no. 15: 2461-2478.

Fried, J.J., P. Muntzer, and L. Zilliox. 1979. Ground-water pollution by transfer of oil hydrocarbons, *Ground Water* 17, no. 6: 586-594.

Green I.R.A., and D. Stephenson. 1986. Criteria for comparison of single events models. *Hydrological Sciences Journal* 31, no. 3: 391-411.

GSchV. 2001. Gewässerschutzverordnung. Switzerland.

Guimera, J., F. Ortuño, E. Ruiz, A. Delos, and A. Pérez-Paricio. 2007. Influence of ground-source heat pumps on groundwater. Conference proceedings: European Geothermal Congress. Unterhaching.

Harbaugh, A.W., E.R. Banta, M.C. Hill, and M.G. McDonald. 2000. MODFLOW-2000, the U.S. Geological Survey modular ground water model, user guide to modularization concepts and the ground water flow process. USGS Open-File Report 00-92.

Hähnlein, S., P. Grathwohl, P. Bayer, and P. Blum. 2008. Cold plumes of ground source heat pumps: Their length and legal situation. *Geophysical Research Abstracts* 10, EGU2008-A-07946.

Hähnlein, S., N. Molina-Giraldo, P. Blum, P. Bayer, and P. Grathwohl. 2009. Ausbreitung von Kältefahnen im Grundwasser bei Erdwärmesonden (Cold plumes in groundwater for ground source heat pump systems). *Grundwasser* (accepted).

Healy, R.W., and A.D. Ronan. 1996. Documentation of computer program VS2DH for simulation of energy transport in variably saturated porous media. USGS Water Resources Investigations Report 96-4230.

Hellström, G., and T. Schmidt. 2005. Ground source cooling – Working paper on usable tools and methods. EU Commission SAVE Programme and Nordic Energy Research.

Hoehn, E., and O.A. Cirpka. 2006. Assessing hyporheic zone dynamics in two alluvial flood plains of the Southern Alps using water temperature and tracers. *Hydrology Earth System Sciences* 10, no. 4: 553–563.

Holzbecher, E. 1998. *Modelling Density-Driven Flow in Porous Media*. New York: Springer Verlag.

Holzbecher, E., and C. Kohfahl. 2008. *Geothermics modelling using COMSOL Multiphysics*. Seminar manual. Berlin.

Hsu, C.T. 2005. *Dynamic Modeling of Convective Heat Transfer in Porous Media*. In: K. Vafai, *Hand Book of Porous Media*, 2nd ed. Boca Raton: CRC-Taylor & Francis Group.

Kangas, M.T. 1996. Modeling of Transport Processes in Porous Media for Energy Applications. Ph.D. diss., Helsinki University of Technology.

Kipp, K.L. 1986. HST3D – A computer code for simulation of heat and solute transport in 3D ground water flow systems. USGS Water Resources Investigations Report 86-4095.

Kipp, K.L., Jr., P.A. Hsieh, and S.R. Charlton. 2008. Guide to the revised ground-water flow and heat transport simulator: HYDROTHERM — Version 3: U.S. Geological Survey Techniques and Methods 6−A25, 160 p.

Kohl, T., and R.J. Hopkirk. 1995. "FRACTure" – A simulation code for forced fluid flow and transport in fractured, porous rock. *Geothermics* 24, no. 3: 333 -343.

Kolditz, O., R. Ratke, H.J.G. Diersch, and W. Zielke. 1998. Coupled groundwater flow and transport: 1. Verification of variable density flow and transport models. *Advances in Water Resources* 21, no. 1: 27–46.

Kolditz, O, A. Habbar, R. Kaiser, T. Rother, C. Thorenz, M. Kohlmeier, and S. Moenickes. 2001. ROCKFLOW user´s manual release 3.5. Institute of fluid mechanics and computer applications in civil engineering. University of Hannover.

Kollet, S.J., I. Cvijanovic, D. Schüttemeyer, R.M. Maxwell, A.F. Moene, and P. Bayer. 2009. The influence of rain sensible heat and subsurface energy transport on the energy balance at the land surface.*Vadose Zone Journal* 8, no. 4: 846-857.

Kupfersberger, H. 2009. Application of groundwater heat transfer modeling to a regional aquifer in Austria. *Environmental Geology* (accepted).

Langevin, C.D., W.B. Shoemaker, and W. Guo 2003. MODFLOW-2000, the U.S. Geological Survey modular ground-water model−Documentation of the SEAWAT-2000 version with the variable-density flow process (VDF) and the integrated MT3DMS transport process (IMT). USGS Open-File Report 03-426.

Langevin, C.D., D.T. Thorne, Jr., A.M. Dausman, M.C. Sukop, and W. Guo. 2008. SEAWAT Version 4: A Computer Program for Simulation of Multi-Species Solute and Heat Transport: USGS Techniques and Methods Book 6, Chapter A22.

Loague, K., and R.E. Green. 1991. Statistical and graphical methods for evaluating solute transport models: Overview and application, *Journal of Contaminant Hydrology* 7, no. 1-2: 51-73. ISSUE

Lund, J.W., D.H. Freeston, and T.L. Boyd. 2005. Direct Application of geothermal energy: 2005 worldwide review. *Geothermics* 34, no. 3: 691-727.

Martin, R.J., S.F. Bender, S.W. Gaulke, and J. Wallace. 2001. Simulation of groundwater flow and heat transport on Grand Cayman Island, *in* Seo, Poeter, Zheng, and Poeter, eds., Conference Proceedings: MODFLOW 2001 and Other Modeling Odysseys. Golden.

Medina, A., G. Galarza, and J. Carrera. 1996. TRANSIN III: Fortran code for solving the coupled non-linear flow and transport inverse problem. ETSE CCPB. UPC. El Berrocal Project. Topical Report 17. ENRESA.

Metzger, T., S. Didierjean, and D. Maillet. 2004. Optimal experimental estimation of thermal dispersion coefficients in porous media. *International Journal of Heat and Mass Transfer* 47, no. 14-16: 3341-3353.

Molson, J.W., and E.O. Frind. 2002. HEATFLOW, version 2.0 user guide. Department of Earth Sciences, University of Waterloo.

Nam, Y., R. Ookaa, and S. Hwanga. 2008. Development of a numerical model to predict heat exchange rates for a ground-source heat pump system. *Energy and Buildings* 40, no 12: 2133–2140.

Nield, D.A., and A. Bejan. 2006. *Convection in Porous Media*, 3rd ed. New York: Springer.

Pawlowski, J. 1991. *Veranderliche Stoffgroben in der Ahnlichkeitstheorie*. Frankfurt: salle+sauerlander.

Pruess, K., C. Oldenburg, and G. Moridis. 1996. THOUGH2 User's Guide, version 2.0, Lawrence Berkeley National Laboratory Report LBL-38383, SN027.

Rühaak, W., P. Schätzl, A. Renz, and H.J.G. Diersch. 2008. Numerical modeling of geothermal processes: issues and examples. 10th International Mine Water Association Congress, Mine Water and the Environment. Karlovy Vary.

Schincariol, R.A., and F.W. Schwartz. 1990. An experimental investigation of variable-density flow and mixing in homogeneous and heterogeneous media. *Water Resources Research* 26, no. 10: 2317–2329.

Schmidt, T., and G. Hellström. 2005. Ground source cooling - working paper on usable tools and methods. EU Commission SAVE Programme and Nordic Energy Research.

Shook, M.G. 2001. Predicting thermal breakthrough in heterogeneous media from tracer tests. *Geothermics* 30, no. 6: 573-589.

Spitz, K., and J. Moreno. 1996. *A practical guide to groundwater and solute transport modeling*. New York: John Wiley & Sons Inc.

Šimůnek, J., M. Šejna, and Th. van Genuchten. 1999. The HYDRUS-2D software package for simulating the two-dimensional movement of water, heat, and multiples solutes in variable-saturated media, version 2. U.S. Department of Agriculture, Riverside.

Therrien, R., R.G. McLaren, E.A. Sudicky, and S.M. Panday. 2006. HydroGeoSphere: a three-dimensional numerical model describing fully-integrated subsurface and surface flow and solute transport, Groundwater Simulations Group, University of Waterloo.

Thorne, D., C.D. Langevin, and M.C. Sukop. 2006. Addition of simultaneous heat and solute transport and variable fluid viscosity to SEAWAT. *Computer and Geosciences* 32, no. 10: 1758-1768.

Tsang, C.F., T. Buscheck, and C. Doughty. 1981. Aquifer Thermal Energy Storage: A Numerical Simulation of Auburn University Field Experiments. *Water Resources Research* 17, no. 3: 647-658.

VDI-Richtlinie 4640. 2001. Thermische Nutzung des Untergrundes, teil 2. Verein Deutscher Ingenieure, VDI-Verlag, Düsseldorf.

Voss, C.I., and A.M. Provost. 2002. SUTRA, a variable-density ground-water flow with solute or energy transport. USGS Water Resources Investigations Report 02-4231.

Zheng, C., and P.P. Wang. 1999. MT3DMS: A modular three-dimensional multi-species model for simulation of advection, dispersion and chemical reactions of contaminants in groundwater systems; documentation and user's Guide, Contract Report SERDP-99-1.

5. Optimization of the Energy Extraction of a Shallow Geothermal System[4]

Abstract: Geothermal energy use from shallow groundwater systems is attractive for the supply of heat and hot water to buildings. It offers economic and environmental advantages over traditional fossil-fuel based technologies, in particular when large scale systems are well adapted to the always unique hydrogeological conditions. Computer based numerical simulations are used to examine the performance of multiple borehole heat exchangers installed in the ground. This paper demonstrates how evolutionary algorithms can be utilized to configure the elements of a geothermal system in an ideal way, and thus substantially enhance the energy extraction rate in comparison to standardized approaches. Differential evolution (DE), evolution strategies (ES) and particle swarm optimizers (PSO) are combined with a local search approach and compared with respect to their efficiency in the optimization of synthetic, real case oriented and static systems. First results are promising, especially for the PSO and the DE with the local search approach.

[4] Reproduced from: Beck, M., Hecht-Méndez, J., de Paly, M., Bayer, P., Blum, P., Zell, A., 2010. Optimization of the energy extraction of a shallow geothermal system. IEEE Congres on Evolutionary Computation (CEC), Barcelona, 18-27 July. ISBN: 978-1-4244-6909-3.

5.1 Introduction

Geothermal energy is a native and environmentally friendly energy. Contrary to most other renewable energy sources, it is available everywhere, independent of geological setting, weather conditions and time of day. For heating and cooling of private houses and other facilities, especially so-called shallow geothermal energy use is on the rise [1]. Here, mostly vertical boreholes are drilled down to a depth of about 100-400 m, and tubes are installed that act as borehole heat exchangers (BHEs). By circulating a glycol/water mixture in these tubes, conductive heat flow is stimulated and the fluid serves as heat carrier. Such systems are called vertical ground source heat pump (GSHP) systems, which, depending on the required energy demand, operate with one single or multiple BHEs. Ultimately the heat is extracted from the subsurface by connecting the BHE with a heat pump [2]. Typically two BHEs are able to sufficiently supply a single-family house with thermal energy. Hence, the simultaneous operation of multiple BHEs may supply an office building, industrial complex or an entire school [3]. Essential for the efficiency of such a BHE field within a given (hydro)geological environment is the overall dimensioning of the field, i.e. the number and depth of boreholes, as well as individual and coordinated arrangement of the BHEs [4]. The appropriate design of such BHE fields to fulfill a certain demand for energy is straightforward and is based on standardized procedures. In contrast, the optimal design of BHE fields can be a challenging task with various degrees of freedom. BHEs might influence each other. Thus, the highly nonlinear mutual influence between the BHEs needs to be considered in the ideal geometric arrangement. Moreover, the performance of BHE(field)s heavily depends on the local natural conditions, which include the geological environment, groundwater flow and in some cases even interference with other GSHP systems in the neighborhood [2]. Considering all of these criteria for the design of GSHP systems yields a mathematically complex, high dimensional optimization problem. This problem cannot satisfactorily be solved and optimized with the

currently available methods or trial-and-error. Currently BHE fields are customarily planned by means of semi-analytical models, such as EED [9] and EWS [8], which are easy to use with short calculation times. These models rely on simplified conditions such as equal heat extraction rates (loads) of all BHEs and a simple geometric arrangement of the BHEs within the field, such as a square lattice. To consider site-specific hydraulic and thermal conditions and to analyze the underground heat transport processes temporally and spatially, numerical models are more suitable [5]. Although numerical models offer much more potential, computational time can be significant and numerical noise often occurs. This is in particular important when the response of such models is used during an automatic optimization procedure. In related studies on model-based optimal water management, Evolutionary optimization Algorithms (EA) are of increasing interest [6], [7]. These algorithms only require objective function values for the optimization of a given problem, are robust and able to handle numerical noise [10]. In the model-based procedure, the design problem is expressed by an objective function that is iteratively evaluated by the EA. In each iteration, candidate solutions are tested by running the numerical model for each candidate and using its response to calculate the objective function value. This concept seems to be promising for larger GSHP systems as well.

In this study we therefore optimize the energy extraction of a BHE field for a synthetic, but real case oriented test case. Selected EAs are used for optimization and the numerical groundwater transport routine MT3DMS [11] is applied for simulating the thermal effects from different configurations of such BHE fields. The GSHP system operates over a defined time span and, as a constraint, resulting groundwater temperatures are not allowed to decrease below a regulative limit [2]. Contrary to available design approaches that drive all BHEs with equal loads and confine possible positions of the BHEs, the technique presented here allows the flexible setting of these parameters. Of major interest is the performance of the selected

EAs: Which variants are computationally most efficient, which can find favorable parameters for this special design problem, and how many iterations are needed?

5.2 Methods

5.2.1 Heat transport model

Heat transport in porous media is governed by two mechanisms: heat conduction and heat advection. Heat conduction is driven by a temperature gradient, while heat advection is the transport of heat due to the moving fluid phase. In the geological porous media of shallow geothermal systems, the moving medium is the groundwater. The governing partial differential equation (PDE) that describes groundwater flow is:

$$\nabla \cdot (k \nabla h) + q = S_s \frac{\partial h}{\partial t}, \tag{5-1}$$

where k is the hydraulic conductivity, h is the hydraulic head, q represents the water source/sink term, S_s is the specific storage of the porous material and t is the time. In heterogeneous systems like the one modeled in the presented study, k is spatially variable. This is typical in natural systems, where for example zones of gravel or sand can be found, all with specific hydraulic properties. For heat transport in the subsurface the PDE is:

$$n\rho_w c_w \frac{\partial T_w}{\partial t} + (1-n)\rho_s c_s \frac{\partial T_s}{\partial t} = (\nabla \cdot [(\lambda_m + n\rho_w c_w \alpha v_a)\nabla T] - \nabla \cdot (n\rho_w c_w v_a T) + q_h, \tag{5-2}$$

Where n is the porosity, $\rho_w c_w$ and $\rho_s c_s$ are the volumetric heat capacities of the materials, λ_m is the arithmetic mean of the thermal conductivity of the water and the solid phase, α represents the thermal dispersivity and v_a is the seepage velocity. The last term q_h represents the source and sink term. The BHE represents a heat source or sink in the subsurface that disturbs the ambient temperature of the surrounding material. Conductive heat flow is enforced by

temperature gradients, in particular by the installed BHEs. Advective heat transport is induced by the prevailing natural head difference, which represents the hydraulic gradient and is linearly proportional to the groundwater flow velocity. Site-specific, often heterogeneous hydraulic and thermal properties of the underground, and the intensity of natural groundwater flow, always create unique conditions.

Two well-established numerical codes used to solve the groundwater flow Equation (5-1) and heat transport equations Equation (5-2) in porous media are MODFLOW [12] and MT3DMS [11], respectively. Both routines are based on a finite difference solution procedure, are open source and written in FORTRAN. According to [13], MT3DMS is suitable for heat transport simulations of BHEs under a wide range of conditions. An important technical aspect is that by separation of the two codes, MODFLOW only has to be applied once at the beginning of the optimization to simulate flow. Since different BHE configurations affect heat transport, just MT3DMS has to be further used to test candidate solutions, and thus total simulation time can be kept down.

5.2.2 Model Setup (Scenarios)

A hypothetical BHE field scenario with 30 BHEs under steady state conditions (800 days) needs to be optimized. The water-bearing stratum (i.e., aquifer) is represented by a one-layer rectangular finite differences model domain. A grid of $\delta x = \delta y = 2.5$ m (Figure 5-1) is defined to simulate a field case over an area of 500 m $\times$ 500 m. Each BHE is represented by a single grid cell with assigned energy extraction values between 20 W/m and 100 W/m. These are typical values reported for sand and gravel aquifers, respectively [14].

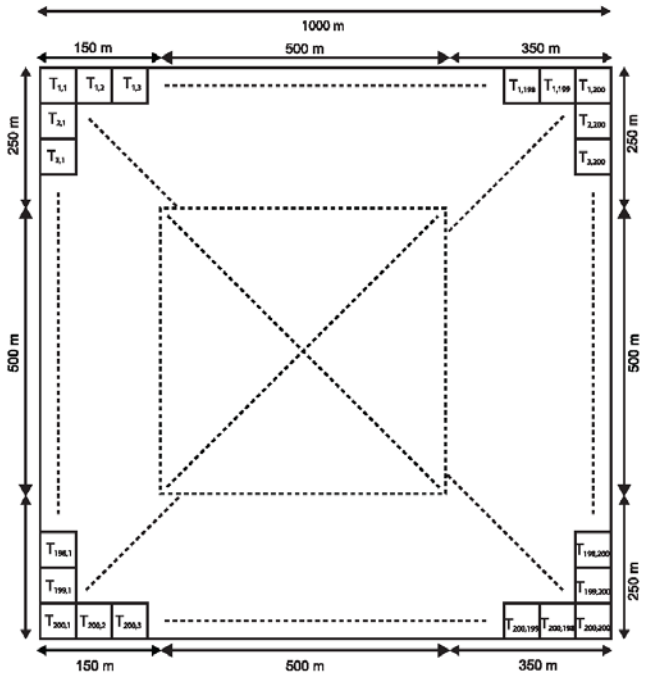

Figure 5-1. Model domain used in MODFLOW and MT3DMS. The dotted square spans the allocation area for the borehole heat exchangers.

In practice, the diameter of a BHE is around 0.10 m. However, the coarse model resolution of 2.5 m is assumed to deliver a sufficiently good approximation of field conditions, since interference between the BHEs as observed in field cases can be well reproduced. For example, Hecht-Méndez et al. [15] show that assuming a BHE size of 3 m × 3 m temperature introduces inaccuracies of only < 0.6 K in the vicinity of a BHE. Higher resolution would significantly increase the computational load of the simulation, which is not desirable for this study, as the focus is set on the performance of the optimization algorithms. The proposed scenario represents an aquifer with three different horizontally distributed hydraulic zones as illustrated in Figure 5-2. These hydraulic zones represent three different aquifer materials: light grey for gravel, black for sand, and dark grey for silty sand. Along the upper and lower model boundaries, Neumann (no-flow) conditions are set. Using Dirichlet boundary conditions (fixed hydraulic head values at the left and right boundaries), groundwater movement from left to right is simulated. Due to the heterogeneous hydraulic conductivity (k) distribution, the groundwater does not flow along a straight pattern and non-uniform flow pathlines are simulated (Figure 5-2). Zones of high hydraulic conductivity (or

high groundwater flow velocity) focus the flow so that the depicted advective pathlines tend to converge. Equivalent to the hydraulic material parameters, the material-specific thermal parameters (thermal conductivity and volumetric heat capacity) are also heterogeneously distributed.

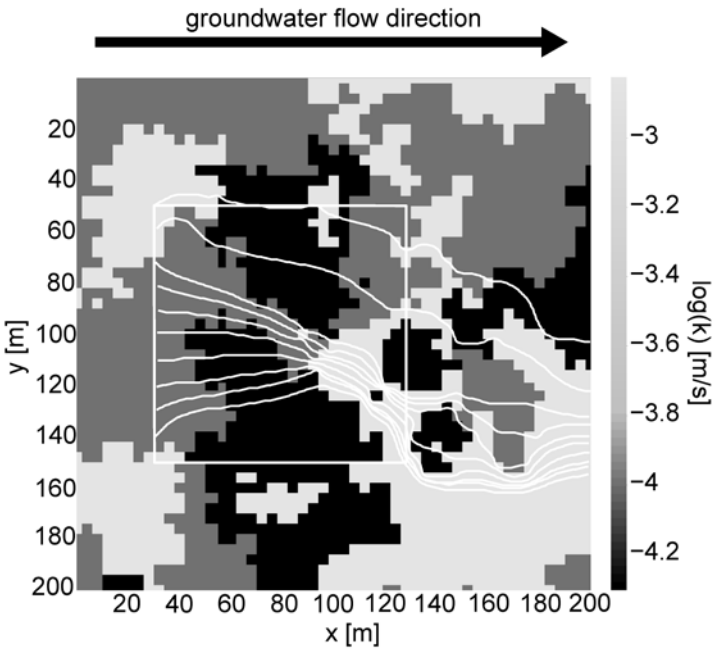

Figure 5-2. Hydraulic conductivity distributions within the model domain. The white lines illustrate flow paths of 10 water particles that are injected into the model domain. These flow paths were created using MODPATH [16]. The white box represents the available placement area for the 30 BHEs.

5.2.3 Objective Function and Constraints

A fixed number of BHEs are to be placed in an area of $250\ \text{m} \times 250\ \text{m}$ in the interior of the model domain as shown in Figure 5-1. This represents typical field conditions, where the placement of the BHEs is restricted to a building plot. The goal is to find a configuration of BHEs that maximizes the possible energy extraction within a defined simulation time:

$$E_{total}(g) = t \sum_{j=1}^{n} l_j, \tag{5-3}$$

where E_{total} is the total extracted energy from the field within the simulation time frame period t for a configuration of BHEs g. n is the number of BHEs in g, and l_j is the

thermal power [W] of each BHE j with $j = 1 \ldots n$. The maximum power of each BHE is restricted by a maximum allowed temperature change ΔT_{max} of the underground in the vicinity of the BHE:

$$\Delta T_c \leq \Delta T_{max}, \tag{5-4}$$

where ΔT_c is the temperature change in cell c caused by the energy extraction of the BHEs. Here ΔT_{max} was set exemplarily to 2.5 K. The influence of a BHE on the aquifer temperature declines with increasing distance. Typical real world applications use a small tolerance area around a given BHE typically between 3 and 10 m [2], and thus the BHE grid cells are not evaluated for this constraint. For the presented study, it is sufficient to evaluate ΔT_c for cells c only in the Moore neighborhoods of all BHE j. The Moore neighborhood comprises the eight cells surrounding the central (BHE) cell on the two-dimensional square lattice.

5.2.4 Constraint Handling

BHE loads and positions are subject to a box constraint. The heat extraction values range between 20 W/m and 100 W/m, while the BHEs are allowed to be set in an area of 250 m $\times$ 250 m in the interior of the simulated domain as shown in Figure 5-1. The temperature constraint (Equation 5-5) is implemented as a penalty term. If the constraint is violated for a candidate solution, the objective function is significantly reduced:

$$P_c = \begin{cases} 0, & \Delta T_c \leq \Delta T_{max} \\ (\Delta T_c - \Delta T_{max}) & otherwise \end{cases}, \tag{5-5}$$

where P_c is the penalty value of cell c. The total penalty value P_{total} for a given configuration of BHEs is calculated by the sum of the penalty values $P_{c(j)}$ of all BHE j. This results in the overall objective (i.e. fitness) function

$$F(g) = E_{total}(g) - P_{total}(g) \cdot \kappa, \tag{5-6}$$

where κ is a scaling factor for the penalty term. The appropriate choice of κ is crucial for the success of the optimization procedure. Values of κ that are too low may yield optimized solutions with higher fitness values for configurations g of BHEs which violate the temperature constraint. Values of κ that are too high generate a very rugged fitness function which is hard to optimize. An ideal value for κ ensures that in cases of constraint violations the influence of the penalty term always surpasses the influence of the energy function, which can be written for each BHE j as:

$$\kappa \cdot P_{c(j)} > t \cdot l_j, \tag{5-7}$$

for all cells c in the Moore neighborhood of BHE j. Assuming the worst case with $\Delta T_{max} = 0$ Equation (5-7) results in

$$\kappa > \frac{l_j \cdot t}{\min(\Delta T_c(l_j))} \tag{5-8}$$

where $\min(\Delta T_c(l_j))$ is the smallest temperature change caused by the load l_j in the Moore neighborhood of BHE j. This relationship enables the determination of a suitable value for κ based on the hydraulic properties of the given scenario prior to the actual optimization procedure.

5.2.5 Encoding of individuals

A configuration of a BHE field g with n BHEs can be written as a vector of the BHEs $j = 1, \ldots, n$, each defined by a position (x_j, y_j) and a thermal power l_j. This yields an overall vector

$$g = (x_1, x_2, ..., x_n, y_1, y_2, ..., y_n, l_1, l_2, ..., l_n) \quad (5\text{-}9)$$

Within the evolutionary optimization process each candidate solution, i.e. individual i of generation m is assigned a single BHE field-vector $g_i^{(m)}$ as defined above. In the studied optimization problem (x_j, y_j) represent cell coordinates which are integer values while the loads l_j are real valued.

5.2.6 A local search approach

In existing designs of BHE fields all BHEs are driven with the same loads. Especially in case of groundwater flow and dominant advective heat transport, such designs do not seem ideal. Unwanted interference between neighboring BHEs can occur, e.g. if one BHE is positioned downwards along the gradient of another one. In such a case, lower loads are favorable for the downgradient BHE in order to comply with the temperature constraint. Similar relationships can be observed for BHEs positioned in areas with different geological properties. As suggested here, a remedy could be to assign different loads to each BHE of the BHE fields. However, using this degree of freedom significantly increases the dimension of the optimization problem.

In the presented study, a hierarchical approach with two separate optimization steps is suggested, one for the geometric design and one for the loads. Each time the EA generates an individual $g_i^{(m)}$ its loads $l_1, ..., l_n$ are separated from its coordinates and optimized independently with a local search approach under the use of an objective function (Equation (5-12) in a separate step. The objective function assigns a single fitness value to every BHE load, depending on the extracted energy of the BHE and the adherence of the temperature constraint. A higher energy extraction of the BHE yields a better fitness value and a violation of the temperature constraint impairs the fitness depending on the extent of the violation. The

local search approach runs over five iteration cycles and, since the result can also be a degraded performance of the BHE field, the global fitness for each local search step is calculated. Depending on the fitness the loads will be increased or reduced in the next iteration step. Finally, the load values of the search step with the best global fitness are assigned to the current individual. Hence the local search never results in reduced global fitness values. In order to achieve maximum energy extraction and concurrently adhere to the temperature constraint each BHE should be driven with loads close to constraint-violating values. The maximum load value l_j^{opt} for a BHE j that does not produce a constraint violation is defined as:

$$l_j^{\text{opt}} = \max(l_j \mid P_j = 0) \tag{5-10}$$

where P_j is the sum of the penalty values P_c of all cells c in the Moore neighborhood of BHE j. The objective function for load l_j of BHE j derives from Equation (5-6)

$$F(g) = E_{total}(g) - P_{total}(g) \cdot k = \sum_{j=1}^{n} l_j - k \cdot \sum_{j=1}^{n} P_j = \sum_{j=1}^{n} (l_j - k \cdot P_j) \tag{5-11}$$

and writes

$$F(l_j) = l_j - k \cdot P_j \tag{5-12}$$

In case of no interaction between the BHEs, l_j^{opt} would be the global optimum of the objective function (5-12), and according to (5-11) and (5-12) the assignment of the load value of each BHE j with l_j^{opt} would be the global optimum of function (5-6). In reality and in our model setup, limited building ground results in a high spatial closeness of BHEs and mutual influence between individual BHEs is inevitable. In the event of positioning a BHE downstream of another BHE it could be more efficient to drive both BHEs with medium loads

than use the first BHE to full capacity and turn down the second one nearly completely. Thus assigning each BHE j with l_j^{opt} will not necessarily lead to the global optimum of (5-6) and the best solution of the overall optimization problem. Although this approach is not able to find the global optimal individual load values for each BHE in each case, it nevertheless can be used to move the loads closer to l_j^{opt} and to support the EA by avoiding individuals with bad fitness values due to extremely high or low load values.

Equation (5-12) represents a convex function in a one dimensional search space. Thus local improvement procedures should be an ideal compromise between speed of convergence and efficiency for the detection of the global optimum. We went for the linesearch algorithm because it is easy to implement and excellent for finding global optima of objective functions in one dimension. The number of linesearch iterations was set to five in each enhancement step.

5.3 Optimization Algorithms and Procedure

5.3.1 Algorithms

We used our open source Evolutionary Algorithm framework EvA2, which is a comprehensive optimization system written in Java, with a wide range of evolutionary algorithms, like evolution strategies (ESs), genetic algorithms (GAs), genetic programming (GP), particle swarm optimization (PSO) and differential evolution (DE) [17]. We applied the following Evolutionary Algorithms on the problem of optimizing a BHE field.

1. Evolution Strategy (ES).

A population of μ parents generates a set of λ children via mutation and recombination operators. A following selection step chooses μ individuals for the next generation from the

set of either the offspring, referred to as (μ,λ)-selection ($\mu < \lambda$ must hold), or both the parents and offspring, referred to as $(\mu+\lambda)$-selection. In this paper we used a $(5,40)-ES$ with $\frac{1}{5}$-success rule as mutation operator and one-point crossover with $(p_c = 0.5)$ for recombination.

2. Particle Swarm Optimization Algorithm (PSO).

In PSO, a set of individuals is represented by a so-called swarm that is composed of a set of particles $P = \{p_1, p_2, ..., p_n\}$. At any time step t, p_i has a position $\vec{x}_i^t$ and a velocity $\vec{v}_i^t$ associated with it. A candidate solution of the optimization problem is represented by the position of a particle. For every particle p_i the best solution it has ever reached until time step t is represented by vector $\vec{b}_i^t$. Further, every particle receives information from its neighborhood $N_i \subseteq P$ while neighborhood relations are commonly represented as a graph $G = \{V, E\}$. The particles' position and velocity are updated by so-called update rules after every time step t. In the presented study we decided on a grid topology and a swarm size of $n = 30$. To update the particles' positions and velocities the constriction mode with $\phi_1 = \phi_2 = 2.05$ is chosen.

3. Differential Evolution (DE).

In DE a population consists of μ individual vectors $x_1, , x_\mu$. A mutation vector v_j is assigned to every individual vector x_j whereas the calculation of v_j depends on the chosen mutation mode and a mutation factor F. In the following recombination step a trial vector u_j composed of elements of x_j and v_j is created. A final selection step calculates the fitness of x_j and u_j and only the vector with the better fitness value will be overtaken in the next

generation. For our optimization runs we decided for a DE/current-to-best/1 Differential Evolution with $F = 0.7$ and a cutoff probability $C_r = 0.8$ for the recombination step.

All algorithms were tested with as well as without the local search approach, so the number of tested algorithms rises to six (ES, PSO, DE, LS-ES, LS-PSO, LS-DE). According to equation (5-8) the scaling factor κ was set to $\kappa = 1250$. To obtain statistically significant results each algorithm run was started 10 times. To keep the overall runtime in an admissible range we limited the number of objective function calls for each algorithm to 75000. For the same reason, we implemented an additional stop criterion that aborts a test run if no better fitness value was found for 6000 objective function calls. With our parameter configuration, one MT3DMS simulation takes about 3 minutes. Hence one optimization run with 75000 objective function calls brings up an overall runtime of 225000 minutes or 156 days. The calculations were executed on AMD Opteron computer cluster and with a tenfold parallelization of the EAs we were able to reduce the runtime for one optimization run to two weeks.

5.4 Results

Figure 5-3 and Table 5-1 show the optimization results of the six tested algorithms. For further evaluation of the results we only consider those algorithms that produced valid solutions in terms of the constraints mentioned in 5.2.4.

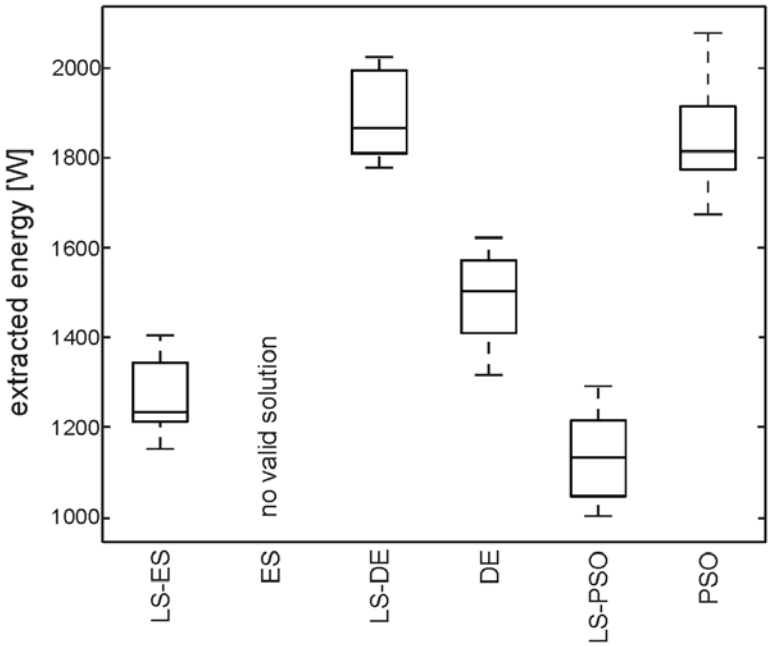

Figure 5-3. Boxplot of the optimization results. The fitness values are expressed in Watt. Every algorithm was tested ten times. On each box, the central mark is the median, the edges of the box are the 25th and 75th percentiles, the whiskers extend to the most extreme data points not considered outliers.

LS-DE and PSO outperformed the other algorithms and achieved the best results. ES is not able to achieve valid solutions without the local search approach. Although PSO gave a better peak result than LS-DE, LS-DE attained a slightly better average performance.

Table 5-1. shows a comparison of the results. The values correspond to the extracted energy of the BHE fields in [W].

Algorithm	Best	Avg.	Std.
DE	1622	1480	112
LS-DE	2024	1887	96
PSO	2077	1853	120
LS-PSO	1291	1139	98
ES	no valid solution	no valid solution	no valid solution
LS-ES	1404	1268	84

LS-DE and PSO are the only algorithms that were not stopped before the limit of 75000 objective function evaluations was reached. The other algorithms were aborted after considerably fewer objective function evaluations according to the stop criterion given in 5.3.1. In comparison, ES, LS-ES and DE showed overly strong convergence behaviour and terminated in local optima very soon. These findings reflect the extremely multimodal

character of the objective function. We suggest that the high selection pressure of the ES is the reason that this algorithm could not detect valid solutions at all. PSO was the only algorithm that achieved significantly better results without the local search approach.

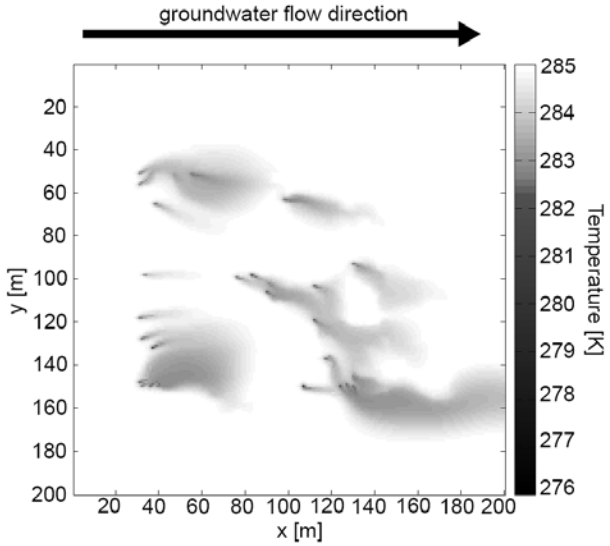

Figure 5-4. Temperature distribution in the underground of the best BHE setup found by PSO. The overall energy extraction of the BHE field equals the energy extraction of the field illustrated in Fig. 5-5 but the defined temperature constraint is respected.

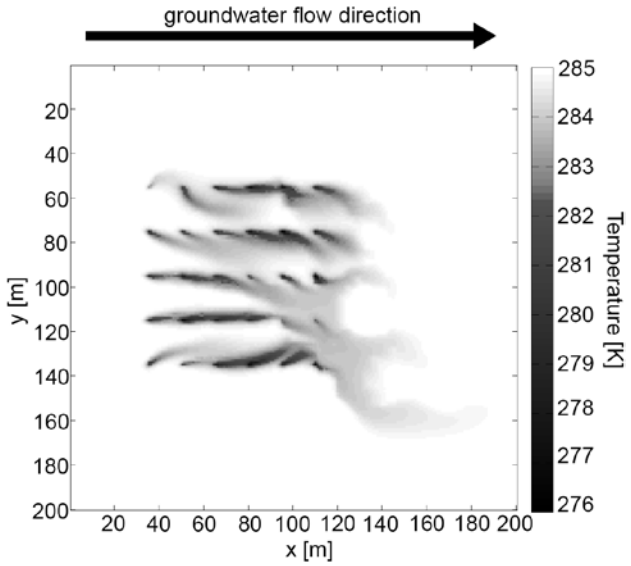

Figure 5-5. Temperature distribution in the underground with a lattice-like arrangement of 30 BHEs and equal loads (67.5 W/m) for all BHEs. The field is parameterized as described in 5.2.2 and the energy extraction of the BHE field equals the energy extraction value of the best BHE field found by PSO (illustrated in Fig. 5-4). 28 of 30 BHE generate temperature changes in the underground that exceed ΔT_{max} at least in one cell in the Moore neighborhood of the BHE cell.

This effect can be attributed to the external change of the individual vectors by the linesearch algorithm between the creation and the evaluation of the individuals by PSO. Because of this

external perturbation, the kinetic energy of the particle swarm remains nearly static and the convergence behaviour of PSO becomes less satisfactory. Figures 5-4 and 5-5 compare the temperature distribution in the underground after one MT3DMS simulation run within two BHE fields.

Both BHE fields extract the same amount of energy. Figure 5-4 presents the best BHE field found by PSO and shows that the temperature constraint is adhered to. The temperature distribution in Figure 5-5 results from a lattice-like arrangement of 30 BHEs and equal extraction rates for each BHE of 67.5 W/m. The loads of this field are assigned to the mean of the loads of the best BHE field found by PSO. That means the load $l_j^{lattice}$ of a BHE j in the lattice arrangement was set to the extracted energy of the best BHE field found by PSO divided by 30. Using this lattice array and without considering the temperature constrain defined in 5.2.4, the temperature change of the subsurface exceeds ΔT_{max} up to 6.5 K. To achieve an adherence of the temperature to the lattice arrangement, the loads would have to be dimmed to 23 W/m. This means a reduction of the loads by 67% compared to the optimal BHE field found by LS-DE.

5.5 Conclusion

In this study we presented an application of three EAs (ES, DE, PSO) to the problem of optimizing the energy extraction of a ground source heat pump system with 30 BHEs over a defined time. A minimum temperature constraint, which ensures that the temperature changes of the subsurface by heat extraction remain in reasonable bounds, was defined. We introduced an objective function and a constraint handling strategy, that ensured the adherence to the minimum temperature criterion of the subsurface. Contrary to current design approaches, which drive all BHEs with equal loads and allow only a constricted arrangement for the positions of the 30 BHEs, our optimizers are allowed to set these parameters freely within

defined ranges. Furthermore, we introduced a local search procedure for an additional fine adjustment of the individual extraction rates. Each EA was tested with and without the local search approach, so the number of tested algorithms rose to six (ES, LS-ES, DE, LS-DE, PSO, LS-PSO). LS-DE and PSO outperformed the other algorithms and achieved the best results, while the ES was not able to achieve valid results without the local search approach at all. The optimized BHE fields ensure a high energy yield and at the same time ensure reasonable temperature changes of the subsurface within the temperature constraint. Fields designed according to the actual lattice shaped design of BHE fields, where all BHEs are assigned with same energy extraction rates, violated the temperature constraint severely. Without violating the temperature constraint, the lattice shape BHE field could only reach 33% of the energy extraction of the optimized BHE fields.

Attractive prospects for future work are to test further EAs with the given problem and to further evaluate the best EAs found in this study (LS-DE and PSO) in respect to various hydrogeological conditions or advanced real case scenarios.

5.6 References

[1] A. H. Demirbas, Global geothermal energy scenario by 2040, *Energy Sources, Part A: Recovery, Utilization, and Environmental Effects*, vol. 30, pp. 1890 - 1895, 2008.

[2] S. Hähnlein, N. Molina-Giraldo, P. Blum, P. Bayer, and P. Grathwohl, Ausbreitung von Kältefahnen im Grundwasser bei Erdwärmesonden (Cold plumes in groundwater for ground source heat pump systems), *Grundwasser*, no. 15(1), 2010.

[3] A. M. Omer, Ground-source heat pumps systems and applications, *Renewable and sustainable energy review*, pp. 344--371, 2008.

[4] S. P. Kavanaugh and K. Rafferty, Ground Soruce Heat Pumps - Design of Geothermal Systems for Commercial and Institutional Buildings, *American Society of Heating, Refrigerating and Air-Conditioning Engineers*, 1997.

[5] T. Schmidt and G. Hellström, Ground Source Cooling Working Paper on Usable Tools and Methods, EU Commission SAVE Programme and Nordic Energy Research, Tech. Rep., 2005.

[6] P. Bayer, C. M. Bürger, and M. Finkel, Computationally efficient stochastic optimization using multiple realizations, *Advances in Water Resources*, no. 31(2), pp. 399 - 417, 2008.

[7] M. de Paly and A. Zell, Optimal Irrigation Scheduling with Evolutionary Algorithms, in *Applications of Evolutionary Computing*, vol. 5484/2009. 1em plus 0.5em minus 0.4em Springer-Verlag Berlin/Heidelberg, April 2009.

[8] M. Wetter and A. Huber, *Vertical Borehole Heat Exchanger EWS Model*, 1997.

6. Summary and concluding remarks

The current design of large GSHP systems follows standardized procedures, in which the demanded energy is commonly achieved by equally operating multiple BHEs. In addition, effects of groundwater flow are usually neglected or indirectly incorporated at the planning stage of the GSHP systems by assuming an “effective” ground thermal conductivity. In the present PhD thesis, two simulation-optimization procedures, that can optimize individual energy extraction of BHE arrays, are developed. Additionally, the effects of groundwater flow in the subsurface heat transport are included in both optimization approaches. In contrast to standard GSHP system design and previous optimization work, special attention is given to the ground temperature changes that are induced by the monthly operation of a BHE field.

In Chapter 2, a linear optimization procedure that is based on superimposed heat transport analytical solutions is developed. The infinite line source mathematical model is selected for estimating the subsurface temperature changes, due to operating the BHEs. Since the overall performance of a GSHP system depends on the temperature of the circulating fluid, which at the same time, strongly depends on the ground temperature, the optimization approach aims at minimizing the maximum temperature change in the ground. As a demonstration case, a synthetic field with twenty-five BHEs that are installed in a homogeneous aquifer without groundwater flow is selected. Subsurface temperature distributions for optimized and non-optimized BHE fields are computed. The use of the optimized BHE field results in a mitigation of the long-term temperature decrease and local temperature anomalies. In spite of the self-regulating effect of the non-optimized case, the optimal system assures a minimal temperature impact in the entire field by distributing more efficiently the operational loads. The absolute temperature decrease in the subsurface is reduced by 18% when combined simulation-optimization is applied.

In Chapter 3, the applicability of the simulation-optimization approach, developed in Chapter 2, is extended to situations where groundwater flow is present. By incorporating an alternative simulation procedure based on the moving infinite line source model, the energy extraction rates of 25 BHEs, which are influenced by groundwater flow, are predicted. Fifteen scenarios characterized by different groundwater flow regimes are inspected. Similar to the conductive case evaluated in Chapter 2, the long-term temperature changes and the temperature anomalies are diminished by using the optimized BHE field. The major finding in this investigation is that optimal adjustment of the monthly energy extraction rates produces typical load patterns that depend on time and groundwater flow velocity. If groundwater flow is small (here $Pe < 1$), radial patterns are suggested, where most of the energy is extracted by the BHEs at the borders. Increase of flow velocity generates optimized patterns that, advantageously, are oriented at the flow direction, using the array column-wise. In general, the benefits from optimization decrease with increasing flow velocity. However, optimal systems always result in lower temperature impact in the subsurface.

The studies presented in Chapters 2 and 3 demonstrate that optimal operative schemes for multiple BHEs can be found by keeping the maximum subsurface temperature change as small as possible. It is also shown that the optimization procedure is not restricted to a specific hydro-geothermal simulation model. Therefore, alternative analytical models, such as the finite line source model (Zeng et al., 2002), the finite moving line source model (Molina-Giraldo et al., 2011) or the planar source model (Domenico and Robbins, 1985), could be utilized. Further, cooling operation can also be accounted for. A significant advantage of the developed optimization procedure is that it does not distinguish between any assumptions regarding the geometry of the field and the geological, hydrogeological and thermal parameters of the ground. Therefore, it can be easily applied to other cases and be readily implemented in planning software. In addition, depending on the specific problem, the

selected temporal resolution of the load profile can also be replaced by a coarser or finer resolution (years, days, minutes). Still, this will be constrained by the associated computational burden, which increases for a finer temporal resolution.

In Chapter 4, a comprehensive evaluation of the well-known solute transport model MT3DMS, for heat transport simulation of GSHP systems, is carried out. Hydro-thermal simulations of three scenarios with different groundwater flow, classified according to the Péclet number, are performed. Two- and three-dimensional numerical results are compared to respective analytical solutions. In addition, the numerical simulations by MT3DMS are compared to alternative temperature-dependent numerical models (FEFLOW and SEAWAT). Based on the overall good agreement of MT3DMS predictions with those by analytical solutions and alternative numerical codes, the use of MT3DMS for heat transport simulation of GSHP systems is feasible. For the temperature ranges at which this type of geothermal technology operates, the influence of the temperature dependencies appear not to be a limitation.

In Chapter 5, MT3DMS is incorporated into a new simulation-optimization approach. The problem to be optimized is now defined as maximizing the total energy extraction of a GSHP system, considering a heterogeneous aquifer. Also, the most suitable position of the BHEs within a predefined area has to be found. Due to the non-linearity and expected non-convexity of the defined optimization problem, three Evolutionary Algorithms (ES, DE, PSO) are selected as the optimization technique. The procedure is tested for a case with 30 BHEs. Using a temperature threshold, the maximum temperature change of the ground is kept within reasonable limits. From the evaluated Evolutionary Algorithms, LS-DE and PSO outperformed the other algorithms and achieved the best results. The obtained optimized BHE fields ensure a high energy yield and, at the same time, ensure reasonable temperature changes of the subsurface within the temperature constraint. In comparison, BHE fields

assigned with equally distributed energy extraction rates violated the temperature constraint severely. Without violating the temperature constraint, the lattice shape BHE field could only reach of the energy extraction of the optimized BHE fields.

The presented theoretical studies have demonstrated the successful application of different optimization procedures for improving the installation and operation of multiple BHEs in closed-loop GSHPs by considering the induced subsurface temperature changes. It has also been shown, through a preliminary study, that optimal positioning of the BHEs is possible and promising, for the improvement of the entire BHE field performance. Since the developed simulation-optimization approaches are independent of the aboveground system, they can be used together with further optimization methods that focus on connected components of the heating or air-conditioning system. Still, the realization of the optimal operation strategies found in this study can be a major technical challenge. Thus, it is strongly recommended to start with first applications at well-controlled test sites, as an experimental prosecution of this work. Furthermore, the overall economic advantage of using optimized BHE fields also has to be assessed at the specific application cases.

7. Acknowledgements

This work was supported by a grant from the Federal Ministry for Education and Research (BMBF) within the International Postgraduate Studies in Water Technologies program (IPSWaT).

I owe special thanks Dr. Peter Bayer for his tireless help, continuous guidance, the motivating discussions and all his constructive critics and good advices during the writing of the manuscripts. Special thanks also to Jun.-Prof. Dr. Philipp Blum for his excellent supervision, patience, the good ideas and for letting me be part of the Hydrogeothermics group. I acknowledge Prof. Dr. Peter Grathwohl for giving me the opportunity to be part of the ZAG.

I am very grateful to Nelson Molina Giraldo, my friend, fellow student and office mate during the last 6 years. Our endless discussions about geothermal systems, analytical solutions and numerical models were fundamental for this work. I also owe special thanks to Michael de Paly and Markus Beck, two of the smartest guys I have ever met. I always enjoyed our short meetings (> 2 hours). It was a pleasure to have them as co-authors. I would like to thank also Prof. Dr. Simone Walker-Hertkorn, Dr. David Kuntz and Dr. Markus Kübert from TEWAG GmbH, for their advices in technical matters.

I thank also all my colleagues from the hydrogeothermics group: Steffi, Ke Zhu, Tao Li, Marc, Steffen, Gita, Valentin, Dr. Javier Rodrigo Ilarri, Jin Shuang and Selcuk for the great time together at the *green building*, *Oberjoch* and at the *Cannstatter*. I am grateful to Fernando Mazo D'Affonseca, Ashutosh Singh and Anibal Pérez for their sincere friendship. All my thanks to Dr. Peter Merkl and Monika Jekelius for their collaboration regarding all administrative issues and to Willi Klapper for his IT support.

I thank my mother for believing in me and for having tender words when I need them most. Last but not least, I want to deeply thank my wife, for supporting me during all my university years in Germany, for her unconditional love und for giving me a beautiful family, and my children Sándor and Sofia, for being the most wonderful inspiration for achieving any goal in my life and for vanishing any worry with only one smile.

8. Ergänzungsblatt zur Eigenleistung

Erklärung nach § 5 Abs. 2 Nr. 7 der Promotionsordnung der Math.-Nat. Fakultät -Anteil an gemeinschaftlichen Veröffentlichungen-

Declaration according to § 5 Abs. 2 No. 7 of the PromO of the Faculty of Science -Share in publications done in team work-

Name: Jozsef Hecht Méndez

List of Publications

1. de Paly, M., Hecht-Méndez, J., Beck, M., Blum, P., Zell, A., Bayer, P., 2012. Optimization of energy extraction for closed shallow geothermal systems using linear programming. Geothermics 43, 57-65.

2. Hecht-Méndez, J., de Paly, M., Beck, M., Bayer, P., Optimization of energy extraction for vertical closed-loop geothermal systems considering groundwater flow. Energy Conversion and Management, submitted.

3. Hecht-Méndez, J., Molina-Giraldo, N., Blum, P., Bayer, P., 2010. Evaluating MT3DMS for heat transport simulation of closed geothermal systems. Ground Water 48, 741-756.

4. Beck, M., Hecht-Méndez, J., de Paly, M., Bayer, P., Blum, P., Zell, A., 2010. Optimization of the energy extraction of a shallow geothermal system. IEEE Congres on Evolutionary Computation (CEC), Barcelona, 18-27 July. ISBN: 978-1-4244-6909-3.

Nr.	**Accepted for publication yes/no**	**Number of all authors**	Position of the candidate in list of authors	Scientific ideas of candidate (%)	Data generation by candidate (%)	Analysis and Interpretation by candidate (%)	Paper writing by candidate (%)
1	yes	6	2nd	20	30	25	10
2	submitted	4	1st	40	60	40	60
3	yes	4	1st	40	80	50	60
3	yes	6	2nd	20	25	17.5	22.5

I certify that the above statement is correct.

_____

Date, Signature of the candidate

I/We certify that the above statement is correct.

_____

Date, Signature of the doctoral committee or at least of one of the supervisors